Lu, Poyang

ENERGY TRANSFER BETWEEN DYE MOLECULES INVESTIGATED BY STEADY STATE AND TIME RESOLVED SPECTROSCOPY

City University of New York PH.D. 1982

ENERGY TRANSFER BETWEEN DYE MOLECULES INVESTIGATED BY STEADY STATE AND TIME RESOLVED SPECTROSCOPY

by

POYANG LU

A dissertation submitted to the graduate faculty in Physics in partial fulfillment of the requirement for the degree of the Doctor of Philosophy, The City University of New York

1982

This manuscript has been read and accepted for the Graduate Faculty in Physics in satisfaction of the dissertation requirement for the degree of Doctor of Philosophy.

August 26, 1982
date

Robert R Alfano
Chairman of Examining Committee

August 26, 1982
date

Executive Officer

Prof. Joel I. Gersten

Prof. Elie Hayon

Prof. Kenneth Rubin

Dr. Ping-Pei Ho

Supervisory Committee

The City University of New York

ACKNOWLEDGEMENT

I wish to thank all the members of my Ph.D. committee. I wish to express my sincere gratitude to my adviser, Professor Robert R. Alfano, for his cogent guidance and continuous encouragement through the entire dissertation work. The helpful discussions with Professor Joel I. Gersten are much appreciated. I also wish to thank the computer center of the Physics Department at City College of New York for using the DEC PDP-10 computer in the theoretical calculation and curve fittings, Mrs. Megan Gibbs for typing the manuscripts, and Mr. Zhen-Xin Yu for his technical assistance in the work. Lastly, I am deeply indebted to my mother, Feng-O Lu, and grateful to my wife, Hui-Hua Lu, for their patience and spiritual support in every aspect.

Abstract

ENERGY TRANSFER BETWEEN DYE MOLECULES INVESTIGATED BY STEADY STATE AND TIME RESOLVED SPECTROSCOPY

by

Poyang Lu

Adviser: Professor Robert R. Alfano

The kinetics of long range resonant energy transfer between photoexcited dye molecules (the donor) and unexcited dye molecules (the acceptor) has been studied with the goal to understand the fundamental processes behind long range resonant energy transfer, to search for the possible mechanisms during the energy transfer, and to find out the factors which parameters affect the energy transfer between the donor and acceptor molecules.

A theoretical model based on the dipole-dipole interaction was established to explain the dynamics of energy transfer between the donor and acceptor dye molecules and fit the kinetic fluorescence profiles of donor and acceptor emission. The measurements by the techniques of steady state and time-resolved fluorescence spectroscopy were performed for the binary mixtures (A) Rhodamine 6G (the donor) and Oxazine 4 Perchlorate (the acceptor), and (B) Rhodamine B (the donor) and Nile Blue A Perchlorate

(the acceptor). It is found that: (1) Not only was the donor decay time short but also the acceptor risetime slowed in the mixed solution. (2) The relative decrease of donor quantum yield followed the increase of quantum yield of acceptor when the energy transfer is operative. (3) The decrease of donor decay time followed the increase of the risetime of the acceptor as the concentration of acceptor increased for a given concentration of donor at room temperature. (4) The long range energy transfer rate increases as the concentration of acceptor and the energy deactivation efficiency increases as the diffusion coefficient increases.

From the thesis research, the long range energy transfer via dipole-dipole interaction plays a dominant role in the mechanism of energy transfer between donor and acceptor binary system ($R \sim 50\text{Å}$) and the diffusion of molecule helps in moving the donors and acceptors so that energy can be transferred more readily. The efficiency of energy transfer can be increased from 49% to 69% when the contribution of diffusion varies from 1% to 38%. Factors such as the typical transfer distance R_o, the concentration and the decay times of donor and acceptor molecules, are important parameters which affect the efficiency and operation of energy transfer.

TABLE OF CONTENTS

CONTENTS PAGE

CONTENTS PAGE

LIST OF ILLUSTRATIONS

CHAPTER 1 INTRODUCTION

The study of the energy transfer between donor and acceptor dye molecules in solution has both theoretical and practical importance. Dyes play a major role in various fields. They are commonly used as biological and industrial stains. In photosynthesis, dyes transfer optical energy from one spectral region to another. Dyes can increase the efficiency in solar energy conversion by absorbing energy in a wide spectral region. It is important to understand the mechanisms for energy losses and transfer in neat and binary dye mixtures in solution. A series of experiments[1-11] on dye mixture have shown that the excitation energy may be efficiently transferred from a photoexcited molecule (the donor) to an unexcited molecule (the acceptor). Dye lasers have been widely used in spectroscopic systems for photosynthesis and photochemistry studies. Energy transfer from an absorber (donor) molecule to an acceptor molecule in a dye laser mixture affects the operation and spectral output of the dye laser. The mixture of two dissimilar dye molecules, for example, rhodamine 6G and cresyl violet, can increase the efficiency of a dye laser of cresyl violet. Lin and Dienes[5] have studied the excitation transfer in a laser dye mixture of rhodamine 6G and cresyl violet by studying the fluorescence kinetics of only the donor molecules. They found a Stern-Volmer quenching relation for the donor system. Rehm and Eisenthal[4] have studied the

donor kinetics and found that the energy transfer between the rhodamine 6G (the donor) and malachite green (the acceptor) is in agreement with the Forster theory.[12] Porter and Tredwell[11] studied the same system of rhodamine 6 G and malachite green and obtained a value of R_o = 52.5 A ± 0.5 A for the Forster mechanism. Recently, Millar, Robbins, and Zewail[13] have investigated the picosecond dynamics of electronic energy transfer between the cresyl violet (the donor) and azulene (the acceptor) dissolved in ethylene glycol and concluded that the Forster dipole-dipole model is valid for that system. However, these investigators[1-11] have only studied the kinetics of the donor system to obtain information on the energy-transfer rates to the acceptor. These measurements do not give a complete picture of energy transfer to the acceptor because of competing nonradiative and radiative rates and concentration quenching from the donor and acceptor, and spatial distribution. It is essential to measure the kinetics of both the donor and acceptor molecules to obtain a complete description of the energy-transfer mechanism operating in the binary components of dyes in a solution.

In order to understand the long range energy transfer process between the donor and acceptor molecules, the following research programs were undertaken:

(1) The steady state measurement of absorption and fluorescence spectra of two kinds of dyes to determine

the critical energy transfer distance parameter R_o and to decide appropriate donor and acceptor dye for our research.

(2) The time-resolved fluorescence measurement of neat and mixed solution of donor and acceptor to determine the change of the rise and decay time of each component in the process of energy transfer.

(3) The concentration dependence of the energy transfer between donor and acceptor to determine the change of decay and rise time of donor and acceptor during the energy transfer process and to find out the efficiency of the energy transfer in strong and weak interaction.

(4) The diffusion effect on the energy transfer between donor and acceptor molecules by varying the temperature.

The theoretical calculations are consistent with the experimental results which was found by curve fitting in all the above research programs.

The dissertation is divided into seven chapters. Chapter 2 describes the experimental setup including the laser system, detection system, and data storage and analysis system. The generation of single pulse selection, and second harmonic generation of the laser pulses will be discussed for the Nd:phosphate oscillator - amplifier glass laser system. The streak camera with white cell delay unit will be covered in the detection system. The digitized data for time-resolved fluorescence stored in the DEC Minc 11

minicomputer are analyzed by the scientific programs. Chapter 3 presents the theoretical model we used to explain and fit our measurements of steady state and time-resolved fluorescence spectroscopy of the neat and binary mixed dyes in the study of long range energy transfer. A detailed derivation of the theoretical equations and computer simulation of the model are covered in this chapter. Chapter 4 through Chapter 6 presents the results, analyses, comparisons, and discussions for the pair of Xanthane dye mixed with Oxazine dye. Specifically, the fluorescence and absorption spectra and the theoretical fitting to the time-resolved fluorescence of the donor and acceptor are included in Chapter 4. The concentration dependence of the donor-acceptor binary system and efficiency of long range energy transfer are presented in Chapter 5. The diffusion effect on the long range energy transfer at different temperatures is discussed in Chapter 6. Chapter 7 gives the summary and conclusion of this investigation and suggests a further research which can be performed. The computer program used in the calculation and curve fitting are included in the appendix.

References

1. R. G. Bennett, J. Chem. Phys. 41, 3037 (1964)
2. S. A. Latt, H. T. Cheung, and E. R. Blout, J. Am. Chem. Soc. 87, 995 (1965)
3. K. B. Eisenthal, Chem. Phys. Lett. 6, 155 (1970)
4. D. Rehm, and K. B. Eisenthal, Chem. Phys. Lett. 9, 387 (1971)
5. C. Lin and A. Dienes, J. of Appl. Phys. 44, 5050 (1973)
6. S. A. Ahmed, J. S. Gergely, and D. Infante, J. Chem. Phys. 61, 1584 (1974)
7. R. W. Anderson, Jr., R. M. Hochstrasser, H. Lutz, and G. W. Scott, J. Chem. Phys. 61, 2500 (1974)
8. R. M. Hochstrasser and A. C. Nelson, Chem. Phys. Lett. 18, 361 (1976)
9. R. Katraro, A. Ron and S. Speiser, Chem. Phys. Lett. 52, 16 (1977)
10. Yu, I. Bukekov, S. A. Tikhomirov, G. B. Tolstorozhev, and D. M. Khalimanovich, Sov. J. Quan. E.ec. 7, 262 (1977)
11. G. Porter and C. J. Tredwell, Chem. Phys. Lett. 56, 278 (1978)
12. Th Forster, Ann. Physik, 2, 55 (1948). Dis. Far. Soc. 27, 7 (1959)
13. D. P. Millar, R. J. Robbins, and A. H. Zewail, J. Chem. Phys. 75, 3649 (1981)

CHAPTER 2 EXPERIMENTAL TECHNIQUES

In this chapter, the experimental setup and techniques will be discussed in detail. The principle of generation of laser train in the laser resonator (cavity), the action of mode locking, the technique of single pulse selection and second harmonic generation, and amplifier system are described sequentially. The streak camera and computer system will be included in the latter part.

2.1 Steady State (Time Integrated) Absorption and Fluorescence Setup

The absorption and fluorescence spectra of dye molecules can be measured using a steady state luminescence apparatus shown in figure 2.1.1.

Light from lamps and monochromator at 530 nm $\pm$ 5 nm was chopped and focussed onto the sample. The fluorescence signal from the sample was focussed onto the Spex double 1/2 m spectrometer, detected by a RCA 7265 photomultiplier and measured by a lock-in amplifier combination. The fluorescence spectrum is recorded on an X-Y recorder. For a given wavelength of pumping light, the transmission light through the sample is converted to optical density (OD) and absorption coefficient. Varying the wavelength of the pumping light, the steady state absorption spectrum can be obtained.

2.2 Time Resolved Experimental Setup

The experimental setup[1] used in picosecond time

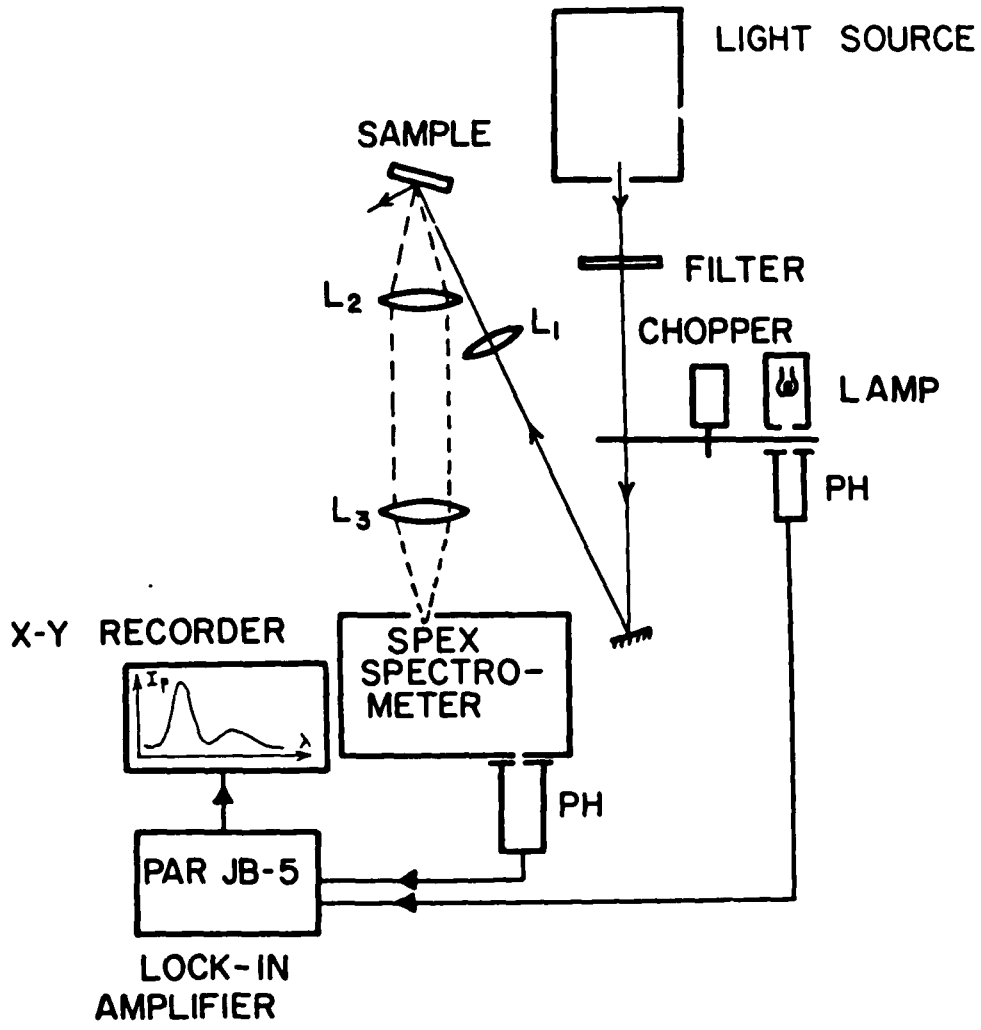

Fig. 2.1.1 Schematic diagram of the steady state luminescence setup.
PH: photomultiplier

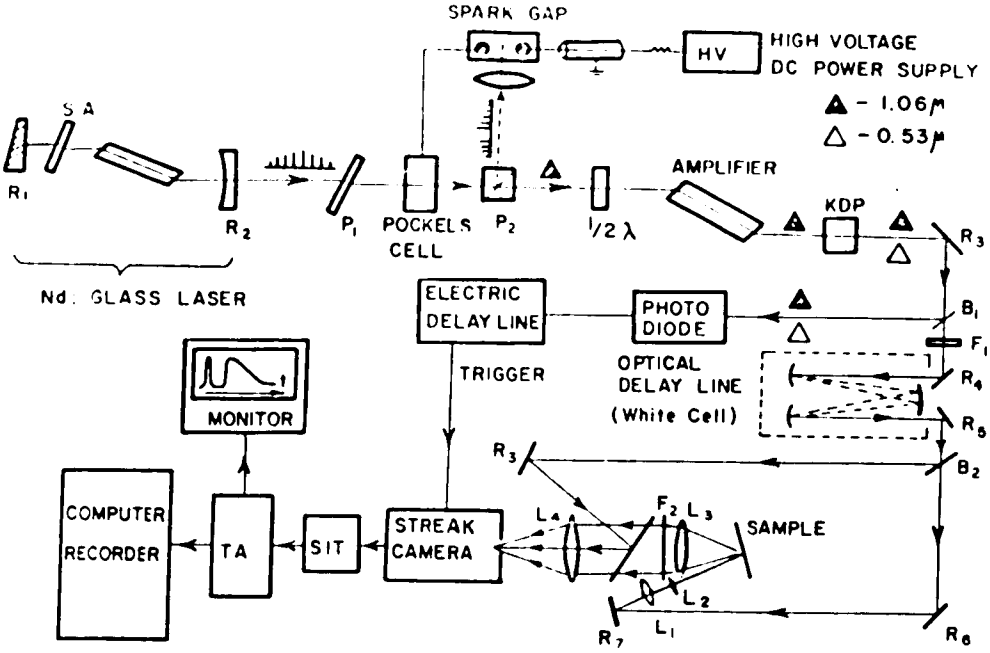

Fig. 2.2.1 Schematic diagram of the picosecond time-resolved fluorescence setup.

resolved studies in figure 2.2.1. It was composed of a laser system with single pulse selection, second harmonic generation, and amplifier; a detection system; and a data storage and analysis system. They are described separately in the following sections.

2.2.1 The Nd:glass Laser System

The single intense picosecond laser pulse at 1.054 μm can be generated by a glass mode-locked oscillator, a single pulse selection, and an amplifier. Two types of laser rods are available - Nd:doped silicate and phosphate rods. The phosphate glass has a larger gain coefficient and lower nonlinear index n_2 than the silicate glass by at least a factor of 1.4 and 1.1. The Nd:glass laser is a 4 level laser system. The energy diagram of Nd:glass laser is shown in figure 2.2.2. The lasing action occurs by the stimulated emission of radiation between level 2 and 1 after the population inverse is achieved. The typical wavelength of Nd:glass laser is 1.06 μm. In order to obtain the population inverse for the lasing material and a stable oscillator for amplification, the Nd:phosphate glass laser used in our experiments then consists of a laser rod within an optical resonator cavity formed by two mirrors aligned parallel to each other, and perpendicular to the axis of the resonator, as shown in fig. 2.2.3. The Q-88 glass laser rod with 3.3% Nd doping was used for the oscillator. The laser rod was 7 1/2 inches long with a diameter of 1/2 inch,

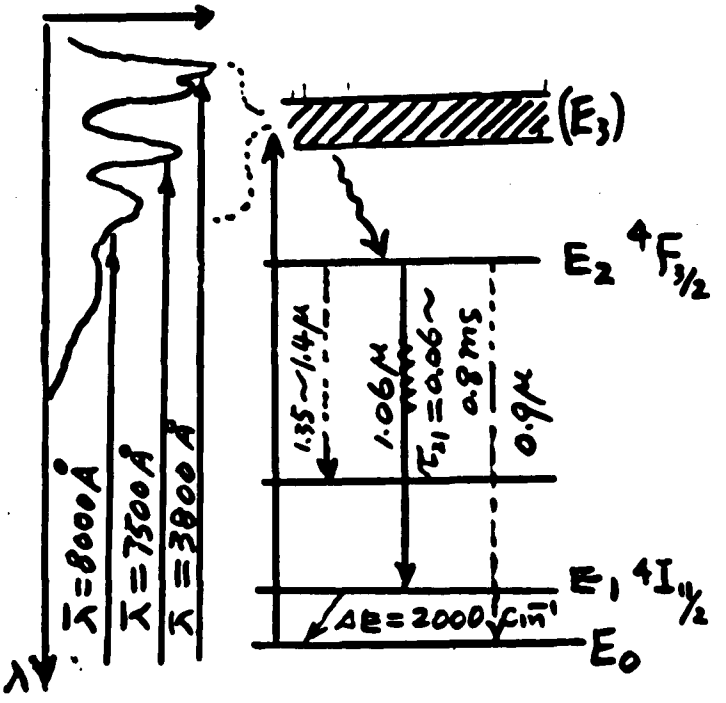

Fig. 2.2.2 Energy level of Nd:glass laser

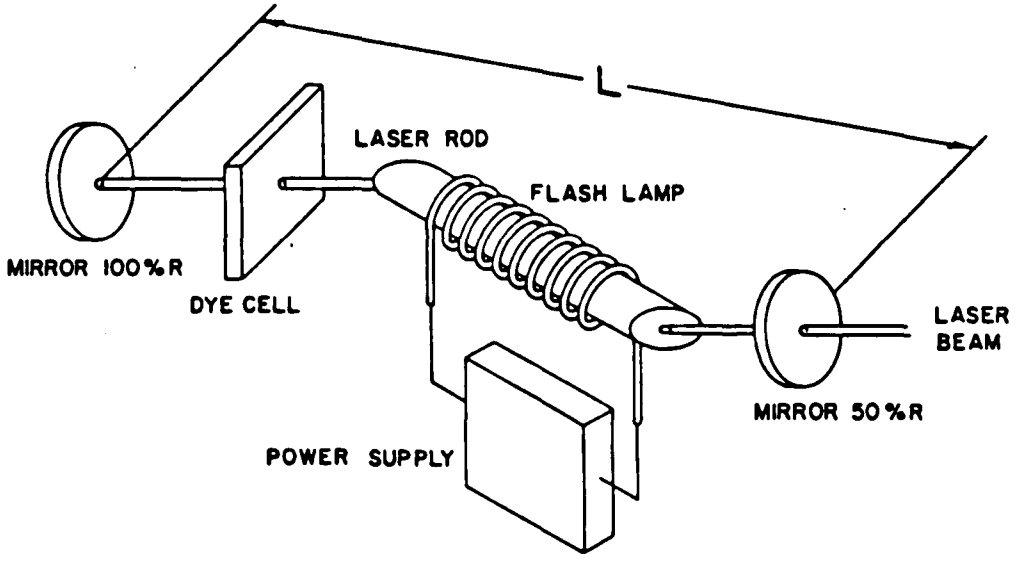

Fig. 2.2.3 Optical resonator cavity configuration

optically polished and cut at Brewster-Brewster angles to reduce multi-cavity resonances, and mounted in a Korad K-1 laser head. Inside the laser head, there is a 5-inch Xenon flash lamp surrounded by the liquid cooled enclosure. The laser head was temperature regulated at $22^{o}C \pm 1/2^{o}C$ with 50-50 ethylene glycol-water mixture by a Neslab HX-50 cooler. The flow rate of the cooling fluid is 7 gal/min and the pressure to have such a flow rate is about 7 psi. The distilled and deionized water was added in the cooling fluid maintaining a low ionic concentration to prevent the shorting of the electrodes in the laser head. The flash lamp is fired by discharging a 400 μf capacitor with a voltage of 2.5 KV supplied by the 5 KV Korad K-1 power supply. The pumping energy is about 1250 joules and the firing rate is about once per minute.

The rear mirror of the stable optical resonator cavity is wedged ($1/2^{o}$) and curved at 5 m with 100% reflection at 1.054 μm. The output mirror is a wedged ($1/2^{o}$) flat mirror with a 50% reflection at 1.054 μm. Both front and output dielectric coated mirrors were purchased from the Laser Energy Company and mounted in lasing mounts with micrometer position adjustment in two dimensions.

2.2.2 Mode-Locked Laser Train

The laser output from the optical resonator usually consists of multimodes without good correlation. In order to have a high power output with all the modes coupled togeth-

er[2-4], a passive mode locked design using the saturable dye absorber for Q-switch and mode-locking is Kodak dye A 9860 (Eastman Co.) dissolved in 1,2-dichloroetbane (Eastman Co.) to a transmission from 65 to 70% at 1.054 μm. The dye solution has a recovery time $\sim$ 10 ps which is faster than the laser cavity round trip time (=2L/c=7.2 ns). The transmission characteristic of this dye is nonlinear and qualitatively shown in fig. 2.2.4. In other words, the saturable absorber dye has the following characteristics: (a) there is a strong absorption at the laser wavelength 1.054μm, (b) the recovery time after each absorption of light by the dye is much smaller than the round trip time 2L/C, and (c) the absorption coefficient tends to be zero when the intensity of light exceeds a certain value I_s. The light generated inside the cavity by the fluorescence emission of lasing medium initially consists of a random noiselike signal with amplitude and phase fluctuation. With the properties of saturable absorber dye, the small light signal will be filtered (absorbed) by the dye because its small intensity. The short pulse of a given mode is built up out of these random fluorescence light signals by bleaching the saturable absorber dye and reflected by front and rear mirrors. Then, the one with the largest intensity in the initial fluorescence emission is selected out and amplified by reflecting back and forth through the lasing medium inside the cavity.

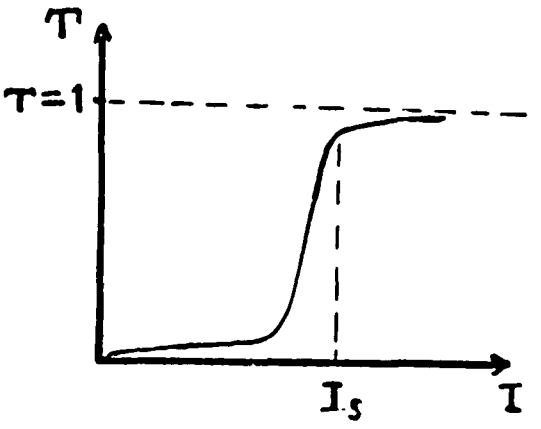

Fig. 2.2.4 Transmission characteristics of saturable absorber dye A9860

This is exactly the same meaning of high Q gain in the resonator (laser cavity) in the sense of engineering. As the high intensity light signal bounces back and forth in the cavity, the saturable absorber dye acts an optical shutter, opening and closing at a frequency equal to the difference in frequency of two adjacent modes (C/2L). Thus, the saturable absorber dye acts as a modulator. Each mode is modulated at the inter-mode frequency (C/2L) and extends to side bands of both the preceding and subsequent modes with frequency difference KC/2L. Through this action, the adjacent oscillating modes inside the cavity interfere and couple together in such a way that the phase relationship among the oscillating modes is definite. When the phase difference of two adjacent modes is fixed, the total electric field of laser beam is equal to the sum of electric field of every mode and shown in the following:

$$E(t) = \sum_{k=-q}^{q} E_0 e^{i[(\omega_0 + k\Delta\omega)t + k\alpha]} \qquad (2.2.1)$$

$$= E_0 e^{i\omega_0 t} \sum_{k=-q}^{q} e^{ik(\Delta\omega t + \alpha)}$$

$$= \frac{\sin\left[\frac{N}{2}(\Delta\omega t + \alpha)\right]}{\sin\left[\frac{1}{2}(\Delta\omega t + \alpha)\right]} E_0 e^{i\omega_0 t}$$

$$= A(t) e^{i\omega_0 t}$$

$$A(t) = \frac{\sin\left[\frac{N}{2}(\Delta\omega t + \alpha)\right]}{\sin\left[\frac{1}{2}(\Delta\omega t + \alpha)\right]} E_0$$

where $\psi_{k+1} - \psi_k = \alpha$

ψ_k = initial phase of kth mode

$\Delta w = 2\pi \left(\frac{c}{2L}\right)$

$w_k = w_o + k$

w_o = Oscillation frequency of center mode

N = total number of oscillation mode inside the cavity

The relationship of E(t) versus time is shown in figure 2.2.5(a) for N=5. The intensity output from the cavity I(t) is proportional to $A^2(t)$ and shown in figure 2.2.5(b). The peak power output is then expressed in equation (2.2.2)

$$P_p = N^2E_o^2 = N(NE_o^2) = NP_o \qquad (2.2.2)$$

where $P_o = NE_o^2$ = total power output of N modes without mode locking.

The saturable absorber dye indeed acts as a Q-switch and mode-locking dye for the laser pulse. This dye is also used to absorb the small intensity "wings" preferentially when an intense pulse bleaches the dye. After hundreds of passes through the saturable absorber dye and amplified by the laser medium in the cavity, the mode-locked pulse becomes more intense and sharpened (narrower pulse width). Upon reflecting on the output mirror, about 50% of the energy of pulse escapes through the mirror and forms one of the periodic picosecond mode locked high intense laser pulse train. Because the recovery time of the saturable absorber

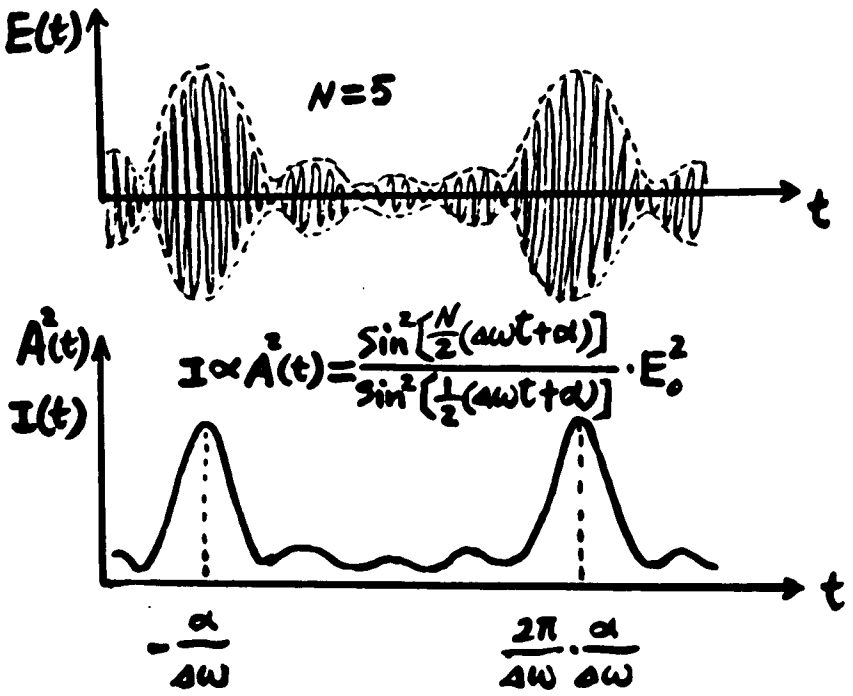

Fig. 2.2.5 (a) The time dependence of the electric field of the mode-locked laser pulse (N=5).

(b) The intensity of the mode-locked laser pulse.

is so short that it recovers very fast after it mode locked for one pulse in the train and be ready for mode-locking for the other successive pulses. The time separation between pulses in the train is about 7.2 ns (2 L/C). The developing process of passive mode-locking for the power output in time and frequency domain is shown in fig. 2.2.6(a) and (b).

The laser pulse train was detected by a Hadron 105C (Hadron Division of ITT) photodiode with S-1 photodiode with S-1 photodetector surface operated at 2.0 kv. The output of the photodiode for the pulse train was displayed on a Tektronix 519 (Beaverton, Oregon) oscilloscope with 1 GHZ bandwidth, and photographed by a high speed camera with manual control of shutter. The picture of the detected pulse train is shown in fig. 2.2.7.

The typical train consists of about 100 pulses and the energy of the train at 1.054 μm is 300 mJ measured by an energy meter.

In short, the mode-locked high intense pulse train was generated with a time separation, τ = 2 L/C, between two adjacent pulses. Each pulse width, $\Delta\tau = \frac{1}{\Delta\nu_g}$ is the reciprocal of frequency width of gain curve of the Nd:glass laser. The peak power of one of the mode-locked pulses is N times larger than the total power of N modes without mode-locking as shown in equation (2.2.2). The pulse width was measured by two photon fluorescence technique (TPF) and will be

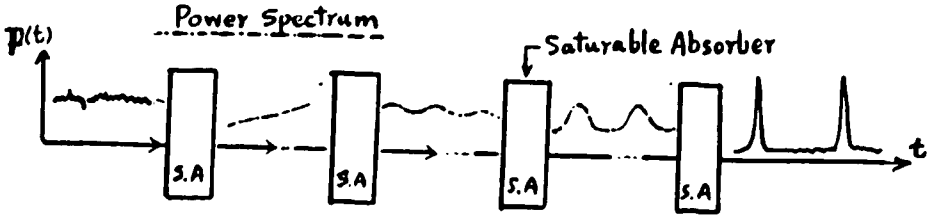

Fig. 2.2.6 (a) The time dependence of power output in the developing process of mode-locking

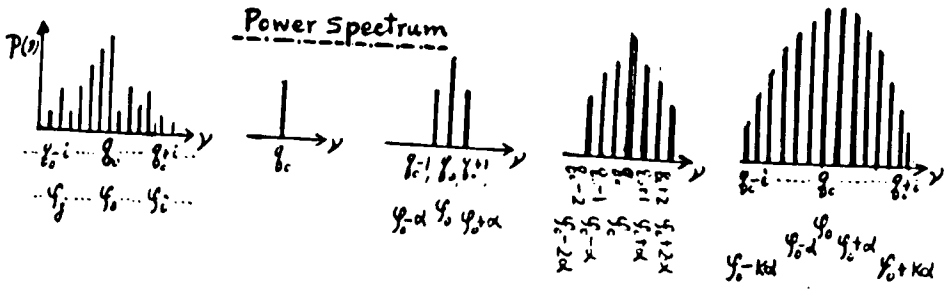

Fig. 2.2.6 (b) The frequency dependence of the power output in the developing process of mode-locking.

$$\tau = \frac{2\pi}{\Delta\omega} = \frac{2\pi}{2\pi\Delta\nu} = \frac{1}{\Delta\nu} = 2L/c$$

Fig. 2.2.7 The typical laser train
$\Delta\tau$ = pulse width
τ = repetition period of each pulse

described in detail in the next section. The pulse width was found to be 6 ps and the power of each pulse is estimated to be 10^9 watts.

It is remarked that the position of the dye cell in the laser cavity is important to get rid of creation of satellite pulses. Satellite pulses can arise when a weak pulse oscillates in the cavity but not strong enough to bleach the dye, passes through the dye cell at the same time when a strong bleaching pulse traveling in the opposite direction. The dye cell may be placed in contact with the rear mirror or is made wider to absorb completely the weaker pulse as it passes through the dye cell. A 1 cm long dye cell with Kodak A 9860 dissolved in 1,2-dichloroethane is suggested to be used to entirely absorb a weak 10 ps pulse since its optical path length is greater than 30 ps. The surface of the dye cell is oriented at the Brewster angle to cavity axis to assure a good polarization of laser pulses output and avoid reflection loss.

It is also remarked that the pumping voltage from the k-1 power supply is set about 10 v to 30 v above the threshold voltage for laser action. This was recommended for a single reproducible train without satellite pulses and multiple trains. The fluctuation of amplitude from shot to shot is about 10%. When the pumping voltage is too high, the distinguishability of two pulse train by the mode-locking dye is not good enough for the double trains to be

build up in the cavity. When the pumping voltage is too close to the threshold voltage, the pulse train occasionally fails to be built up.

With these techniques and criteria, the pulse train with longitudinal mode-locking and lowest transverse mode (uniform burn pattern of photo film without hot spot by pulse train) was generated by Nd:phosphate glass laser system.

2.3 Single Pulse Selection and Two Photon Fluorescence

In this section, the principle and technique of single pulse selection and measurement of pulse duration (width) by two photon fluorescence will be discussed.

A schematic diagram of the experimental apparatus is shown in Fig. 2.3.1. The single pulse can be selected from the train by a pair of cross polarizers sandwiched with a Pockell cell (Lasermetrics Co., Teaneck, N.J.) in between and connected to a spark gap. The spark gap is filled with Nitrogen gas at a pressure of 80 psi and connected to the high voltage power supply (16 kv) through a 10 MΩ resistor by a double sheathed cable (3 ft), which forms the transmission lines from the electrode of the spark gap. The output of the Pockells cell was dumped into a 50 Ω resistor through a 15 ft long cable to eliminate the high voltage pulse reflection from returning to the Pockell cell. A 4 cm focal length cylindrical lens was used to focus the laser pulses into the spark gap. The 16 kv, 5 ns voltage pulse

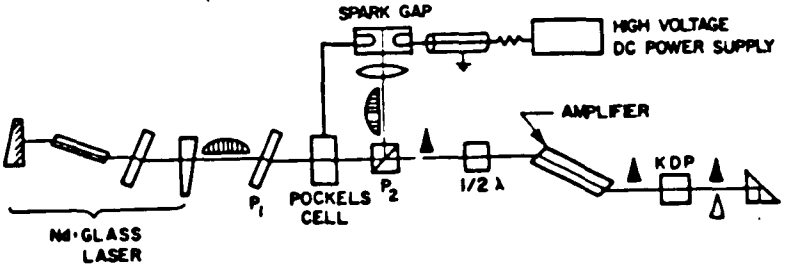

Fig. 2.3.1 Nd:glass laser with second harmonic generation and amplifier

can be performed by the 10 MΩ resistor and 3 ft, 50 Ω double sheathed cable. The first polarizer is polarized along the direction of polarization of the output laser train at 1.054 μm from the cavity. The second polarizer is a dielectric type prism. When the first few pulses pass through the first polarizer and Pockells cell and is reflected by the second polarizing prism and focused into the spark gap, the Nitrogen gas in the spark gap is ionized by the first few laser pulses and the avalanche breakdown across the electrode appears to form a conductive path for the preformed high voltage pulse (16 kv). Because of the impedance matching between two ports of the cable, a high voltage pulse 8 kv, 5 ns is then applied to the Pockells cell. The axes of the index ellipsoid of refraction of the crystal (KDP) inside the Pockells cell are rotated because of the nonlinear electro-optical effect. The polarization of the next subsequent incoming laser pulse just after the first few pulses is then rotated to match the polarization direction of the second prism polarizer and escape through it. Since the high voltage (8 kv) acting on the Pockells cell lasts for about 5 ns, there is not a long enough time period to have another single pulse being transmitted. Actually, the time separation between two adjacent single pulses is about 7 ns, which is longer than the time period for the Pockells cell to be functioning. Therefore, we have only one single pulse selected from the pulse train. The

rest of the pulse train are all rejected by the second prism polarizer and detected by a Hadron 105-C, S-1 photodiode. The rejected pulse train in the output from the photodiode was displayed on a Tektronix 519 oscilloscope with a sweep speed of 5 ns/cm. The photo-picture for the rejected train is shown in Fig. 2.3.2.

The selection of single pulse is better than 80%. Using the selected single pulse, a two photon fluorescence (TPF) technique[5-6] was applied to measure the pulse duration. The schematic diagram of TPF was shown in Fig. 2.3.3. The TPF technique requires a superposition of the pulse propagating in one direction and its own reflection. TPF is a second order nonlinear optical effect.

A beam splitter with 50% transmission is used to separate the selected single pulse into two equal portions with the same optical path from the beam splitter to the center of the rectangular cell containing rhodamine 6G in ethanol at 10^{-5} M. In front of the glass cell, a camera with a magnification of unity was ready to take the picture of two photon fluorescence light. Ideally, the signal to noise ratio of the two photon fluorescence intensity is 3:1 for a pulse with Gaussian form in time dependence. Our measurements gave 2:1 for multi-transverse modes. From the width of the yellow bright spot (shown in Fig. 2.3.4) of the fluorescence of rhodamine 6G by absorption of two photons of 1.054 μm, the pulse width, which is usually defined as the full width of half maximum power, is found to be 6 ps.

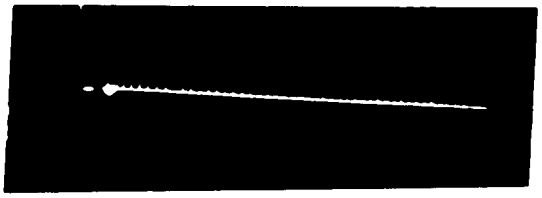

Fig. 2.3.2 (a) The picosecond laser pulse train with one pulse selected

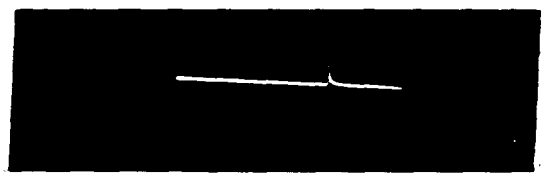

Fig. 2.3.2 (b) The selected laser pulse

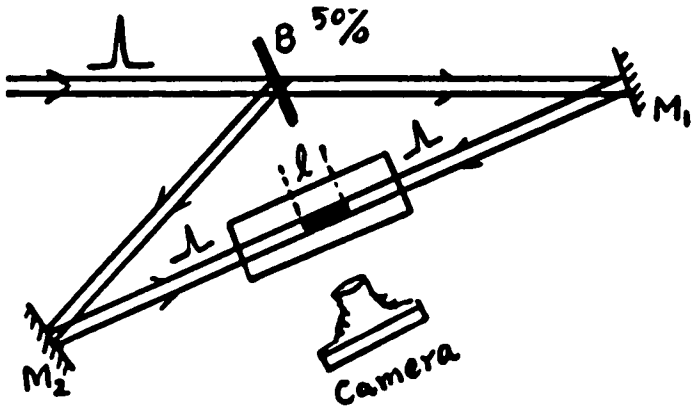

Fig. 2.3.3 Schematic diagram of the setup of two photon fluorescence measurement

Fig. 2.3.4 The photographic picture of two photon fluorescence.

$$\tau = \frac{\tau_c}{\sqrt{2}} = \frac{nd}{\sqrt{2}\,c} = \frac{1.359}{\sqrt{2}}\frac{d}{c} = 6 \pm 0.3\ \text{PS}$$

2.4 Second Harmonic Generation

In studying the excitation - fluorescence kinetics of dyes or semiconductors, energy difference between the ground and excited states (band) exceeds the photon energy of infrared 1.054 μm. Therefore, a generation of shorter wavelength with higher energy photon laser pulse is necessary. The pulses at 527 nm can be obtained by second harmonic generation[7-9] of 1.054 μm pulses by passing the 1.054 μm beam through a KDP (Potassium Dihydrogen Phosphate) crystal. When properly phase matched, a maximum of 10% power conversion from 1.054 μm to 527 nm is obtained. The pulse width of 527 nm is $\sqrt{2}$ shorter than that of 1.054 μm and becomes 4 ps. The third harmonic or fourth harmonic generation at 353 nm and 256 nm can be achieved by using an additional KDP crystal after the first one. The power conversion of 353 nm is about 1%.

The second harmonic generation is a nonlinear optical effect. It is a 3-wave mixing phenomenon to generate a photon at twice the fundamental frequency from two photons at the fundamental frequency. The ratio[10] of power conversion of second harmonic generation to the fundamental pulse was written as

$$\frac{P^{2w}}{P^{w}} = 2\left(\frac{\mu}{\epsilon}\right)^{\frac{3}{2}} \frac{w^2}{n^3} d_{ijk}^2 L^2 \frac{P^{w}}{A} \frac{\sin^2\left(\frac{\Delta KL}{2}\right)}{\left(\frac{\Delta KL}{2}\right)^2} \qquad (2.4.1)$$

where w = fundamental frequency

$2w$ = second harmonic frequency

A = effective area of incident light beam at fundamental frequency

μ = permeability of free space

ϵ = dielectric constant of free space

n = index of refraction of KDP crystal

L = optical path

$\Delta k = k_{2w}^{j} - k_{w}^{i} - k_{w}^{k}$

d_{ijk} = nonlinear susceptability tensor and

k_{w}^{k} = propagating vector in k direction for the light at fundamental frequency

k_{2w}^{j} = propagating vector in j direction for the light at second harmonic generation

$$\vec{k}_{w}^{i} = \frac{n^{(w)} c}{w} \hat{i}$$

If the lights at the fundamental and second harmonic frequency are propagating in the same direction, then

$$\Delta k = n^{(2w)} \frac{(2w)}{c} - 2 n^{(w)} \left(\frac{w}{c}\right)$$

$$= \frac{2w}{c} \left[n^{(2w)} - n^{(w)} \right] \qquad (2.4.2)$$

When $k = o$, the maximum power conversion is obtained by equation (2.4.1). In general, the index of refraction n increases as frequency increases. For a negative uniaxial crystal like KDP, the index of refraction n_e for extra-

ordinary light is smaller than that (n_o) of ordinary light at a given frequency. So, it is possible to have an index of refraction n_e at second harmonic frequency equal to n_o at fundamental frequency, to obtain a phase matching condition for maximum power conversion. In reality, the relation between n_e, n_o and angle between the propagation direction and optical axis θ is expressed as

$$\frac{1}{n_e^2(\theta)} = \frac{\cos^2\theta}{n_o^2} + \frac{\sin^2\theta}{n_e^2} \qquad (2.4.3)$$

It is necessary to find an angle θ^* so that, $n_e^{(2w)}(\theta^*) = n_o^{(w)}$ to satisfy the phase matching condition. A technical method[11] to determine the θ^* was shown in Fig. 2.4.1.

At the phase matching angle θ^*, the intensity of the light at second harmonic frequency reaches its maximum and the photographic picture shows a bright spot. While at an angle slightly different from the phase matching angle, an additional bright ring appears around the bright spot due to the forward scattered light, which is shown in Fig. 2.4.2.

The polarization of light at fundamental frequency (1.054 μm) is perpendicular to the plane determined by the propagating vector and the normal to incident plane. The polarization of second harmonic light is perpendicular to that of fundamental light.

Similar TPF technique can be used to measure the pulse

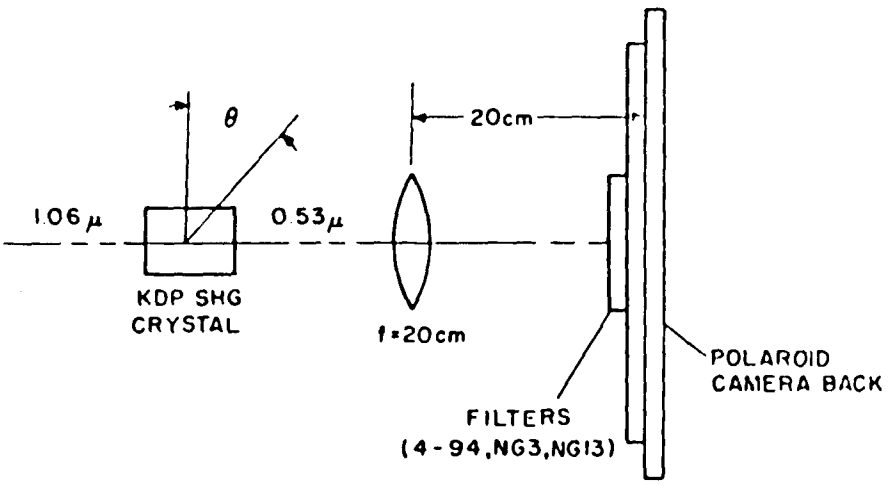

Fig. 2.4.1 Schematic diagram of the technical method to determine the phase matching angle θ^* in the second harmonic generation

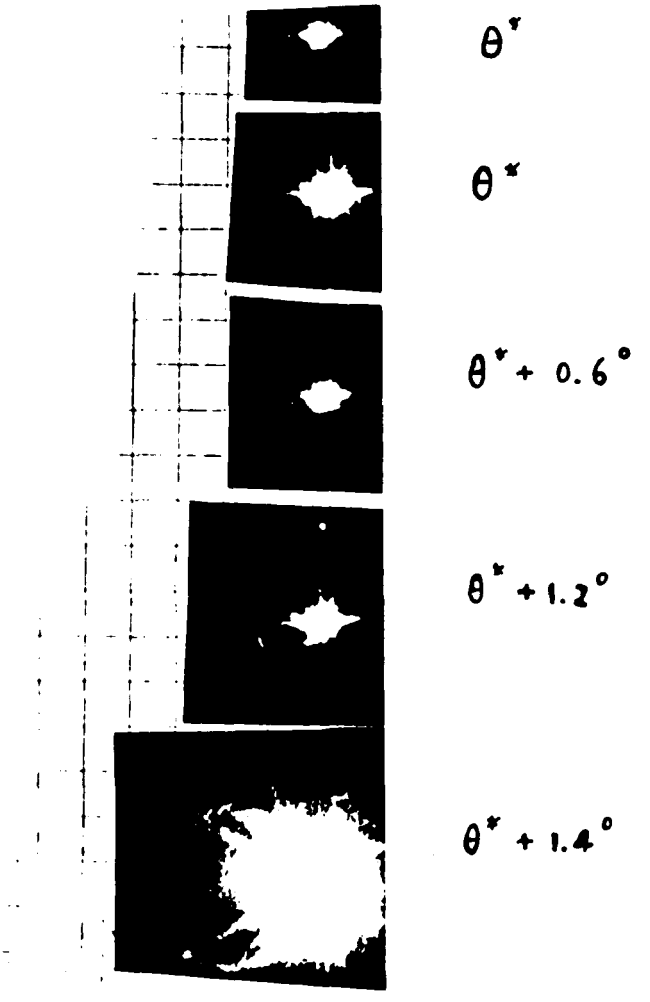

Fig. 2.4.2 Photographic picture of the phase matching angle and its deviations

duration of laser pulse at second harmonic frequency. The dye solution is a super saturable solution of 7 diethylamino 4-methyl coumarin dissolved in ethanol.

2.5 Amplifier

In the previous sections, the mode-locked picosecond single pulse at fundamental and second harmonic frequency were discussed. In order to have higher power laser pulse, an amplifier is added after the oscillator. The amplifier rod was 10 inches long by a diameter of 3/4 inch, cut with 6^{o}-6^{o} wedges and mounted in a Korad K-2 laser head with an 8 inch pumping length. This laser rod was still temperature regulated at $22^{o}C \pm 1/2^{o}$ C with the same cooling system as the oscillator. In order to increase the extinction ratio, a Kodak A9860 dye with 4 percent transmission at 1.054 μm was placed in the optical path before the amplifier to improve the extinction ratio from 400:1 to 1000:1. The energy measurement referring directly to the gain of the amplifier was obtained by either using a Hadron thermopile and a microvolt meter or a digitized energy meter. The noise from the flashlamp and the laser pulse train leakage through the cross polarizers was measured by blocking the spark gap. Excluding this noise, the energy of the selected pulse at 1.054 μm was 3.5 mj. The output energy from a single pass through the amplifier was 100 mj at a pumping energy of 8.1 kj (9.0 kv). The gain was measured as a function of flashlamp. The small signal gain coefficient

was calculated with the parameters of input energy and effective pumping length. The results are tabulated in Table I. The amplifier having a Q-88 phosphate glass rod has a higher amplification gain over the silicate rod by at least a factor of 2. However, we found that the output face of the phosphate amplifier rod is susceptible to damage at this high pulse energy. Extra care is necessary to keep the surface clean when performing experiments requiring intense picosecond pulses with an energy density above 30 mJ/cm^2.

2.6 Streak Camera System

2.6.1 Composition of Streak Camera

The new detection system using the streak camera is successful in order to obtain a direct measurement of the time resolved profile for single shot of excitation laser pulse and extend the time range to 10 ns.

The streak camera was introduced to measure the picosecond phenomena in the early 1970's by Bradley et al. and Shelev et al.[12-13] A schematic diagram of the streak tube operation is shown in Fig. 2.6.1. The photoelectrons generated by light incident on the photocathode are accelerated by an accelerating mesh and deflected by an applied voltage ramp in time in the streak tube. Since the sweeping voltage ramp decreases its voltage linearly in time, the photoelectron being emitted at an earlier time will be deflected a longer distance vertically. This is the basic principle of the conversion of the time dependent to a space dependent profile.

GAIN AND GAIN COEFFICIENT FOR AN INPUT ENERGY E_i = 3.5 mJ AND PUMPING LENGTH 20.32 cm

Pumping flashlamp energy	Measured energy gain G	Calculated gain coeff. α (cm⁻¹)
5.6 kJ	10 ± 1	0.113
6.9 kJ	16 ± 2	0.137
8.4 kJ	24 ± 2	0.159
9.1 kJ	33 ± 2	0.172

TABLE I: Gain and Gain Coefficient of Amplifier

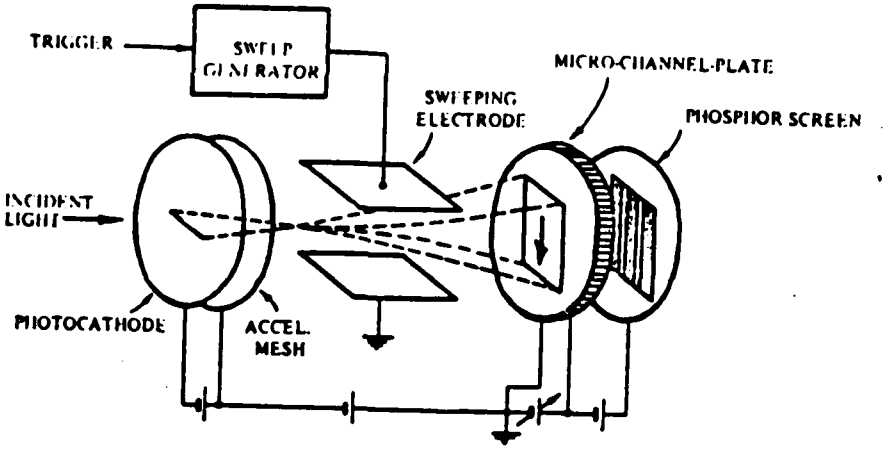

Fig. 2.6.1 Schematic diagram of streak tube operation[15]

These photoelectrons then strike a microchannel plate which produces electron multiplication through the secondary emission. The secondary electrons released at a different time domain corresponding to the incident light signal impinge upon a phosphor screen to form the streak image in different channels. The intensity distribution of the space dependent profile among all the channels are in proportion to that of the time dependent profile of the original light signal and thus forms a time resolved profile correspondingly. The streak image on the phosphor screen can be recorded by a polaroid film or by an electronic readout video or photodiode array device connected to a data storage and analysis system.

The streak camera used in these research programs was the Hamamatsu C979 model[15] (Hamamatsu Corporation, Middlesex, N.J.). It consists of a temporal disperser (streak tube), silicon-intensified target (SIT) camera, and a temporal analyzer. The temporal disperser mentioned above was used to convert the time dependent signal to space dependent signal. The silicon-intensified target camera was a vidicon camera with S-20 photocathode used to intensify the streak image. The temporal analyzer is a microprocessor-based video image analyzer with a TV screen used to display the digitized intensity distribution of the time-resolved signal versus channels. The streak camera was sensitive for a spectral region from 400 nm to 850 nm. There are four

streak rates 15 mm/ns, 7.5 mm/ns, 3 mm/ns, and 1.5 mm/ns for people to use.

2.6.2 Calibration of Streak Rate and Intensity

The streak camera must be calibrated for streak rate because it affects the linearity of the intensity. A 6 ps, 530 nm laser pulse and an etalon were used to calibrate the streak rate. The 6 ps, 530 nm calibration pulse was separated into a series of pulses with a known time interval by reflecting in between an etalon (Fig. 2.6.2(a)). The etalon was formed by an aluminum spacer with a known length d accurate to 10^{-3} inch. In each side of the etalon, there is a 92% reflection (8% transmission) dielectric mirror coated at 530 nm. The time separation between two adjacent pulses arising from the round trip reflection from the dielectric mirror on the etalon is 2d/c. The ratio of intensity of these two adjacent pulses is $(1-T)^2$.

If the intensity of the first calibration pulse is I_o, then the intensity of a series of pulses due to reflection by the etalon are

$$I_o(1-T)^2,\ I_o(1-T)^4,$$

Since $I_k = I_o(1-T)^{2k}$ and $I_{k+1}/I_k = (1-T)^2$,

An exponential decay expression can be approximated to the intensity of the k^{th} calibration pulse, i.e.

$$I_k = I_o \exp\left[\frac{t_k}{\Delta\tau} I_n (1-T)^2\right] \qquad (2.6.2)$$

where $t_k = k\,\Delta\tau = K\left(\frac{2d}{c}\right)$

The output of the calibration pulses were shown in Fig. 2.6.2(a) and Fig. 2.6.2(b).

The intensity calibration can be done by knowing the streak rate at a given channel, and is written in the following equation:

$$I(t) = i(x)\ \frac{\Delta x}{\Delta t}$$

Because of the non-uniform streak rate, the intensity for a given channel must be compensated for with a faster streak rate at that channel.

2.6.3 The Resolution and Total Response Time of The Streak Camera

The total time resolution Δt_r of the streak camera is given by the equation

$$\Delta t_r = \left[\Delta t_1^2 + \Delta t_2^2 + \Delta t_3^2 \right]^{\frac{1}{2}} \qquad (2.6.3)$$

The Δt_1 is due to the time spread occurring between the photocathode and mesh electrode Δt_{11}, and the mesh and microchannel plate Δt_{12}. The Δt_2 is caused by the spatial spread of the slit width and Δt_3 is caused by the deflection electric field (ramp voltage) on the emitted photoelectron from the photocathode.

The Δt_{11} is given by

$$\Delta t_{11} = 2.34 \times 10^{-6} \sqrt{\frac{\Delta \varepsilon}{E}}$$

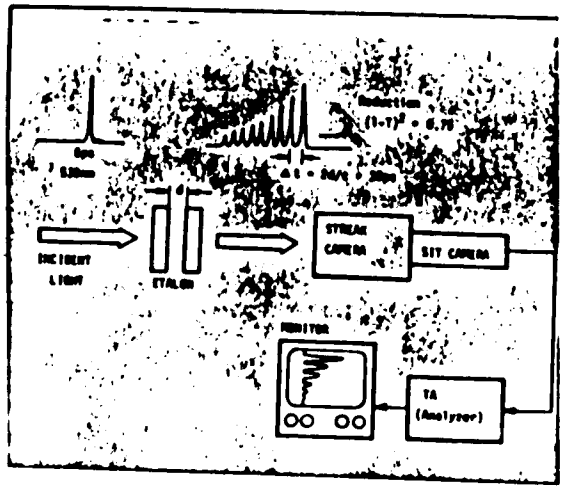

Fig. 2.6.2 (a) Schematic diagram of calibration technique of a streak camera system.[15]

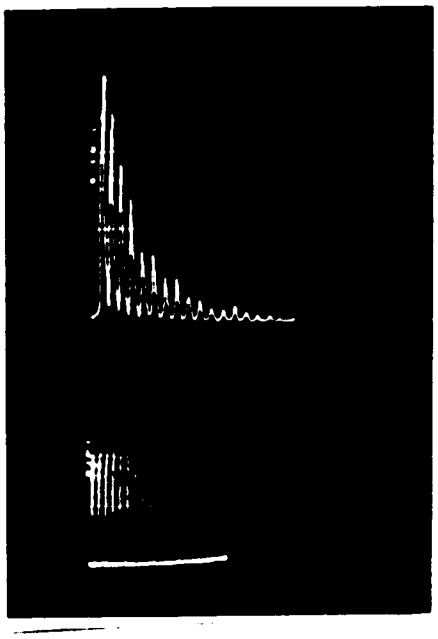

Fig. 2.6.2 (b) Graphic representation of the intensity profile for a 6 ps laser pulse passing through a 30 ps etalon[15].

(From N. H. Schiller et al's paper)

where $\Delta \mathcal{E}$ = the full width of half maximum of the energy distribution of the generated photoelectron and E is the accelerating electric field near the photocathode. Typically, the value of Δt_1, Δt_2, and Δt_3 are in the order of 1 picosecond. The response time of the detection system is the convolution of the real laser pulse and the resolution of the streak camera. For an ideal gaussian pulse in time (Δt_p) and space, the response time is Δt_o and $\Delta t_o^2 = \Delta t_p^2 + \Delta t_r^2$. For the fastest sweep rate 15 mm/ns, the system response time is about 10 ps. In addition, for a stable operation of streak camera, the jittering of streak camera is not more than 15 channels.

2.6.4. Delay Unit of Streak Camera

The speed of light is always faster than the response of the electronic components. In order to match the time for triggering the streak camera and excitation of sample by a single laser pulse, two delay units are needed. One is the electronic delay box for delaying the triggering signal from the pin diode, the other is an optical delay device called a white cell. The white cell consists of two curved mirrors with a radius of curvature of 2 m, separated by 1 m, and coated for 99% reflection at 530 nm. One part of the white cell is composed of two semi-circular curved mirrors with a dimension of 2 inches, the other part is a curved mirror with a dimension of 4 inches and two notches cut on the top for light input and output. After the excitation 530 nm

pulse bouncing back and forth inside the White cell, a total delay of (2N-1) optical paths is generated. N is the number of bright spots on the second curved mirror of the White cell. By adjusting the proper delay time of the electronic delay unit for the triggering the pin diode, a clear picture of time-resolved signal is shown on the TV screen of the temporal analyzer. These two delay units eventually play the same role as the delay prisms for the gate-opening and excitation pulse in the optical Kerr gate technique. The starting point (t=o) of the detected signal can be found by using a marker prepulse prior to the fluorescence signal. A typical diagram for fluorescence kinetics setup is shown in Fig. 2.6.3. A wedged beam splitter is used to isolate a portion of excitation pulse as a marker prepulse. The absolute zero time point of fluorescence was found by measuring the time separation between the prepulse and the scattered excitation light from the surface of the sample.

2.7 Data Storage and Analysis System

A DEC Minc 11 minicomputer was used to store the digitized data from the temporal analyzer. A program written in BASIC version fetched the data by questioning the necessary information step by step. The data were stored in the disk and a built-in graphing subroutine was used to get the hard copy of the time-resolved fluorescence profile.

A standard interfacing hardware RS 232 was connected to the PDP 10 and Minc 11 computer for data transferring. The

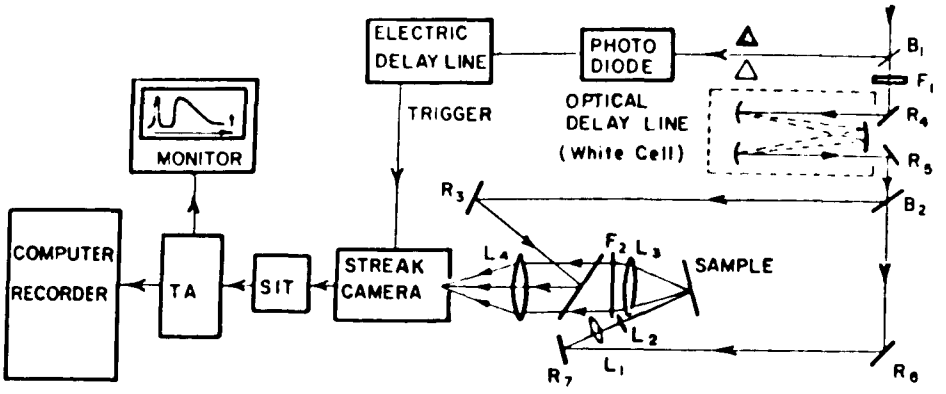

Fig. 2.6.3 Schematic diagram of the fluorescence kinetics study using streak camera.

programs in Fortran version were used to construct the data files and correct the streak rate and intensity. The complicated programs written in RATFOR and FORTRAN version were used for the data manipulation. The scientific subroutine for integral from Bell Laboratories was included in the theoretical calculation. The theoretical curve fitting to the experimental results confirms a reasonable and consistent model to explain the long range energy transfer kinetics between the donor and acceptor molecules. The significant parameters were deduced and generalization of the model to include the diffusion effect was made. All the useful data were stored in the tape to extend the capability of data storage and handling.

In the treatment of curve fitting, the excitation pulse was first deleted from the whole experimental fluorescence spectroscopy (intensity versus channel). The starting channel of the fluorescence spectroscopy was chosen such that a tendency of a monotonically increasing function of intensity versus channel exists in the region from the starting point to the peak of fluorescence intensity. Then, a program was used to correct the streak rate and intensity for the corresponding channels from the starting point to the end of the fluorescence intensity, and convert it to a time-resolved fluorescence spectroscopy. Therefore, the theoretical calculation of the time-resolved fluorescence spectroscopy can easily be compared and fitted to the experimental measurements.

References

1. P. Y. Lu, P. P. Ho, and R. R. Alfano, IEEE., J. of Quan. Electron. QE-15, 406 (1979)
2. A. J. DeMaria, D. A. Stetser, W. H. Glenn, Jr., Science 156, 1559 (1967)
3. A. J. DeMaria, W. H. Glenn, Jr., M. J. Brienza, and M. E. Mack, Proceed. of IEEE., 57, 2 (1969)
4. P. W. Smith, M. A. Duguay, and E. P. Ippen, Process in Quan. Electron. 3, 107 (1975)
5. J. R. Klauder, M. A. Duguay, J. A. Giordmaine, and S. L. Shapiro, Applied Phys. Lett. 13, 174 (1968)
6. D. J. Bradley and Geoffrey H. C. New, Proceed. of IEEE., 62, 313 (1974)
7. P. A. Franker and J. F. Ward, Rev. of Modern Phys., 35, 23 (1963)
8. B. Green and R. R. Alfano, Opt. Comm., 20, 305 (1977)
9. B. Green, J. C. Liu, R. R. Alfano, and D. Anafi, Opt. Comm. 22, 119 (1977)
10. A. Yariv, Quantum Electronics, Second Edition (Chap. 16, John Wiley, N.Y. 1975)
11. R. R. Alfano, Private Report in GTE., "Interaction of Picosecond Laser Pulses with Matter" (GTE Inc. Bayside, N.Y. 1972)
12. D. J. Bradley, J. F. Higgins, and M. H. Key, Appl. Phys. Lett. 16, 53 (1971)
13. D. J. Bradley, B. Liddy, and W. E. Sleat, Opt. Comm. 2, 391 (1971).

14. M. Ya. Shelev, M. C. Richardson, and A. J. Alcock, Appl. Phys. Lett. 18, 354 (1971)

15. N. H. Schiller, Y. Tsuchiya, E. Inuzuka, Y. Suzuki, K. Kamiya, H. Iida, and R. R. Alfano, Opt. Spec. 14, 55 (1980)

CHAPTER 3 THEORY AND COMPUTER SIMULATION OF ENERGY TRANSFER BETWEEN DONOR AND ACCEPTOR BINARY SYSTEM

In the first half of this chapter, the Forster mechanism for the long range energy transfer is reviewed. A theoretical model on the rate equations and initial conditions for donor and acceptor is presented in section 3.1. The detailed derivation of the solutions for the time-resolved fluorescence profile of donor and acceptor will be covered in sections 3.2 and 3.3. The theory of the fluorescence and absorption of a neat dye will be discussed in section 3.4.

The second half of this chapter will theoretically simulate the long range energy transfer process by the model proposed in section 3.1 for various parameters: critical transfer distance R_o, ratio of donor and acceptor absorption cross section β, donor fluorescence decay time τ_D, and acceptor fluorescence decay time τ_A. The results will be shown in sections 3.5 through 3.8. The experimental data fitted to this theoretical model are compared in chapter 4.

3.1 Forster Mechanism and Theoretical Model

Let us consider the long range energy transfer between a pair of donor and acceptor molecules. Qualitatively, the resonance energy transfer is similar to the behavior of two coupled oscillators. Just as the two oscillators should have the same energy for optimum coupling, the transition

in the donor ($D^* \rightarrow D$) and the transition in the acceptor ($A^* \rightarrow A$) should involve nearly the same energy as shown in Fig. 3.1. If there is a small difference in the electronic energy gaps for the two transitions, it can be adjusted by including vibrational levels of the donor and acceptor. This coupling interaction between the initial (Ψ_I) and the final (Ψ_F) states can be expressed as follows:

$$U = \langle \Psi_I | H | \Psi_F \rangle \qquad (3.1.1)$$

where the Ψ_I = the initial state at which the donor is excited and acceptor is in ground state; Ψ_f = the final state at which the donor is deexcited and the acceptor is excited; H = Interaction Hamiltonian.

The first term of expansion of interaction Hamiltonian H is a dipole-dipole interaction, the second term is a dipole-quadrupole interaction. The energy of interaction between the two dipoles is inversely proportional to the third power of separation distance between the dipoles (R^{-3}) and is directly proportional to the oscillator strengths to the extent of spectral overlap, and a dipole-dipole orientation factor. According to the Fermi-Golden rule, the energy transfer rate is proportional to the square of interaction energy, and thus is proportional to the sixth power of the separation distance between the two oscillators:

$$K_{D^* \to A} = \frac{2\pi}{\hbar} \sum_f \overline{\sum_i} |\langle \Psi_I | H | \Psi_F \rangle|^2 \qquad (3.1.2)$$

Forster[1-4] has derived a quantitative expression for the rate of energy transfer due to dipole-dipole interaction

$$K_{D^* \to A} = \frac{9000(\ln 10)\kappa^2 \Phi_D}{128\pi^5 n^4 N \tau_D R^6} \int_0^\infty F_D(\nu)\, \epsilon_A(\nu)\, \frac{d\nu}{\nu^4} \qquad (3.1.3)$$

where ν = wave number

$\epsilon_A(\nu)$ = molar absorptivity of the acceptor

$F_D(\nu)$ = spectral distribution of fluorescence of donor, normalized to unity on a wave number scale

N = Avogadro's number

R = distance between the donor and acceptor

Φ_D = quantum yield of fluorescence of the donor

n = index of refraction of solvent

τ_D = mean lifetime of the excited state

κ = orientation factor

= $\cos\theta_{DA} - 3\cos\theta_D \cos\theta_A$

θ_{DA} = angle between the dipole vectors of D and A

θ_D, θ_A = angle between these vectors and the direction D A

For a random distribution of dipoles, $\kappa^2 = 2/3$. If we define a typical transfer distance R_0 to be the rate of energy transfer is equal to the sum of all other donor deactivation rates, this is

$$K_{D^* \to A} = \frac{1}{\tau_D} \quad at \quad R = R_0 \qquad (3.1.4)$$

$$R_o^6 = \frac{9000[\ln 10]\,\kappa^2 \Phi_D}{128\pi^5 n^4 N}\int_0^\infty F_D(\nu)\,\epsilon_A(\nu)\,\frac{d\nu}{\nu^4} \qquad (3.1.5)$$

The efficiency of resonance transfer η_R is expressed as

$$\eta_R = \frac{\frac{1}{\tau_D}\left(\frac{R_o}{R}\right)^6}{\frac{1}{\tau_D} + \frac{1}{\tau_D}\left(\frac{R_o}{R}\right)^6} = \frac{\left(\frac{R_o}{R}\right)^6}{1 + \left(\frac{R_o}{R}\right)^6} \qquad (3.1.6)$$

Dexter[5] extended this theory and included the exchange and higher multiple interaction in the study of energy of energy transfer. Yokota and Tanimoto[6] developed a model treating the diffusion of the excited molecule as a perturbation to the theory of long-range transfer. Later, Klein et al.[7] formulated the theory considering the diffusion effect and long-range energy transfer. Recently, Auerbach et al.[8] have considered a diffusion modulated donor-acceptor energy transfer in a disordered system and obtained the result that the fastest acceptor rise times occur in the limit of the slowest donor diffusion, and faster rise times also result from shortening of the range of the donor-acceptor transfer interaction. Furthermore, Allinger and Blumen[9] used statistics to investigate the direct energy transfer in the donor-acceptor system. Most of the theories and measurements emphasized the results of the donor in the energy-transfer process. There is lack of a concise theory which will fit the experimental results for the kinetics of both donor and acceptor.

In order to study the kinetics of both the donor and acceptor molecules to obtain a complete description of the energy-transfer mechanism operating in the binary components of dyes in solution, a theoretical model including the spatial distributions of the molecules and relaxation rates is derived.

The energy-level diagram for the donor and acceptor is shown in fig. 3.1. The rate equations describing the energy dynamics for photoexcited donor (D) and acceptor (A) molecules are as follows. The donors are photoexcited to a vibrational state denoted by S_1^* in the electronic manifold:

$$\dot{D}_{2n} + \rho_D D_{2n} = \sigma_D I_0 \delta(t) \qquad (3.1.7)$$

Likewise, some acceptors are photoexcited to vibrational states S_1^* of the electronic manifold.

$$\dot{A}_{2m} + \rho_A A_{2m} = \sigma_A I_0 \delta(t) \qquad (3.1.8)$$

The population of excited donor and acceptor molecules are described by the equations

$$\dot{D}_{1n} + (\gamma_D + \Gamma_D) D_{1n} = \rho_D D_{2n} - \sum_m^{N_A} \delta_{nm} D_{1n} \qquad (3.1.9)$$

$$\dot{A}_{1m} + (\gamma_A + \Gamma_A) A_{1m} = \rho_A A_{2m} + \sum_n^{N_D} \delta_{nm} D_{1n} \qquad (3.1.10)$$

respectively.

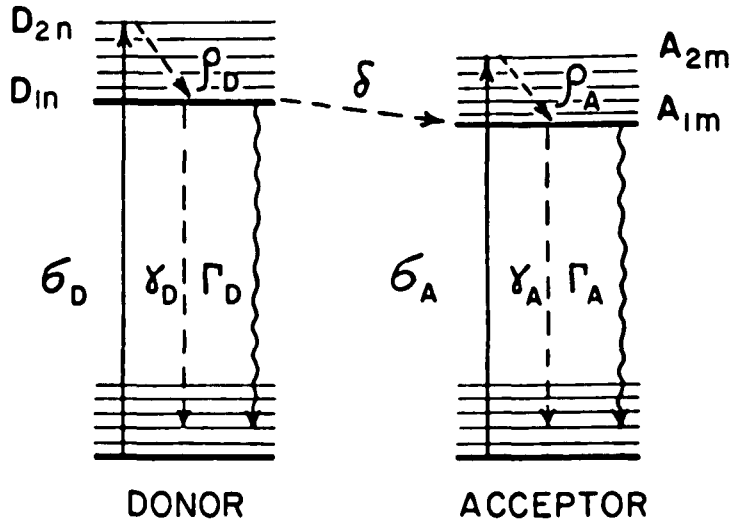

Fig. 3.1 The energy diagram for the theoretical model for the resonance energy transfer in the binary mixture solution. D_{1n} is the excited electronic state of the nth donor molecule. D_{2n} is the vibronic state associated with D_{1n}. Similarly, A is used for acceptor and δ is the transfer rate.

The following is a list of the symbols:

I_o (t) = ultrashort laser pulse (photons/cm^2 sec);

D_{jn} = probability for the nth donor molecule to be in the jth excited state;

A_{jn} = probability for the nth acceptor molecular to be in the jth excited state;

ρ_A, ρ_D = excited-state vibrational relaxation rate of acceptor and donor molecule;

σ_A, σ_D = absorption cross sections in the acceptor and donor molecules;

γ_D = nonradiative decay rate of donor molecule;

γ_A = nonradiative decay rate of acceptor molecule;

Γ_D = radiative decay rate of donor molecule;

Γ_A = radiative decay rate of acceptor molecule;

δ_{nm} = transfer rate from the nth donor to mth acceptor;

$$= \frac{1}{\tau_D} \left(\frac{R_o}{R}\right)^6$$

τ_D = fluorescence decay time of donor

The initial conditions at t=o for donor and acceptor probabilities are as follows:

$$D_{2n}(0^+) = \sigma_D I_o \qquad (3.1.11)$$

$$A_{2m}(0^+) = \sigma_A I_o \qquad (3.1.12)$$

$$D_{1n}(0^+) = 0 \qquad (3.1.13)$$

and

$$A_{1m}(0^+) = 0 \qquad (3.1.14)$$

3.2 Fluorescent Donors

Integrate the equations (3.1.7) and (3.1.8) immediately.

$$D_{2n} = \sigma_D I_0 e^{-\rho_D t} \tag{3.2.1}$$

$$A_{2m} = \sigma_A I_0 e^{-\rho_A t} \tag{3.2.2}$$

Substituting equations (3.2.1) and (3.2.2) in the equations (3.1.9) and (3.1.10), we have

$$\dot{D}_{1n} + (\gamma_D + \Gamma_D) D_{1n} = \rho_D \sigma_D I_0 e^{-\rho_D t} - \sum_m^{N_A} \delta_{nm} D_{1n} \tag{3.2.3}$$

$$\dot{A}_{1m} + (\gamma_A + \Gamma_A) A_{1m} = \rho_A \sigma_A I_0 e^{-\rho_A t} + \sum_n^{N_D} \delta_{nm} D_{1n} \tag{3.2.4}$$

For convenience, let us use the notations

$$E_D(t) = \rho_D \sigma_D I_0 e^{-\rho_D t} \tag{3.2.5}$$

$$E_A(t) = \rho_A \sigma_A I_0 e^{-\rho_A t} \tag{3.2.6}$$

$$g_A = \gamma_A + \Gamma_A \tag{3.2.7}$$

and

$$g_D = \gamma_D + \Gamma_D \tag{3.2.8}$$

The equations (3.2.3) and (3.2.4) are rewritten as:

$$\dot{D}_{in} + g_D D_{in} + \left(\sum_m^{N_A} \delta_{nm}\right) D_{in} = E_D(t) \qquad (3.2.9)$$

$$\dot{A}_{im} + g_A A_{im} - \left(\sum_n^{N_D} \delta_{nm}\right) D_{in} = E_A(t) \qquad (3.2.10)$$

The fluorescence of donor and acceptor are then expressed as:

$$d = \Gamma_D \sum_n D_{in} \qquad (3.2.11)$$

$$a = \Gamma_A \sum_m A_{im} \qquad (3.2.12)$$

From equation (3.2.9), we obtain

$$D_{in}(t) = \int_0^t dt' E_D(t') \exp\left[-\left(g_D + \sum_m^{N_A} \delta_{nm}(t-t')\right)\right] \qquad (3.2.13)$$

Averaging over the spatial distribution of molecules is essential to describe the observed donor kinetics. The equations for the fluorescence per unit volume for donor is denoted by D(t) in the following:

$$D(t) = \frac{1}{V}\left\langle \Gamma_D \sum_{n=1}^{N_D} D_{in} \right\rangle = \frac{\Gamma_D}{V} \prod_{k=1}^{N_A} \left(\frac{1}{V}\int dr_k 4\pi r_k^2\right) \sum_{n=1}^{N_D} D_{in} \qquad (3.2.14)$$

Substituting (3.2.5) and (3.2.13) into (3.2.14), we have

$$\mathcal{D}(t) = \frac{\Gamma_D}{V} \prod_{K=1}^{N_A} \left[\frac{1}{V} \int dr_K 4\pi r_K^2 \right] \sum_{n=1}^{N_D} \int_0^t dt' \sigma_D \rho_D I_0$$

$$\exp\left[-\rho_D t' - \left(g_D + \sum_{m=1}^{N_A} \delta_{nm}(t-t') \right) \right] \qquad (3.2.15)$$

$$= \frac{\Gamma_D}{V} \sum_{K=1}^{N_A} \frac{1}{V} \int dr_K 4\pi r_K^2 \exp\left[- \sum_{m=1}^{N_A} \delta_{nm}(t-t') \right]$$

$$\sum_{n=1}^{N_D} \int_0^t dt' \sigma_D \rho_D I_0 \exp\left[-\rho_D t' - g_D(t-t') \right] \qquad (3.2.16)$$

The first integral in equation (3.2.16) becomes:

$$\prod_{K=1}^{N_A} \frac{1}{V} \int_0^R 4\pi r_K^2 dr_K \exp\left[- \sum_{m=1}^{N_A} \delta_{nm} \tau \right]$$

$$= \left[\frac{1}{V} \int_0^R dr\, 4\pi r^2 \exp(-\delta\tau) \right]^{N_A}$$

$$= \left[\frac{1}{V} \int_0^R dr\, 4\pi r^2 (\exp(-\delta\tau) - 1 + 1) \right]^{N_A}$$

$$= \left[1 - \frac{1}{N} n_A \int_0^\infty 4\pi r^2 dr \left(1 - \exp\left(-\frac{\tau\Delta}{r^6} \right) \right) \right]^{N_A}$$

$$= \exp\left[-n_A \int_0^\infty 4\pi r^2 dr \left(1 - e^{-\frac{\tau\Delta}{r^6}} \right) \right] \qquad (3.2.17)$$

where

$$\Delta = \frac{R_0^6}{\tau_D} \quad , \quad \tau = t - t'$$

Now, the integral $\int_0^\infty 4\pi r^2 dr \left[1 - e^{-\frac{\tau\Delta}{r^6}} \right]$ in equation (3.2.17) can be calculated in the following.

Let $u = \frac{1}{r^3}$, then

$$\int_0^\infty 4\pi r^2 dr \left[1 - e^{-\frac{\tau\Delta}{r^6}} \right]$$

$$= \int_0^\infty \frac{4\pi}{3u^2} du \left[1 - e^{-\tau\Delta u^2} \right] \qquad (3.2.18)$$

Again, let $U = 1 - e^{-\tau\Delta u^2}$

$$V = -\frac{1}{u}$$

then equation (3.2.18) becomes

$$\frac{4\pi}{3}\left\{-\frac{1}{u}\left(1-e^{-\tau\Delta u^2}\right)\Big|_0^\infty+\int_0^\infty\frac{1}{u}2\tau\Delta\tau\, e^{-\tau\Delta u^2}du\right\}$$

$$=\frac{4\pi}{3}2\tau\Delta\int_0^\infty du\, e^{-\tau\Delta u^2}$$

$$=\frac{4\pi}{3}\sqrt{\pi\Delta\tau} \qquad (3.2.19)$$

Putting (3.2.19) in (3.2.17) and substituting in equation (3.2.16) we obtain

$$\mathcal{D}(t)=\Gamma_D n_D \rho_D \sigma_D I_0\int_0^t dt' e^{-\rho_D t'-g_D(t-t')-\frac{4\pi}{3}n_A\sqrt{\pi\Delta(t-t')}}$$

$$=\Gamma_D n_D \rho_D \sigma_D I_0\int_0^t d\tau\, e^{-\rho_D(t-\tau)-g_D\tau-\frac{4\pi}{3}n_A\sqrt{\pi\Delta\tau}} \qquad (3.2.20)$$

3.3 Fluorescent Acceptors

In this section, we will calculate the fluorescence of acceptor. Let $\sum_{m=1}^{N_A} A_{1m}=A_1$, and sum over the number of acceptor on the equation (3.2.10), we have

$$\dot{A}_1+g_A A_1=N_A E_A(t)+\sum_m^{N_A}\sum_n^{N_D}\delta_{nm}D_{1n} \qquad (3.3.1)$$

Taking derivative of equation (3.2.13) with respect to time t, we obtain

$$\dot{D}_{1n} = E_D(t) - \vartheta_D D_{1n} - \sum_{\nu}^{N_A} \delta_{n\nu} D_{1n} \qquad (3.3.2)$$

Sum over the number of donors on the equation (3.3.2), we get

$$\sum_{n}^{N_D} \dot{D}_{1n} = N_D E_D(t) - \vartheta_D \sum_{n}^{N_D} D_{1n} - \sum_{n}^{N_D} \sum_{\nu}^{N_A} \delta_{n\nu} D_{1n} \qquad (3.3.3)$$

Let $\sum_{n}^{N_D} D_{1n} = D_1$, equation (3.3.3) becomes

$$\dot{D}_1 = N_D E_D(t) - \vartheta_D D_1 - \dot{A}_1 - \vartheta_A A_1 + N_A E_A(t), \text{ and}$$

$$\dot{A}_1 + \vartheta_A A_1 = -\dot{D}_1 - \vartheta_D D_1 + N_D E_D(t) + N_A E_A(t) \qquad (3.3.4)$$

The spatial averaged fluorescence of acceptor per unit volume is:

$$\mathcal{A}(t) = \frac{\langle \Gamma_A \Sigma_n^{N_A} A_{1n} \rangle}{V} = \frac{\langle \Gamma_A A_1 \rangle}{V}$$

$$\dot{\mathcal{A}} + \vartheta_A \mathcal{A} = -\frac{\Gamma_A}{V}(\dot{D}_1 + \vartheta_D D_1) \qquad (3.3.6)$$

$$+ \Gamma_A [n_D E_D(t) + n_A E_A(t)]$$

$$\doteq -\frac{\Gamma_A}{\Gamma_D}(\dot{\mathcal{D}} + \vartheta_D \mathcal{D}) + \Gamma_A (n_D E_D + n_A E_A)$$

Take the derivative of (3.2.20) with respect to time, we have

$$\dot{\mathcal{D}} = -\rho_D \mathcal{D} + \Gamma_D n_D \rho_D \sigma_D I_0 e^{-\vartheta_D t} - \frac{4\pi}{3} n_A \sqrt{\pi \Delta t} \qquad (3.3.7)$$

Substituting equation (3.3.7) in equation (3.3.6), equation (3.3.6) is then expressed as

$$\dot{A} + g_A A = \Gamma_A (n_D E_D + n_A E_A) - \frac{\Gamma_A}{\Gamma_D} \{ (g_D - \rho_D) D(t) \} - \Gamma_A n_D \rho_D \sigma_D I_0 e^{-g_D t - \frac{4\pi}{3} n_A \sqrt{\pi \Delta t}} \quad (3.3.8)$$

The solution of A(t) can be found by integrating the equation (3.3.8). This is shown by equation (3.3.9):

$$A(t) = \int_0^t dt' e^{-g_A(t-t')} \Gamma_A (n_D \sigma_D \rho_D I_0 e^{-\rho_D t'} + n_A \sigma_A \rho_A I_0 e^{-\rho_A t'}) - \frac{\Gamma_A}{\Gamma_D} (g_D - \rho_D) \int_0^t dt' e^{-g_A(t-t')} D(t') - \Gamma_A n_D \rho_D \sigma_D I_0 \int_0^t dt' e^{-g_A(t-t') - g_D t' - \frac{4\pi}{3} n_A \sqrt{\pi \Delta t}} \quad (3.3.9)$$

Substituting D(t') from equation (3.2.20) into equation (3.3.9), we obtain the acceptor fluorescence per unit volume in the following equation:

$$A(t') = \Gamma_A \sigma_A I_0 \{ n_D \rho_D \beta \frac{(e^{-\rho_D t} - e^{-g_A t})}{g_A - \rho_D} + n_A \rho_A \frac{(e^{-\rho_A t} - e^{-g_A t})}{g_A - \rho_A} - (\frac{g_D - \rho_D}{g_A - \rho_D}) n_D \rho_D \beta e^{-\rho_D t} \int_0^t d\tau \exp[(\rho_D - g_D)\tau - \frac{4\pi}{3} n_A \sqrt{\pi \Delta t}] \quad (3.3.10)$$

$$+ (\frac{g_D - \rho_D}{g_A - \rho_D}) n_D \rho_D \beta e^{-g_A t} \int_0^t d\tau \exp[(g_A - g_D)\tau - \frac{4\pi}{3} n_A \sqrt{\pi \Delta \tau}] - n_D \rho_D \beta e^{-g_A t} \int_0^t d\tau \exp[(g_A - g_D)\tau - \frac{4\pi}{3} n_A \sqrt{\pi \Delta \tau}] \}$$

3.4 Fluorescence and Absorption of A Neat Dye

For a neat solution the fluorescence intensity profile versus time is described by the equation

$$F(t) = \frac{\rho_F}{\rho_F - \gamma_F} \left[e^{-\gamma_F t} - e^{-\rho_F t} \right] \qquad (3.4.1)$$

where ρ_F = vibrational relaxation rate

γ_F^{-1} = fluorescence decay time.

The absorption of light by a neat dye solution is determined by Beer's law, that is:

$$I_a = I_0 \left[1 - e^{-2.3 \epsilon c d} \right] \qquad (3.4.2)$$

where I_a = intensity of absorbed light

I_o = intensity of incident light

ϵ = molar absorptivity (molar extinction coefficient)

C = molar concentration

d = path length

The O.D. is defined as $\log_{10}\left(\frac{I_o}{I_t}\right)$

where I_t = intensity of the light transmitted through the sample.

For most systems, the O.D. is conveniently determined using Beer's law and given by O.D. = ϵ Cd.

If O.D. > 2, then all the incident light is absorbed, $I_a = I_o$, (100%). If O.D. $\leq$ 0.05, then there is only a very little of

light is absorbed (10%) and I_a is approximated by 2.3 ϵ CdI_o.

In the following sections, the computer simulation for out theoretical model is obtained on the time resolved fluorescence intensity of the donor and acceptor molecules for various parameters.

3.5 Ro Variation

The parameter R_o was varied from 20A to 100A for the calculation of the fluorescence of donor and acceptor molecules. These results are shown in figure 3.2(a) and 3.2(b). The other parameters such as P_D, P_A, g_D, g_A, and β in the equation (3.2.20) and (3.3.10) remain fixed. The values of the parameters are given in the figure caption of figure 3.2. In figure 3.2(a), for a given concentration of molecules (2.5×10^{-3}M), gives $\bar{R}^{DA} = 43.5\mathring{A}$, $\bar{R}^{DD} = \bar{R}^{AA} = 54\mathring{A}$, the peak intensity of donor fluorescence decreases as R_o increases indicating more energy transfer. In figure 3.2(b), the peak intensity of the acceptor increases and the risetime becomes slower as R_o increases. Physically, this means the energy transfer is more efficient if the separation distance R between the donor and acceptor molecules for a given concentration is less than R_o. If R_o increases continuously, the energy transfer becomes so efficient that the donor acts like a pumping laser pulse which provides the energy. The intensity of the fluorescence profile of the acceptor abruptly increases because of a much higher energy absorp-

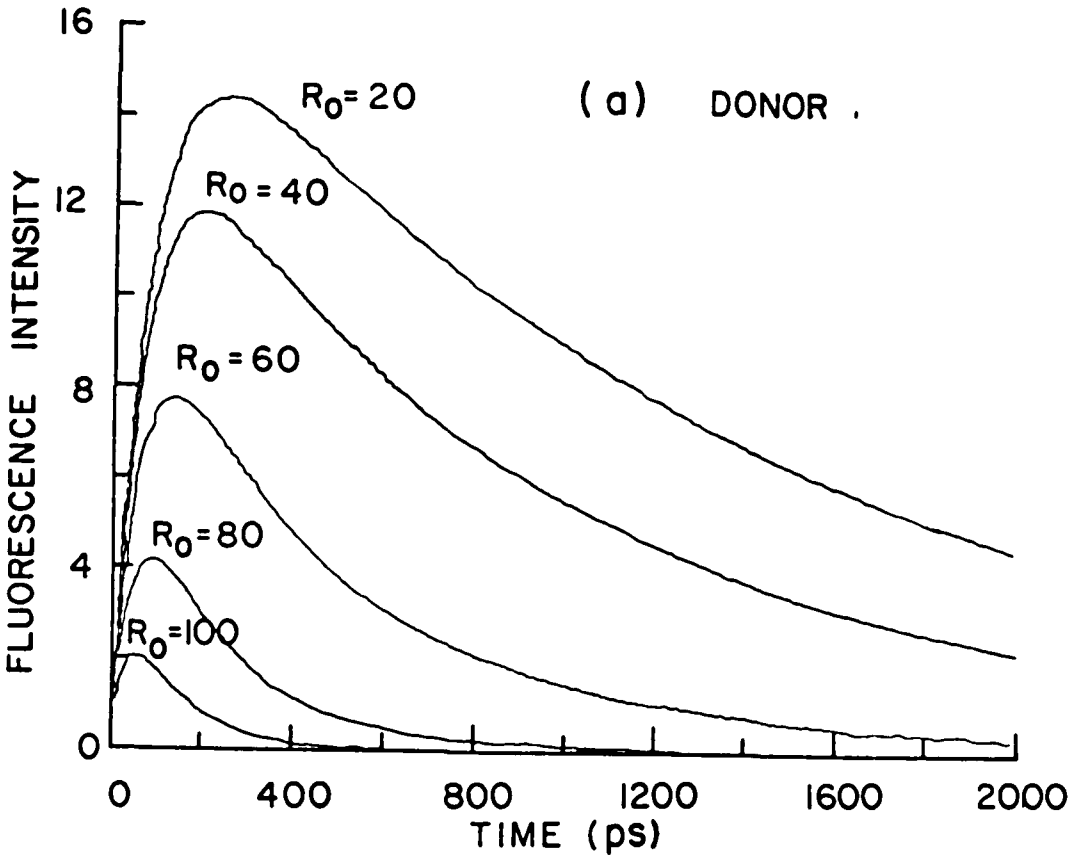

Fig. 3.2 The theoretical calculation of fluorescence profile versus time obtained by equation (3.2.20) and (3.3.10) for (a) donor and (b) acceptor for various R_o = 20Å, 40Å, 60Å, 80Å, and 100Å. The detection system risetime is assumed to be 80 ps considering the resolution of streak camera. The fluorescence decay time is assumed to be 1.5 ns and 0.75 ns for donor and acceptor, respectively. The ratio of absorption coefficient of donor to acceptor is 17.5. The concentration is 2.5×10^{-3} M

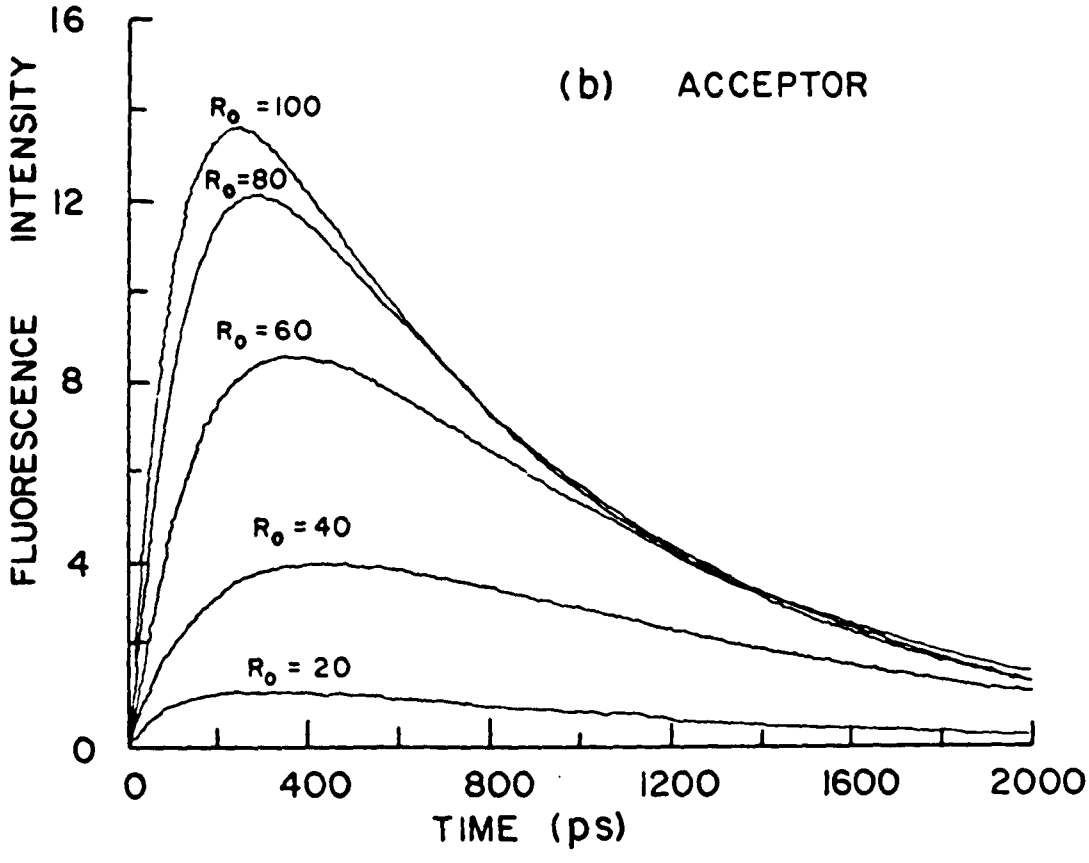
(b) ACCEPTOR
FLUORESCENCE INTENSITY
16
12
8
4
0
R_0 =100
R_0=80
R_0 = 60
R_0 = 40
R_0 = 20
0
400
800
1200
1600
2000
TIME (ps)

Fig. 3.2 (b)

tion ability of the donor, which provides almost all the energy it absorbed to the acceptor. In this case, the acceptor fluoresces in the same way as though it was pumped directly by a laser pulse in a neat solution (actually, it gained energy from the donor). So, the risetime of the acceptor looks very much like that in the neat solution and we observe the time displacement between the peak and the starting point of the fluorescence profile becomes smaller as R_o reaches 100 A.

3.6 Ratio of Donor and Acceptor Absorption Cross-Section β

The ratio β of the absorption cross-sections of the donor to that of the acceptor was varied from 10 to 30. The fluorescence of the donor and the acceptor for different values of β are shown in figure 3.3(a) and 3.3(b), respectively. The value of β defines the amount of energy of the incident laser pulse absorbed directly by the donor and acceptor. A large value of β indicates a smaller absorption by the acceptor. The acceptors are chosen such that the direct absorption ability of laser energy is much weaker than the donor. In our case, the fluorescence from the acceptors occurs from the optically excited donors via energy transfer. Thus, the fluorescence kinetics depends on the energy transfer from the donor to the acceptor for large values of β .

3.7 Effect of the Donor Fluorescence Decay Time; τ_D

By changing the value of the donor decay time, the

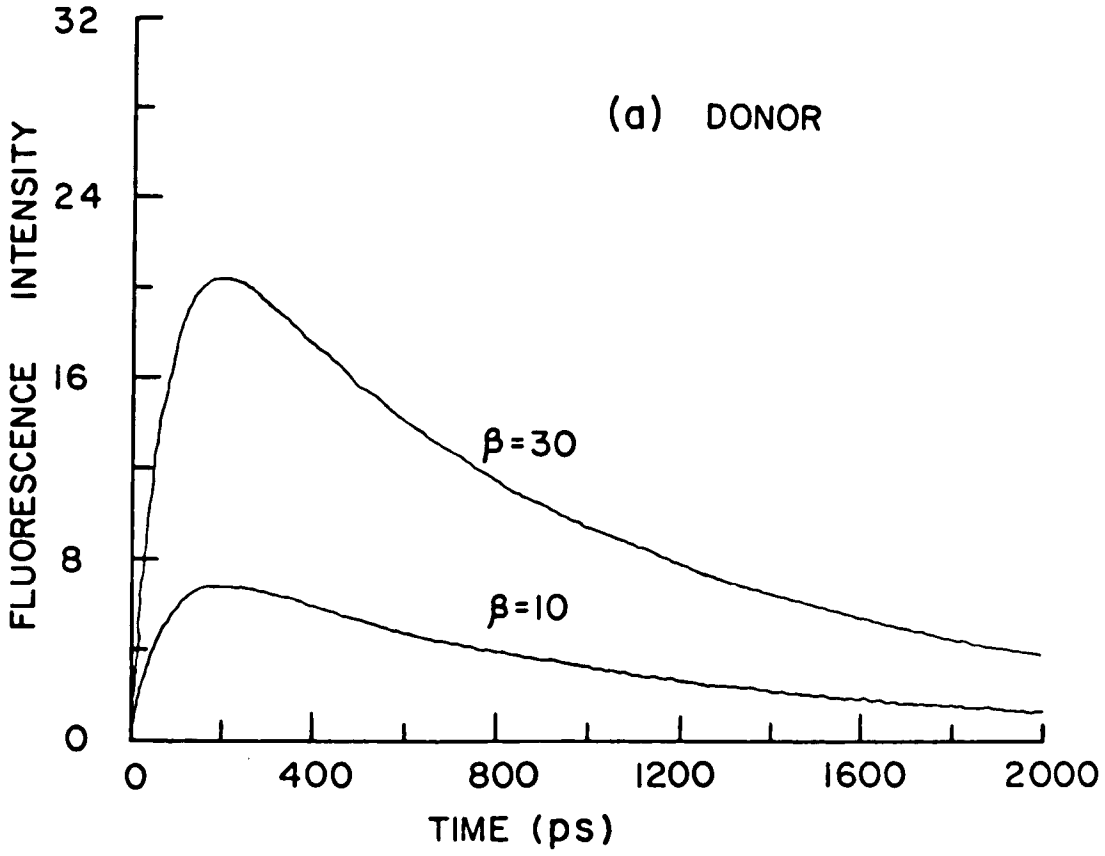

Fig. 3.3 (a) The theoretical calculation of fluorescence profile versus time obtained by eq. (3.2.20) and (3.3.10) for (a) donor and (b) acceptor for different ratios of absorption of donor and acceptor, β = 30 and 10. The detection risetime is 80 ps. The fluorescence decay time is assumed to be 1.5 and 0.75 ns for donor and acceptor, respectively. The concentration is 2.5×10^{-3} M and R_o = 40Å

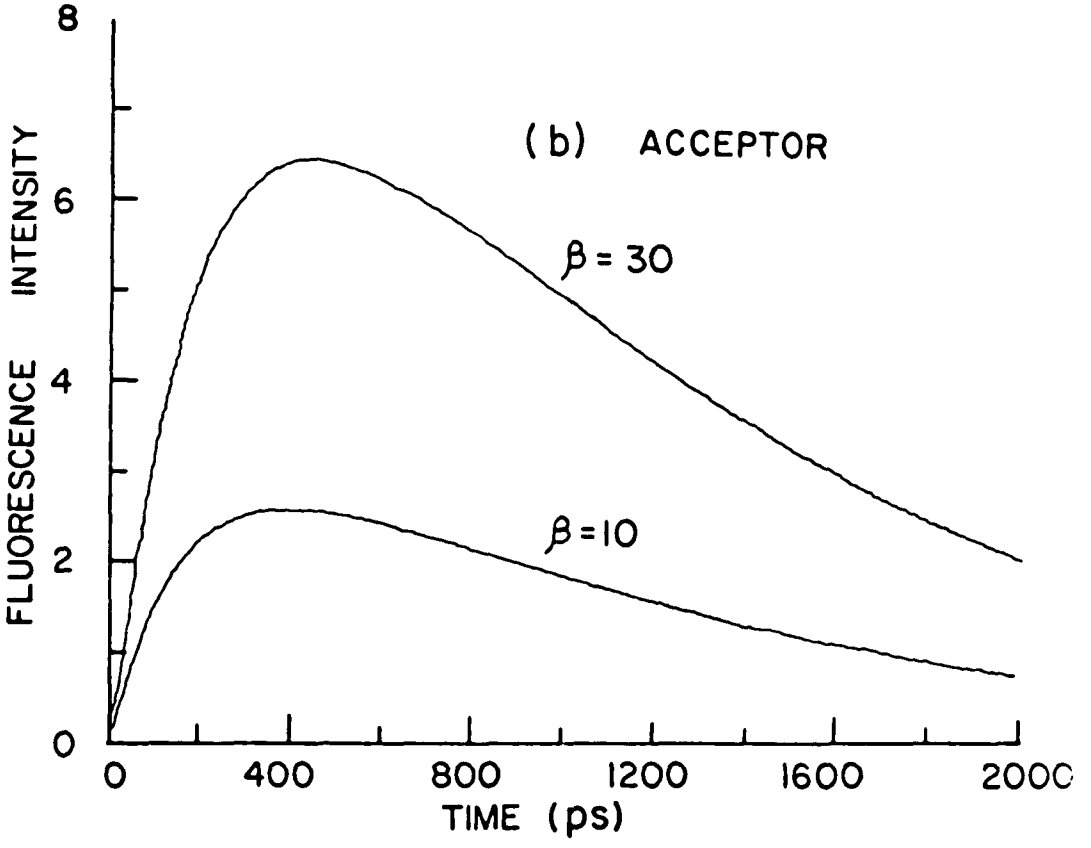
8
6
4
2
0
FLUORESCENCE INTENSITY
(b) ACCEPTOR
β = 30
β = 10
0
400
800
1200
1600
2000
TIME (ps)

Fig. 3.3 (b)

fluorescence kinetics profiles of the donor and acceptor are calculated in figures 3.4(a) and 3.4(b). The fluorescence decay time of acceptor τ_A for this calculation is fixed at 0.75 nsec. In the neat donor solution, the longer the fluorescence decay time, the larger the fluorescence quantum yield and more light is emitted. In the binary dye mixture, as the fluorescence decay time increases, the fluorescence intensity of the donor molecules increases. In this case, the resonant energy transfer through the dipole-dipole interaction is decreased because energy is spread out over a larger time interval (transfer rate $\sim 1/\tau_D$). Therefore, the fluorescence intensity of the acceptor decreases in the low energy transfer case when the fluorescence decay time of the donor molecule increases.

3.8 Effect of Acceptor Fluorescence Decay Time: τ_A

The calculated kinetic profiles of the acceptor molecule in the dye mixtures are shown in figure 3.5 for different fluorescence decay times of the acceptor molecule. The donor decay time is fixed at 1.5 nsec. These results show that the acceptor molecule excited by energy transfer from the donor fluoresces with complex behavior. The acceptor molecules are excited by resonant dipole-dipole interaction and then fluoresce. So, the longer the fluorescence decay time, the slower the decay of the acceptor in the mixture solution. As expected, there is little effect on the fluorescence kinetics of the donor in the mixture for different fluorescence decay times of the acceptor.

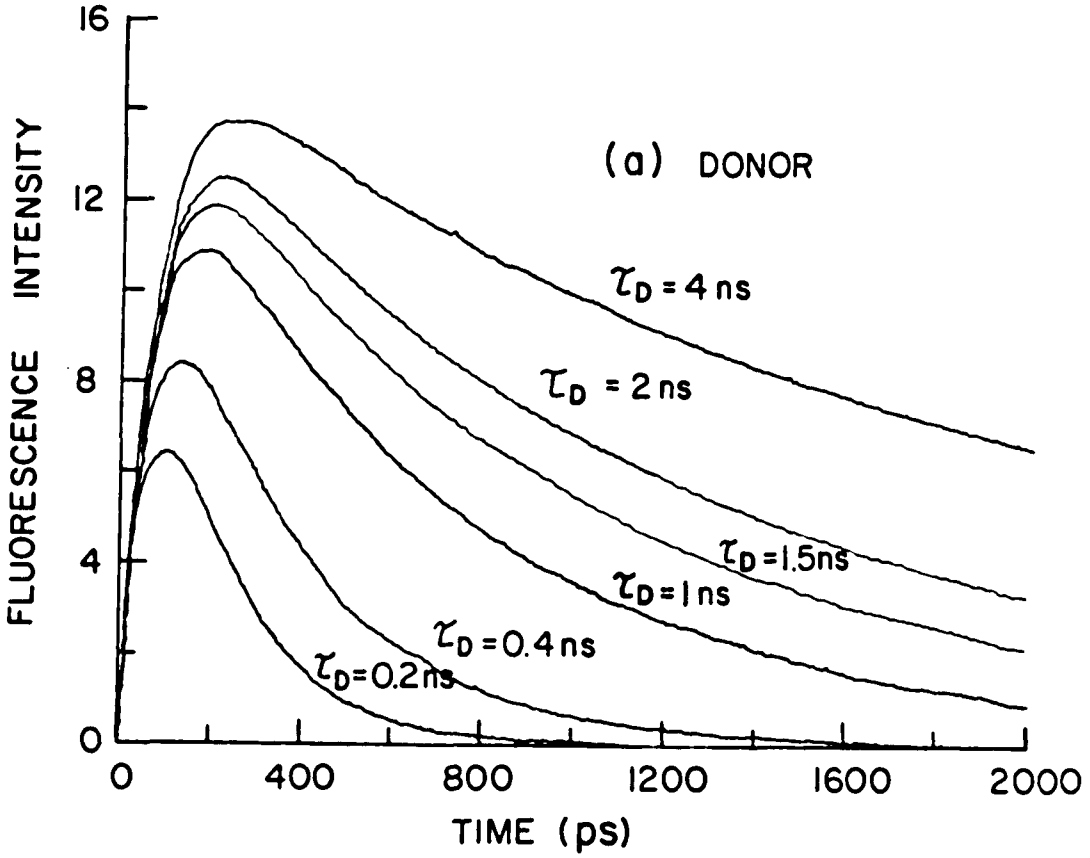

Fig. 3.4 (a) The theoretical calculation of fluorescence profile versus time obtained by equation (3.2.20) and (3.3.10) for (a) donor and (b) acceptor for different fluorescence decay times of donor (4, 2, 1.5, 1, 0.4, 0.2 ns). The detection system risetime is 80 ps. The fluorescence decay time is 0.75 ns for the acceptor. The concentration is 2.5×10^{-3} M and the ratio of absorption coefficient is 17.5 and R_o = 40Å

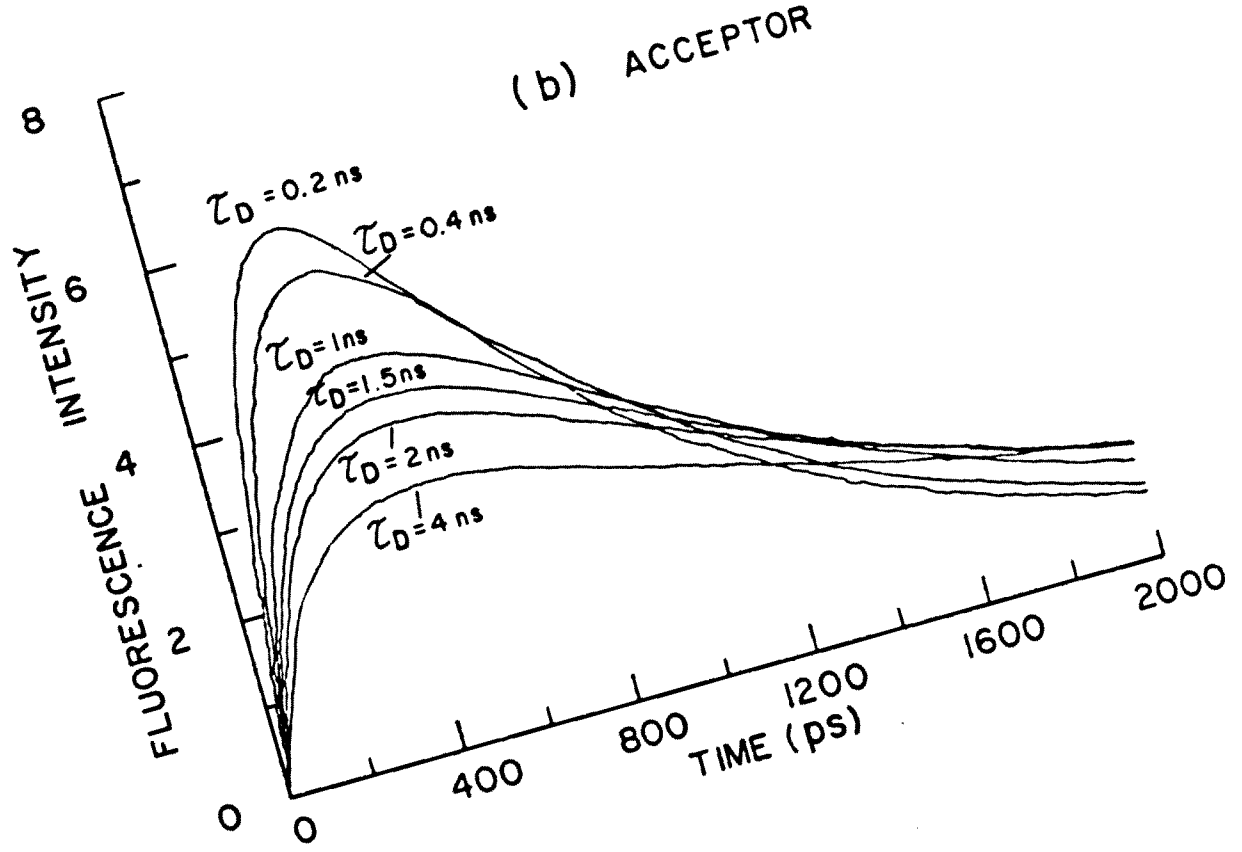
(b) ACCEPTOR
FLUORESCENCE INTENSITY
8
6
4
2
0
0
400
800
1200
1600
2000
TIME (ps)
τ_D = 0.2 ns
τ_D = 0.4 ns
τ_D = 1 ns
τ_D = 1.5 ns
τ_D = 2 ns
τ_D = 4 ns

Fig. 3.4 (b)

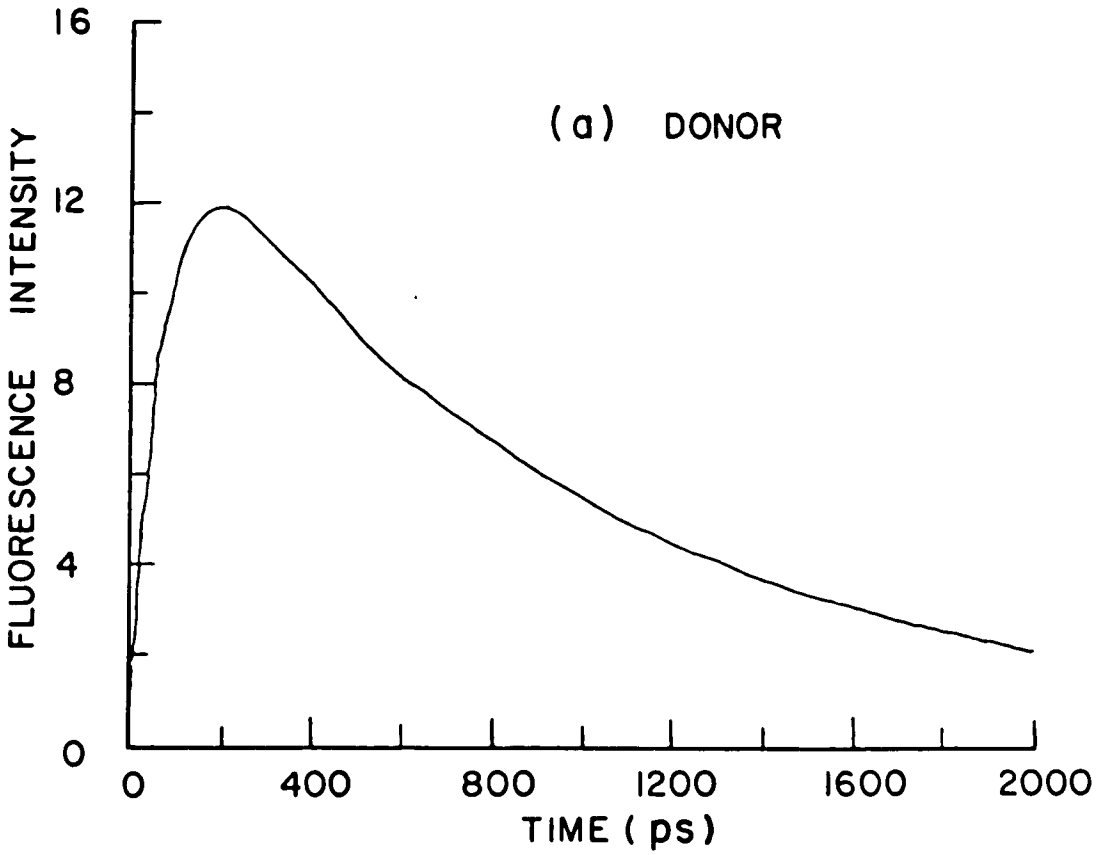

Fig. 3.5 (a) The theoretical calculation of fluorescence profile versus time obtained by equations (3.2.20) and (3.3.10) for (a) donor and (b) acceptor for different fluorescence decay time τ_A (1.25, 0.75, 0.4, 0.2, 0.1 ns). The detection risetime is 80 ps. The fluorescence decay time is 1.5 ns for the donor. The concentration is 2.5×10^{-3} M. The ratio of absorption coefficient is 17.5, and R_o = 40A. The fluorescence decay time of the donor τ_D = 1.5 ns.

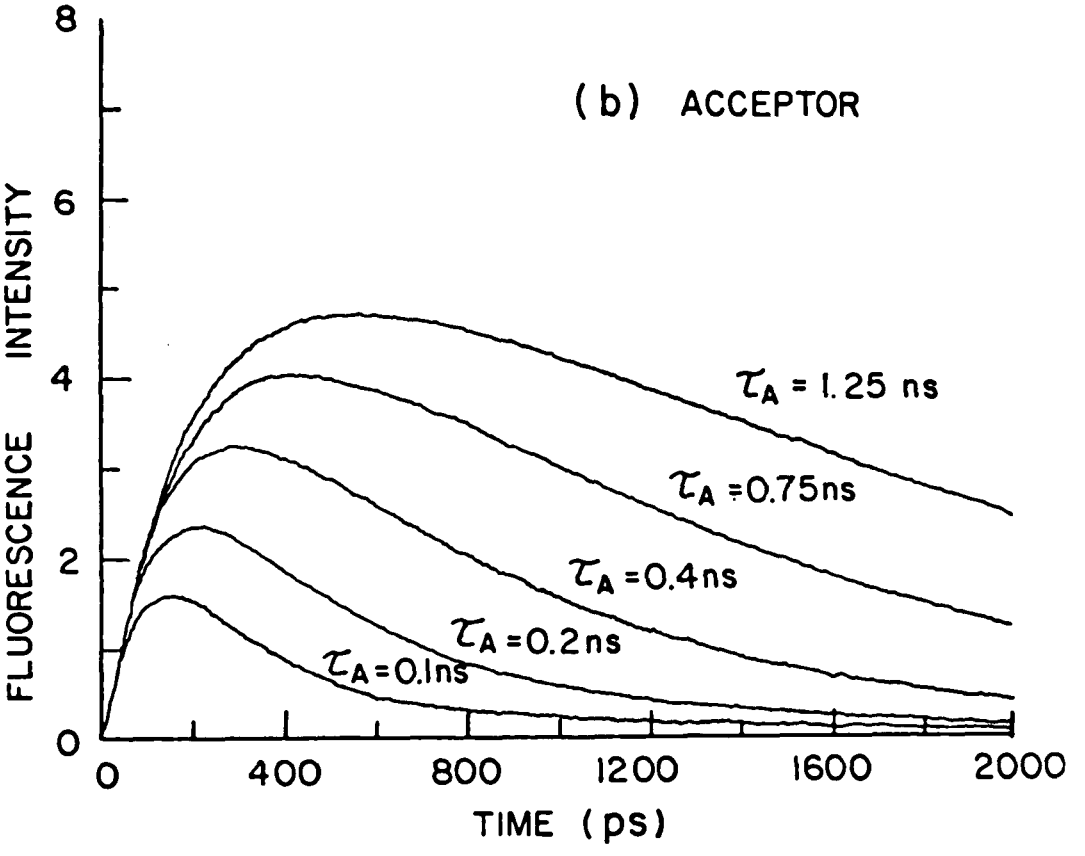
(b) ACCEPTOR
FLUORESCENCE INTENSITY
TIME (ps)
τ_A = 1.25 ns
τ_A =0.75ns
τ_A =0.4ns
τ_A =0.2ns
τ_A =0.1ns
0
2
4
6
8
0
400
800
1200
1600
2000

Fig. 3.5 (b)

References

1. Th Forster, Ann. Physik, 2, 55 (1948). Dis. Far. Soc. 27, 7 (1959)
2. K. B. Eisenthal and S. Siegel, J. Chem. Phys. 41, 652 (1964)
3. J. B. Birks, Photophysics of Aromatic Molecules, John Wiley, N.Y. (1970)
4. R. G. Powell and Z. G. Soos, J. Lum. 11, 1 (1975)
5. D. L. Dexter, J. Chem. Phys. 21, 836 (1953)
6. M. Yokota, and O. Tanimoto, J. Phys. Soc. of Japan 22, 779 (1967)
7. U. K. A. Klein, R. Frey, M. Hauser and U. Gosele, Chem. Phys. Lett. 41, 139 (1976)
8. R. A. Auerbach and G. W. Robinson, and R. W. Zwanzig, J. Chem. Phys. 72, 3528 (1980)
9. K. Allinger and A. Blumer, J. Chem. Phys. 72, 4608 (1980)

CHAPTER 4 THE ENERGY TRANSFER BETWEEN DONOR AND ACCEPTOR BINARY SOLUTION AT FIXED CONCENTRATION

4.1 In this chapter, the experimental measurements and theoretical calculations for the energy transfer dynamics in two mixtures composed of (1) Rhodamine 6G (the donor) and Oxazine 4 Perchlorate (the acceptor), and (2) Rhodamine B (the donor) and Nile Blue A Perchlorate (the acceptor) are presented. The fluorescence kinetics for neat dyes and for both the donor and acceptor dyes in the binary mixture were investigated at concentration 2.5 x 10^{-3}M in ethylene glycol at room temperature. The absorption and fluorescence spectra for the donors and acceptors used are displayed in fig. 4.1.

From equation (3.1.5), the critical transfer distance R_o can be calculated from the fluorescence spectrum of donor and the absorption spectrum of acceptor as shown in figure 4.1. The R_o can be re-expressed as

$$R_0 = \sqrt[6]{\frac{9000(\ln 10)\,\kappa^2 \Phi_D}{128\pi^5 n^4 N}\,J} \qquad (4.1.1)$$

where

$$J = \int I_\lambda \epsilon_\lambda \lambda^4 d\lambda \qquad (4.1.2)$$

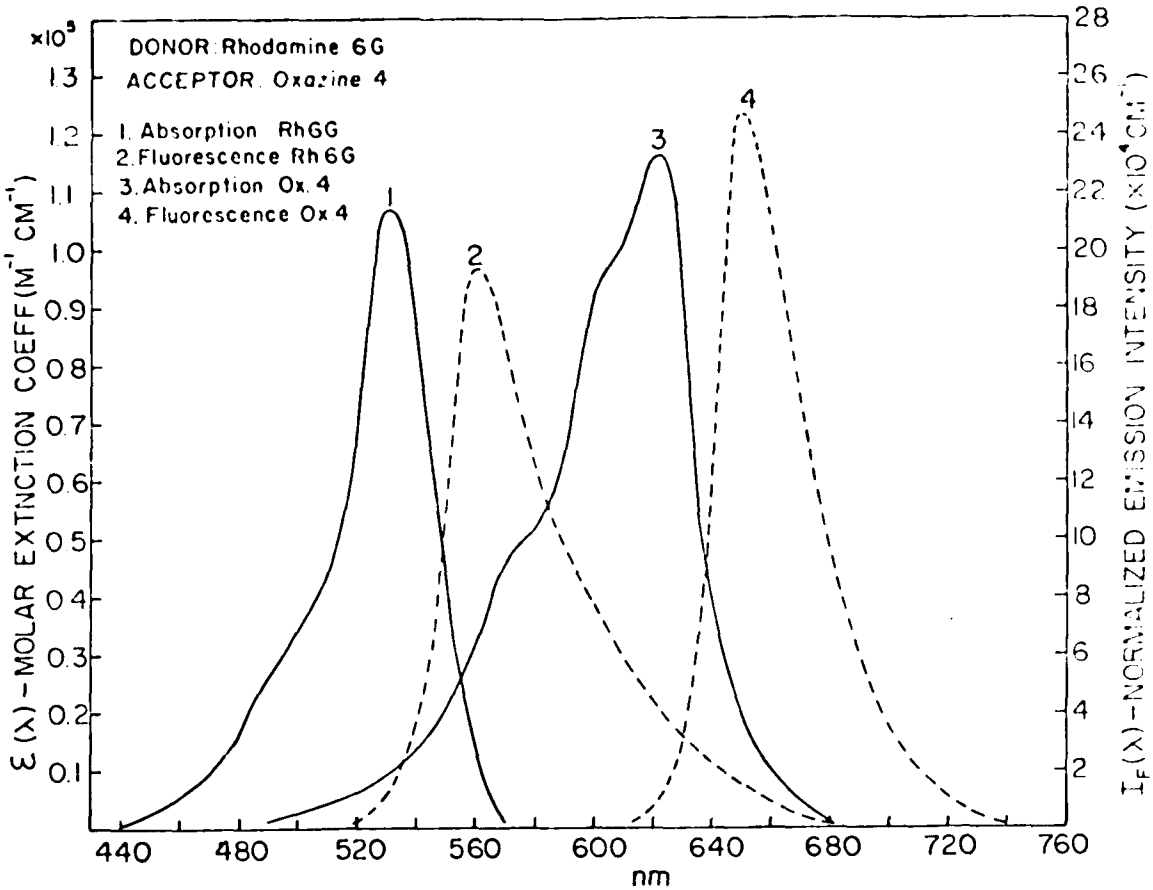

Fig. 4.1 (a) **Steady state absorption and fluorescence spectra for donor and acceptor dye molecules. (a) Rh6G(D)-OX(A)**

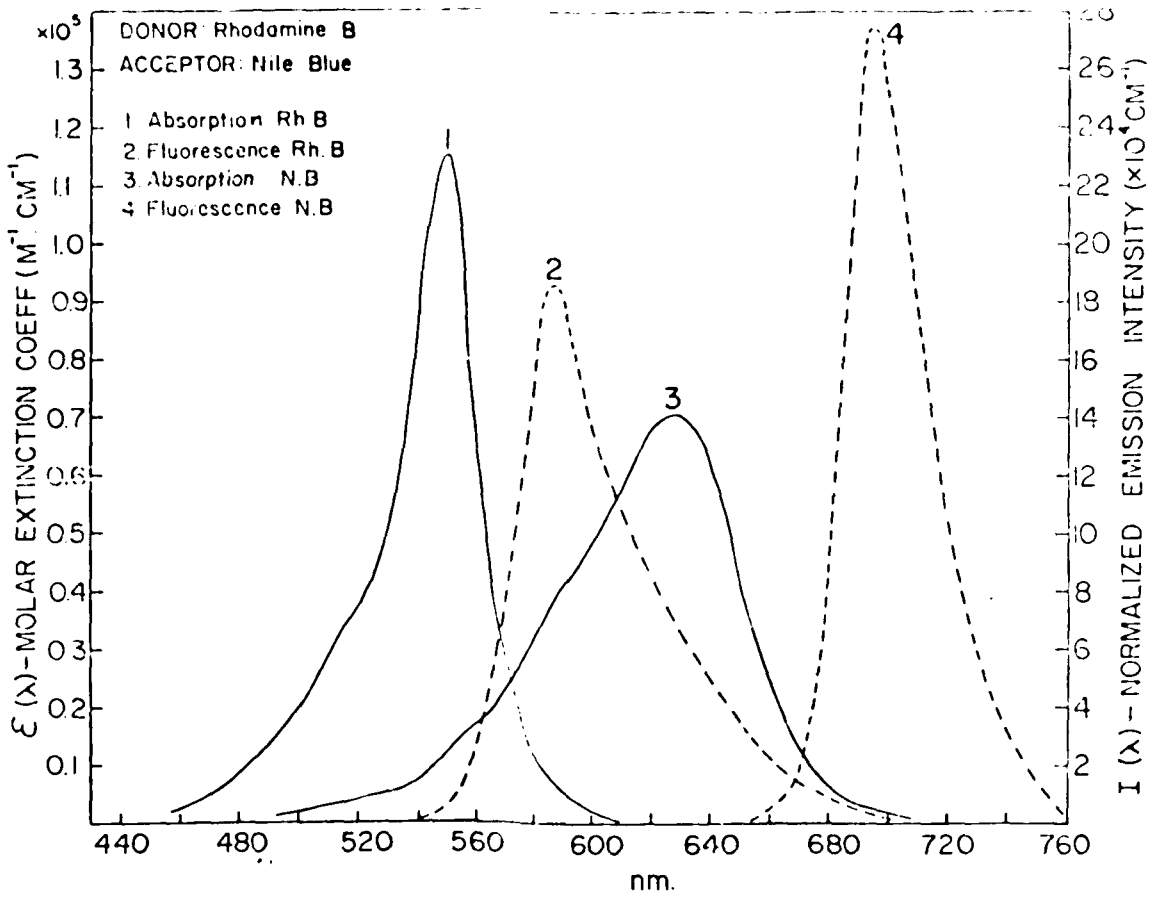

Fig. 4.1 (b) **Steady state absorption and fluorescence spectra for donor and acceptor dye molecules. (b) RhB(D)-NB(A)**

and K^2 = 2/3

n = 1.42

N = 6.02×10^{23}

Φ_D = 0.98 for R6G

= 0.9 for RB

J = 0.3537×10^{35} $[Å]^6$ for R6G- R6G

= 2.1819×10^{35} $[Å]^6$ for Ox4 - R6G

= 0.2964×10^{35} $[Å]^6$ for RB - RB

= 1.9132×10^{35} $[Å]^6$ for NB - RB

J is the overlap integral between the normalized donor fluorescence I_λ by the definition of $\int I_\lambda d\lambda = 1$, and the absorption extinction coefficient ϵ_λ. From the fluorescence spectra of rhodamine 6G, the donor, the normalized intensity I_λ was determined by the unity of the integral (area) of I_λ with respect to the wavelength λ. The molecular extinction coefficient ϵ_λ of oxazine 4 perchlorate (the acceptor) was found by measuring the absorption coefficient in terms of O.D. The ϵ_λ can be related to O. D. as

$$\epsilon_\lambda = \frac{O.D.}{C \cdot d} \qquad (4.1.3)$$

where C = concentration of oxaxine 4 perchlorate

d = optical path of cuvette

knowing the value of I_λ and ϵ_λ, the overlap integral

was calculated by equation (4.1.2). Then the value of R_o was found by equation (4.1.1) for donor-acceptor and donor-donor pairs. The value of R_o^{DD} is 41.3Å and 40.2Å for R6G and RB respectively. The value of R_o^{DA} is 56Å for R6G-Ox4 and 54Å for RB-NB.

4.2 Experimental Method and Samples

The experimental setup used in this research program is shown in figure 2.2.1. The 1.054 μm laser beam is generated by the Nd:phosphate glass oscillator and amplifier. The single pulse selector is used to select a single pulse from the mode-locked pulse train. A second harmonic generator, KDP converts the frequency of the 1.054 μm to 0.527 μm.

The 0.527 μm single pulse is delayed by an optical delay unit (white cell), and incident onto the sample. The excitation pulse is filtered by a Corning filter 3-67 from the fluorescence from the sample. A cyan Dichroic filter is used to separate the fluorescence component of Rhodamine 6G, and Hoya R-66 filter is used for the component of Oxazine 4 Perchlorate. The Ditric short pass filter at 620 nm is used to separate the fluorescence component of Rhodomine B, and Hoya R-68 filter is used for the component of Nile Blue A Perchlorate. The fluorescence is collected by lenses and focussed into the slit Hamamatsu streak camera (C 979). The streak camera output is recorded and digitized by a SIT (Silicon Intensified Target) camera and Hamamatsu Temporal Analyzer. The data are stored by DEC Minc 11 minicomputer.

On the full time display of 3.1 nsec, the overall resolution of streak camera at this streak rate for these measurements is 80 ps. The system response for a laser pulse (pulse duration = 6 ps measured by two photon fluorescence technique) is shown in figure 4.2. The system time response at full width at half maximum power is around 80 ps for the convolution of the laser pulse signal with the system function in time on the 3.1 nsec full scale. Only the 2 nsec part of the total display is displayed in fig. 4.2. A portion of the excitation pulse is directed into the streak camera as a marker prepulse.

The laser-grade dye samples (Eastman Kodak Company) were dissolved in the certified ethylene glycol (Fisher Scientific Company). A concentration of 2.5×10^{-3}M for both the neat (similar, monocomponent system) and binary mixture (dissimilar, two-component system) solution was prepared. At this concentration the average distance R between the donor and acceptor molecules is about 43.5 Å, and the average distance between donor-donor molecules in the mixture is 54 Å. The solution was contained in a 1-mm or 2-mm optical path cuvette. The ratio of absorption coefficient β at λ = 530 nm for Rhodamine 6G to that of Oxazine 4 Perchlorate, and Rhodamine B to that of Nile Blue A Perchlorate was measured to be 22 and 17.5, respectively. At these absorption ratios, very little direct pumping of the acceptor molecules is possible in the mixed system.

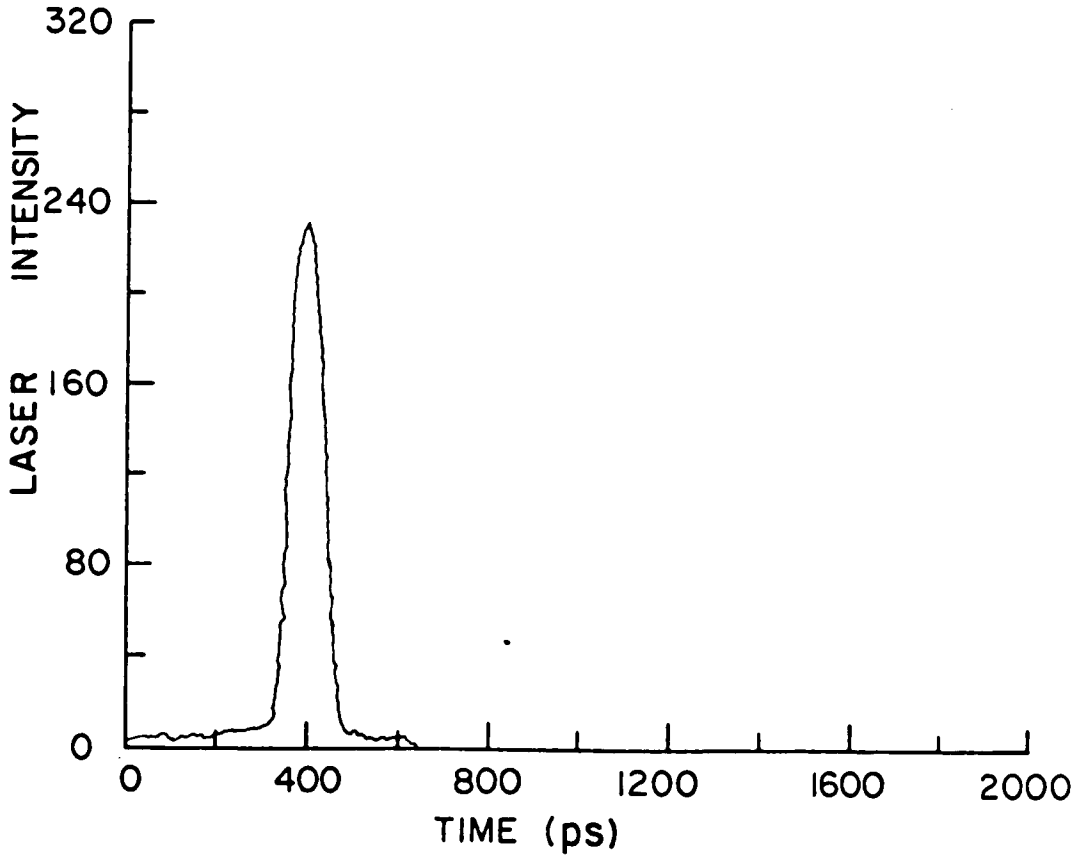

Fig. 4.2 Time response of the streak camera system on a 3 nsec sweep scale - a 6 picosecond, 530 nm laser pulse profile versus time measured by streak camera system. This is the time convolution of the laser pulse and the system function of the detection apparatus. The pulse width at half maximum is about 80 ps. This is the time response function of the detection system on the streak rate being used (3.1 nsec full time display).

4.3 EXPERIMENTAL RESULTS

Neat Sample Kinetics

The fluorescence kinetics from neat monocomponent solutions of dyes of Rhodamine 6G, Oxazine 4 Perchlorate, Rhodamine B, and Nile Blue A Perchlorate in neat solution are shown in figures 4.3, 4.4, 4.5 and 4.6, respectively. The risetime of fluorescence is the time convolution of the system response function (80 ps) of our detection system on the 3.1 nsec full-time scale. The fluorescence decay time is determined by a least square single exponential data fitting. The decay times are 1.8, 1.52, 1.5, and 0.75 ns at C= 2.5 x 10^{-3} M for figures 4.3 (R6G), 4.4(OX), 4.5 (RB), and 4.6 (NB), respectively. The standard error for these decay times is $\leq$ 0.2 nsec.

Donor-Acceptor Mixture Kinetics

The fluorescence of Rhodamine 6G (the donor) and Oxazine 4 Perchlorate (the acceptor) system; and Rhodamine B (the donor) and Nile Blue A Perchlorate (the acceptor) system are shown in figures 4.7, 4.8, 4.9 and 4.10 respectively.

From figures 4.7 and 4.3, we found that 1/e time of the donor in the mixture becomes shorter compared to the fluorescence decay time of the donor molecule in the neat solution. The shortening is about 700 ps and 200 ps for Rhodamine 6G and Rhodamine B, respectively. From figures 4.8 and 4.4, we found that the risetime of the acceptor in the binary mixture becomes slower compared to that of the

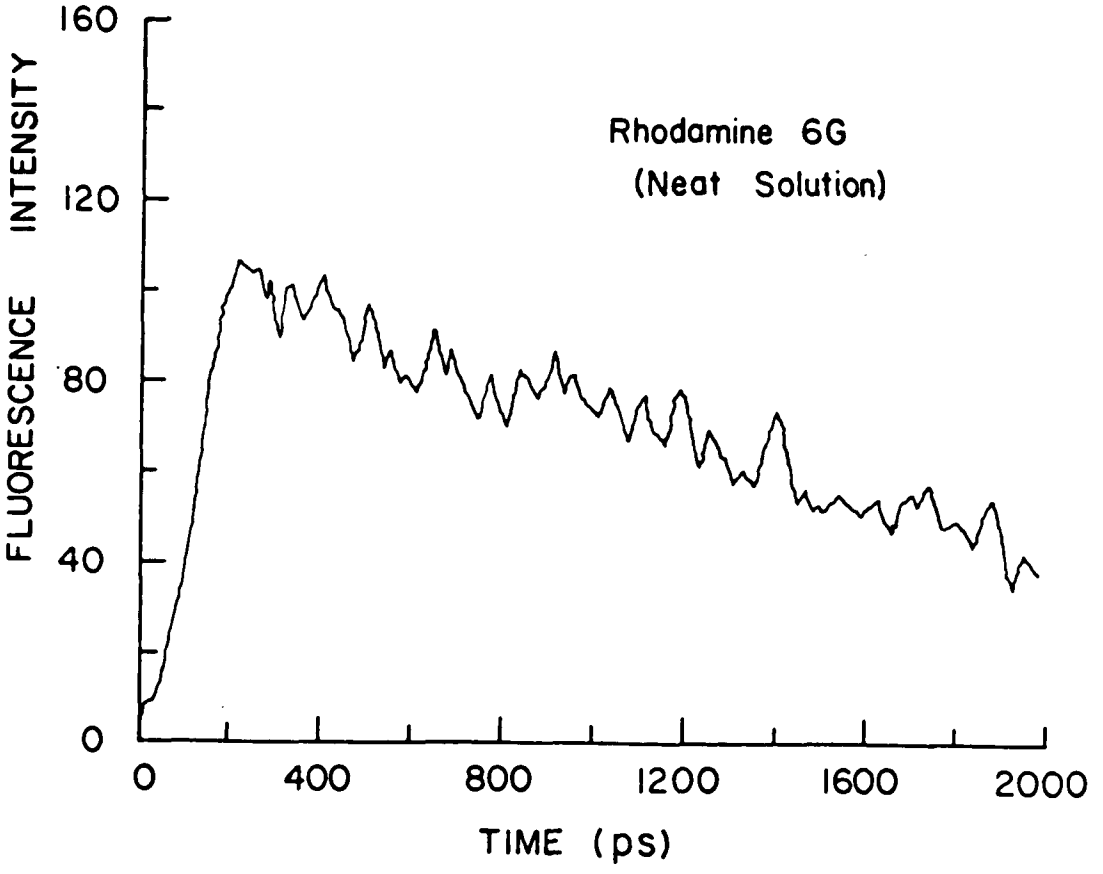

Fig. 4.3 Experimental measurement of fluorescence profile versus time of neat Rhodamine 6G in ethylene glycol at a concentration 2.5×10^{-3} M. Using Corning 3-67 filters and a Cyan Dichroic filter, the fluorescence decay time is found to be 1.8 ns $\pm$ 0.15 ns (5300 Å$<\lambda<$6000 Å) by least square data fitting.

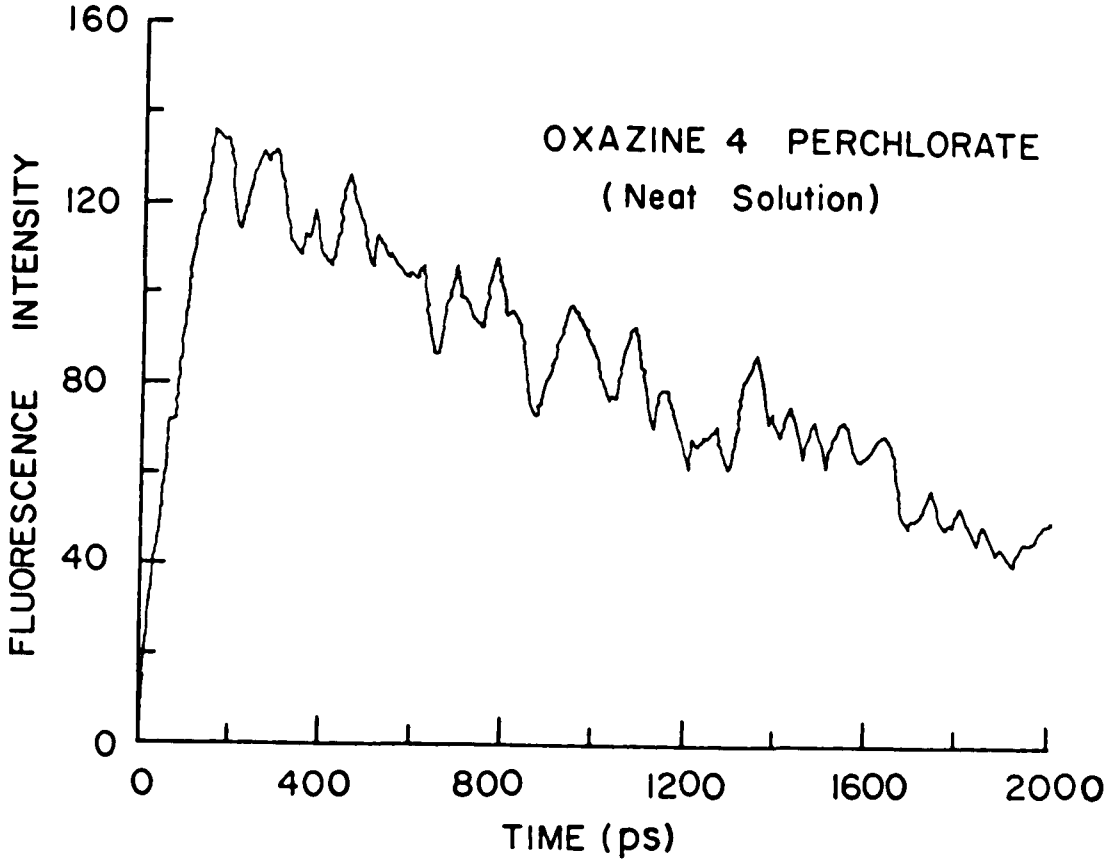

Fig. 4.4 Experimental measurement of fluorescence profile versus time of neat Oxazine 4 Perchlorate in ethylene glycol with a concentration 2.5×10^{-3} M. Using Corning 3-67 filters and Hoya R-66 filter, the fluorescence decay time is found to be 1.52 ns $\pm$ 0.1 ns ($\lambda >$ 6600Å) by least square fitting.

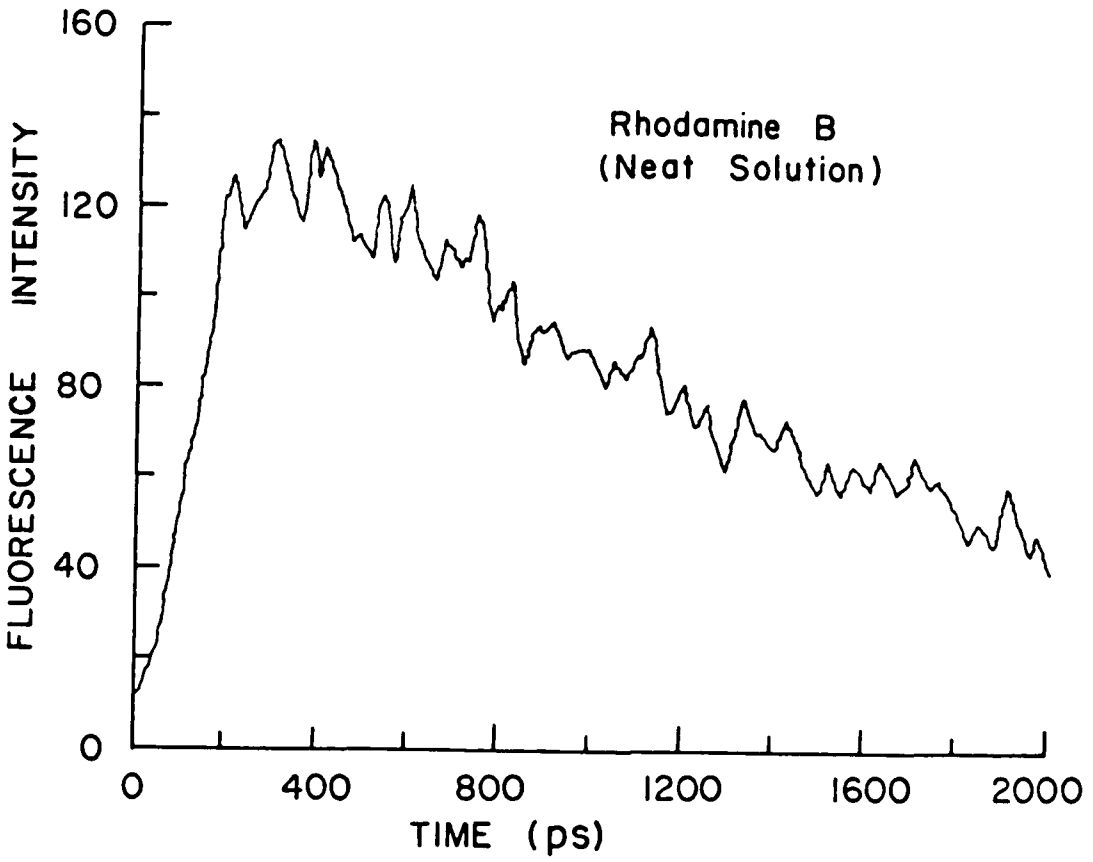

Fig. 4.5 Experimental measurement of fluorescence profile versus time of neat Rhodamine B in ethylene glycol with a concentration 2.5×10^{-3} M. Using 3-67 filters and Ditric short pass filter at 620 nm, the fluorescence decay time is found to be 1.5 ns $\pm$ 0.16 ns (5300Å $< \lambda <$ 6200Å) by least square data fitting.

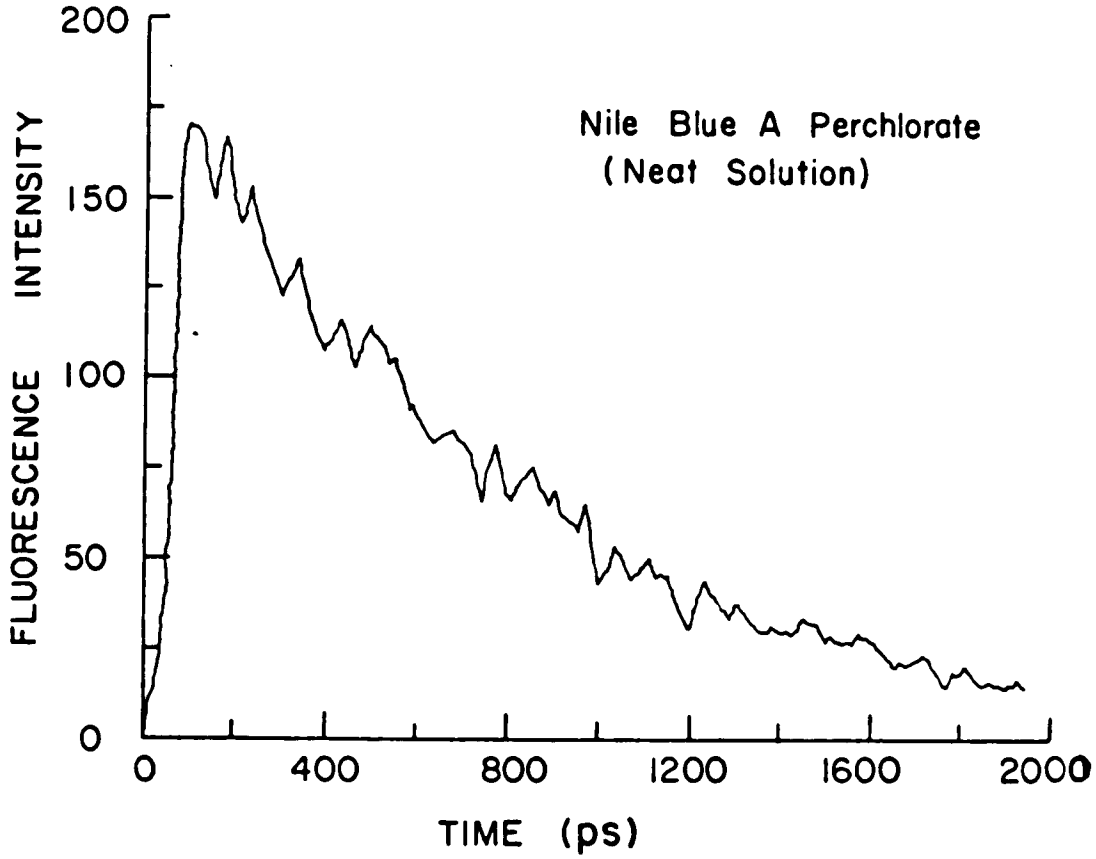

Fig. 4.6 Experimental measurement of the fluorescence profile versus time of neat Nile Blue A Perchlorate in ethylene glycol with a concentration 2.5×10^{-3} M. Using Corning 3-67 and Hoya R 68 filters, the fluorescence decay time is found to be 0.75 ns $\pm$ 0.05 ns ($\lambda > 6800$Å) by least square data fitting

neat solution. The measured risetime is 650 ps and 400 ps slower than neat Oxazine 4 Perchlorate and neat Nile Blue A Perchlorate of 80 ps (system time resolution), respectively. This is attributed to the energy transfer from the donor to the acceptor because the rate of energy transfer to the excited state of the acceptor molecule is much slower than the feeding rate by vibrational relaxation.

4.4 DISCUSSION

The experimental fluorescence kinetics profiles of both the donor and acceptor were fitted by subsituting the experimental value of P_D, g_D, P_A, g_A, and β in equations (3.2.20) and (3.3.10)) for a different value of R_o. The experimental results of the donor and acceptor can be fitted very well with an appropriate value of R_o. This is a one-parameter fit (R_o). The parameter R_o for the best fit to the data for (1) the mixture of Rhodamine 6G and Oxazine 4 Perchlorate system is 55 Å, and (2) Rhodamine B and Nile Blue A Perchlorate system is 48 Å.

We have performed the first measurements for fluorescence kinetics of both the donor and acceptor dye molecules and theoretically fitted the decay profiles for both the donor and the acceptor molecules. The theory for the energy transfer kinetics was developed to explain the change of decay of fluorescence of the donor, and the risetime of the fluorescence of the acceptor molecules. The theoretical

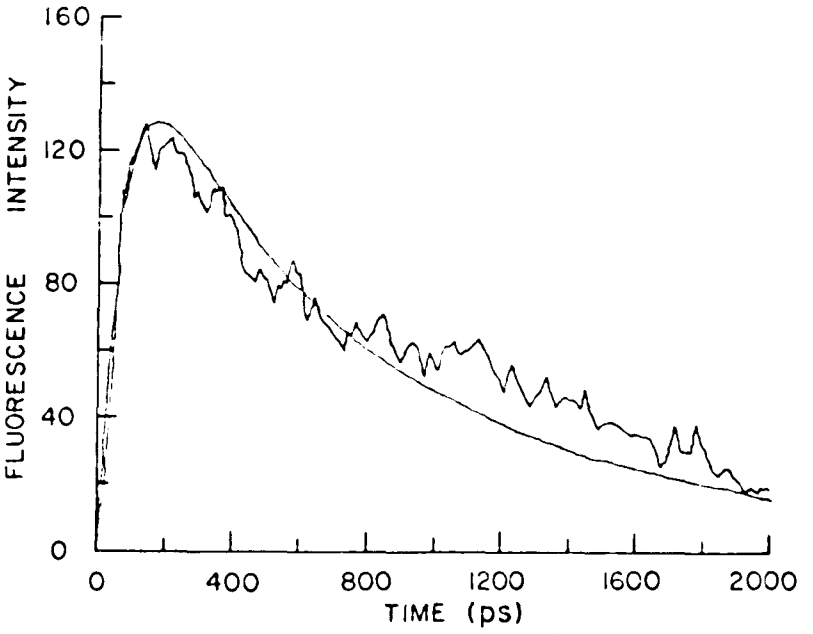

Fig. 4.7 Experimental measurement of fluorescence profile versus time of Rhodamine 6G (the donor) mixed with Oxazine 4 Perchlorate (the acceptor) in ethylene glycol with a single concentration of 2.5×10^{-3} M (5300Å $< \lambda <$ 6000Å). The filters used are Corning 3-67 and Cyan Dichroic filters. The measurement is fitted by a solid curve generated theoretically from equation (3.2.20). The parameters used to fit the donor data are: the system risetime of 80 ps, the fluorescence decay time of 1.8 ns and 1.52 ns for the donor and acceptor molecule respectively, the ratio of absorption coefficient of the donor and acceptor of 22, and value R_o=55Å

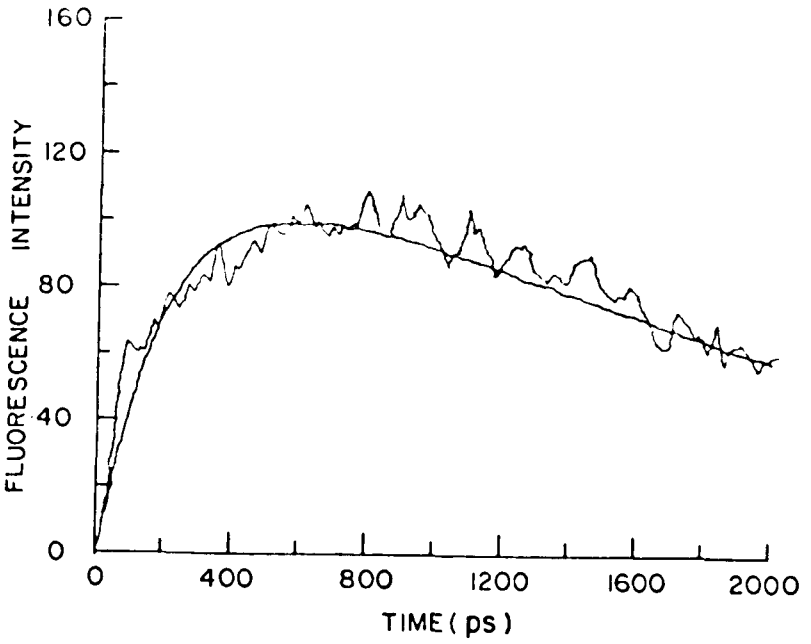

Fig. 4.8 Experimental measurement of fluorescence profile versus time of Oxazine 4 Perchlorate (the acceptor) mixed with Rhodamine 6G (the donor) in ethylene glycol with a single concentration of 2.5×10^{-3} M ($\lambda > 6600$Å). The filters used are Corning 3-67 and Hoya R-66 filters. The measurement is fitted by a solid curve generated theoretically from equation (3.3.10). The parameters used to fit the acceptor data are: The system response of 80 ps, the fluorescence decay time of 1.8 ns and 1.52 ns for the donor and acceptor respectively, the ratio of absorption coefficient of donor and acceptor of 22, and value $R_o = 55$Å

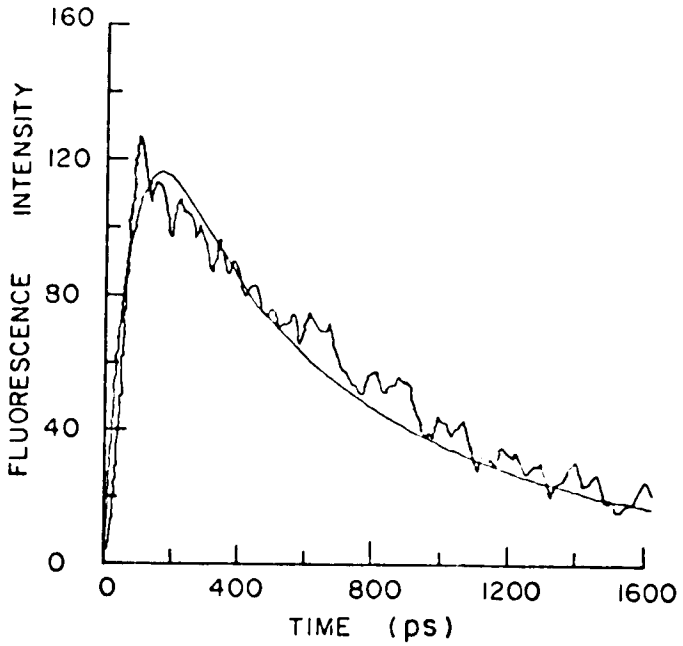

Fig. 4.9 Experimental measurement of fluorescence profile versus time of Rhodamine B (the donor) mixed with Nile Blue A Perchlorate in ethylene glycol with single concentration of 2.5×10^{-3} M (5300Å $< \lambda <$ 6200Å). The filters used are Corning 3-67 and Ditric short pass filter at 620 nm. The measurement is fitted by a solid curve generated theoretically from equation (3.2.20). The parameters used to fit the donor data are: The system risetime of 80 ps, the fluorescence decay time of 1.5 ns and 0.75 ns for donor and acceptor respectively, the ratio of absorption coefficient of donor and acceptor of 17.5, and value R_o = 48Å

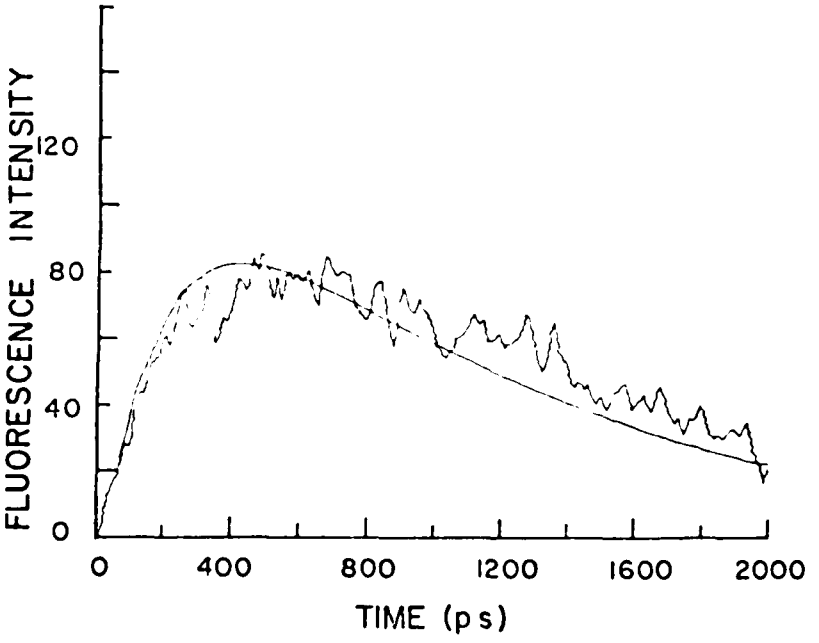

Fig. 4.10 Experimental measurement of fluorescence profile versus time of Nile Blue A Perchlorate (the acceptor) mixed with Rhodamine B (the donor) in ethylene glycol with a single concentration of 2.5×10^{-3} M ($\lambda > 6800$Å). The filters used are Corning 3-67 and Hoya R-68 filters. The measurement is fitted by a solid curve generated theoretically from equation (3.3.10). The parameters used to fit the acceptor data are: the system risetime of 80 ps, the fluorescence decay time of 1.5 ns and 0.75 for the donor and acceptor respectively, the ratio of absorption coefficient of 17.5, and value of R_o = 48Å

fitting to the experimental kinetics profiles is excellent and consistent.

Theoretically, the parameter R_o is the distance at which the rate of energy transfer is equal to the sum of all other donor deactivation rates. It can be expressed in terms of the overlapping integral of the emission spectrum of the donor and absorption spectrum of acceptor. The meaning of R_o is just the strength of interaction between the donor and acceptor molecule. It is the distance parameter from which we can estimate if there is energy transfer, what concentration of solution we are able to make to get the efficient energy transfer. The values of R_o were calculated[1] from spectroscopic data of fluorescence of the donor and absorption spectra: for Rh6G - OX 4, R_o = 56 Å and for RhB - NB, R_0 = 54 Å. These values are in excellent agreement with the values of R_o obtained from fitting the time resolved measurements of donor and acceptor in this study. In addition, the critical transfer distance R_o^{DD} for donor-donor excitation transfer was calculated to be 41 Å and 40 Å for R6G-R6G and RB-RB, respectively. The donor-donor excitation transfer will occur at high concentration of donors[3] when the critical distance R_o^{DD} for D-D transfer is larger than the average distance R (44Å) between the molecules. In our case, R_o^{DD} is 41Å (R6G) or 40Å (RB), and smaller than $\bar{R}$. The long range energy transfer rate between molecules decreases

tremendously when the critical distance R_o is less than the average distance R in the Forster mechanism. If $R_o > \bar{R}$, there will be an increase in the long range transfer. In order to enhance the energy transfer between donor and acceptor molecules, it is necessary to choose a pair of donors and acceptors such that (a) the absorption spectrum of the acceptor overlaps with the tail portion of the emission spectrum of the donor towards the longer wavelength region as shown in figure 4.1; (b) the critical distance R_o^{DA} for donor-acceptor molecules is greater than that (R_o^{DD}) of donor-donor and $R_o^{DA} > \bar{R}^{DA}$, $\bar{R}^{DD} > R_o^{DD}$; and the absorption of laser energy by donors is high enough to overcome the absorption of laser energy by acceptors and to reduce the long range D-D energy transfer to a minimum. In our cases the donor-donor energy transfer is not as important as donor-acceptor energy transfer because $R_o^{DA} > \bar{R}^{DA}$ and $\bar{R}^{DD} > R_o^{DD}$. If $R_0 = 0$, for instance, there is no overlapping of the emission spectrum of donor and absorption spectrum of acceptor. In this case, there is no energy transfer at all. This can be easily double-checked by inserting $R_o=0$ in the equations (3.2.20) and (3.3.10) to yield equation (3.4.1) immediately. The value of R_o found for the Rhodamine 6G and Oxazine 4 Perchlorate is larger than that of Rhodamine B and Nile Blue A Perchlorate. These results give us another consistency check between the theory and experimental results.

References

1. J. B. Birks, Photophysics of Aromatic Molecules, John Wiley, N.Y. (1970)

2. G. Porter and C. J. Tredwell, Chem. Phys. Lett. 56, 278 (1978)

3. D. P. Millar, R. J. Robbins, and A. H. Zewail, J. of Chem. Phys. 75, 3649 (1981)

CHAPTER 5 CONCENTRATION DEPENDENCE OF THE ENERGY TRANSFER BETWEEN DONOR AND ACCEPTOR MOLECULES IN SOLUTION

In chapter 4 we have measured the rise and decay of the fluorescence profiles of the donor and acceptor molecules at a fixed concentration (2.5×10^{-3}M). A theoretical model was formulated to fit the experimental results for the time-resolved fluorescence profiles of the donor and acceptor molecules. The consistency of the theory with the experimental data has given some of the conditions for efficient energy transfer between the donor and acceptor dye molecules. In order to obtain additional information on the energy transfer mechanisms and transfer efficiency and show consistency, a series of measurements with different concentrations of donor and acceptor molecules were performed.

In this chapter, experimental measurements and theoretical calculations were performed on mixed solutions with different concentrations of acceptor molecules at a fixed concentration of donor molecules for the following pair of dyes: (1) Rhodamine 6G (the donor) and Oxazine 4 Perchlorate (the acceptor); and (2) Rhodamine B (the donor) and Nile Blue A Perchlorate (the acceptor). The dyes were dissolved in ethylene glycol at room temperature where diffusion is small and can be neglected.

5.2 Theoretical Review

The fluorescence intensity per unit volume from the donor

and acceptor molecules as function of time were formulated in chapter 3 and are given by:

$$\mathcal{D}(t) = \Gamma_D \sigma_D I_0 n_D \rho_D \int_0^t d\tau \exp[-\rho_D(t-\tau) - g_D\tau - \frac{4\pi}{3} n_A \sqrt{\pi D \tau}] \quad (5.1)$$

and

$$\begin{aligned} \mathcal{A}(t) = \Gamma_A \sigma_A I_0 \Big\{ & n_D \rho_D \beta \frac{(e^{-\rho_D t} - e^{-g_A t})}{g_A - \rho_D} + n_A \rho_A \frac{(e^{-\rho_A t} - e^{-g_A t})}{g_A - \rho_A} \\ & - \left(\frac{g_D - \rho_D}{g_A - \rho_D}\right) n_D \rho_D \beta e^{-\rho_D t} \int_0^t d\tau \exp\left[(\rho_D - g_D)\tau - \frac{4\pi}{3} n_A \sqrt{\pi D \tau}\right] \\ & + \left(\frac{g_D - \rho_D}{g_A - \rho_D}\right) n_D \rho_D \beta e^{-g_A t} \int_0^t d\tau \exp\left[(g_A - g_D)\tau - \frac{4\pi}{3} n_A \sqrt{\pi D \tau}\right] \\ & - n_D \rho_D \beta e^{-g_A t} \int_0^t d\tau \exp\left[(g_A - g_D)\tau - \frac{4\pi}{3} n_A \sqrt{\pi D \tau}\right] \Big\} \end{aligned} \quad (5.2)$$

where Γ_D = radiative decay rate of donor molecule,

Γ_A = radiative decay rate of acceptor molecule,

σ_D, σ_A = absorption cross section of donor and acceptor molecule,

ρ_D = excited state vibrational relaxation rate of donor molecule,

ρ_A = excited state vibrational relaxation rate of acceptor molecule,

n_D = number of donor molecule per unit volume,

n_A = number of acceptor molecule per unit volume,

$\beta = \frac{\sigma_D}{\sigma_A}$ = ratio of absorption cross sections of the donor and acceptor,

$\Delta = \frac{1}{\tau}(\frac{R_o}{R})^6$,

τ_D = fluorescence decay time of donor,

R_o = the critical distance for donor-acceptor which the rate of energy transfer equals the sum of all other donor deactivation rate,

g_D^{-1} = fluorescence decay time of the donor in a neat solution, and

g_A^{-1} = fluorescence decay time of the acceptor in a neat solution.

Using equations (5.1) and (5.2), the fluorescence profiles versus time were calculated numerically for a given concentration (1.25×10^{-3}M) of the donor mixed with various concentrations of acceptors. The calculated fluorescence profiles of the donor and acceptor molecules are displayed in figures 5.1 and 5.2. In figure 5.1, the fluorescence intensity and quantum yield of the donor decreases as the concentration of acceptor increases. In figure 5.2, the fluorescence intensity and quantum yield of the acceptor increases as the concentration of the acceptor increases. This implies a larger and more efficient energy transfer in the higher concentration of acceptor molecules because there are more acceptor molecules surrounding a given donor

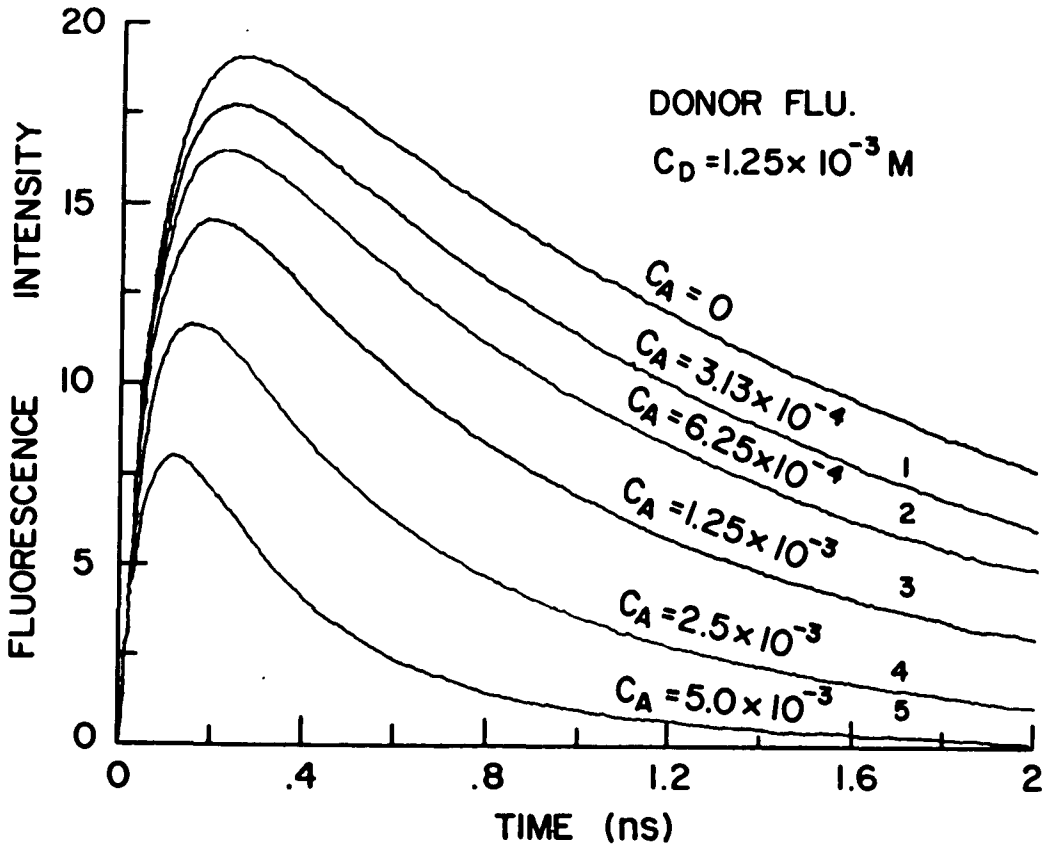

Fig. 5.1 The theoretical calculation of the fluorescence profiles versus time obtained by equation (5.1) for the donor at concentration 1.25×10^{-3} M and various concentrations of acceptors. The detection system risetime is assumed to be 80 ps considering the convolution of signal and streak camera. The critical transfer distance R_o is assumed to be 55 Å. The ratio of absorption cross section of donor to acceptor is 22. The decay time of donor is 1.85 ns

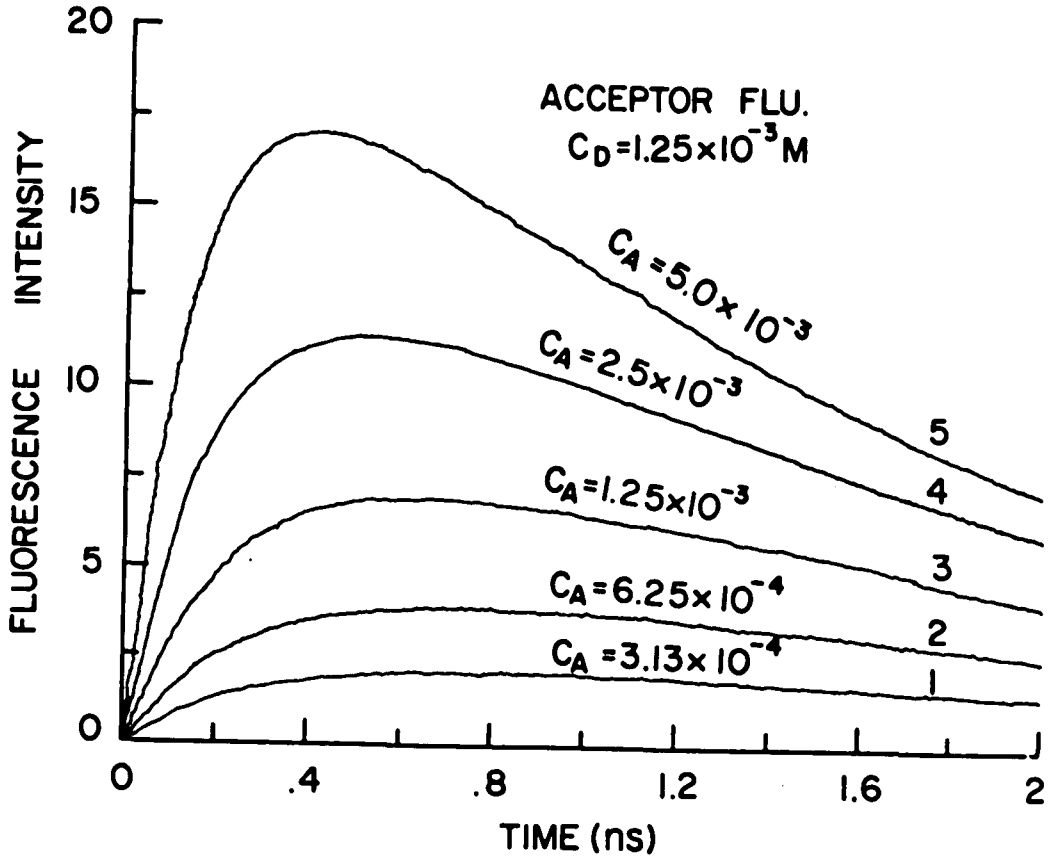

Fig. 5.2 The theoretical calculation of the fluorescence profiles versus time obtained by equation (5.2) for the acceptor at various concentrations and the donor at a concentration at 1.25×10^{-3} M. The system response function is 80 ps. The decay times of donor and acceptor are assumed to be 1.85 and 1.45 ns, respectively. The critical transfer distance is 55 Å. The ratio of absorption cross section of donor to acceptor is 22

molecule. The mean distance between the acceptor and donor is smaller than critical energy transfer distance R_o for higher energy transfer.

According to the theoretical model, the efficiency of the energy transfer η_E, is defined as follows

$$\eta_E = 1 - \frac{\int_0^\infty \int_0^t \exp\left[-\rho_D(t-\tau) - g_D\tau - \frac{4\pi}{3} n_A \sqrt{\pi \Delta \tau}\right] d\tau dt}{\int_0^\infty \int_0^t \exp\left[-\rho_D(t-\tau) - g_D\tau\right] d\tau dt} \quad (5.3)$$

On the other hand, the efficiency of energy transfer at average distance between donor and acceptor can be written as

$$\eta_{\bar{R}} = \frac{k_{ET}}{k_{ET} + g_D} = \frac{\frac{1}{\tau_D}\left(\frac{R_o}{\bar{R}}\right)^6}{\frac{1}{\tau_D}\left(\frac{R_o}{\bar{R}}\right)^6 + \frac{1}{\tau_D}} = \frac{\left(\frac{R_o}{\bar{R}}\right)^6}{1 + \left(\frac{R_o}{\bar{R}}\right)^6} \quad (5.4)$$

where K_{ET} is the average energy transfer rate. The value of η_E can be used to check the consistency of the theoretical calculation by comparing the results obtained from equations (5.3) and (5.4) with the experimental measurements for the different concentrations of acceptors mixed with a fixed quantity of donors.

5.3 Experimental Results

The experimental results are divided into two subsections: (1) steady state measurements and (2) time resolved measurements.

Subsection (1): Steady State Measurements

The fluorescence spectra (pumped by 530 nm) of solutions composed of Rhodamine 6G (the donor) at a fixed concentration 1.25×10^{-3}M, mixed with Oxazine 4 Perchlorate in ethylene glycol at different concentrations are shown in figure 5.3. The results of the binary mixed solution of Rhodamine B and Nile Blue A Perchlorate are shown in figure 5.4. From data displayed in figures 5.3 and 5.4, it is clear that when the concentration of the acceptors is increased, there is a decrease of the fluorescence yield of the donors and a corresponding increase in the fluorescence yield of the acceptors. We have observed an increase in the fluorescence intensity and quantum yield of the acceptors in the presence of the donor molecules in the binary solution. This is expected if long range energy transfer from the donors to acceptors is operative.

Subsection (2): Time Resolved Measurements

Typical time-resolved fluorescence profiles of the donor and acceptor molecules in binary mixtures are shown in figures 5.5 and 5.6, respectively. The theoretical fitting of the profiles by equations (5.1) and (5.2) to the experimental data using the known parameters P_o, P_A, β, g_D, g_A, C_D, and C_A in figures 5.5(a) to 5.5(e) and 5.6(a) to 5.6(e) are shown by the solid lines for $R_o = 55\text{Å}$. Neat fluorescence curves are on page 85 to 88. The fitting is excellent. Similar results for the other pair of dyes:

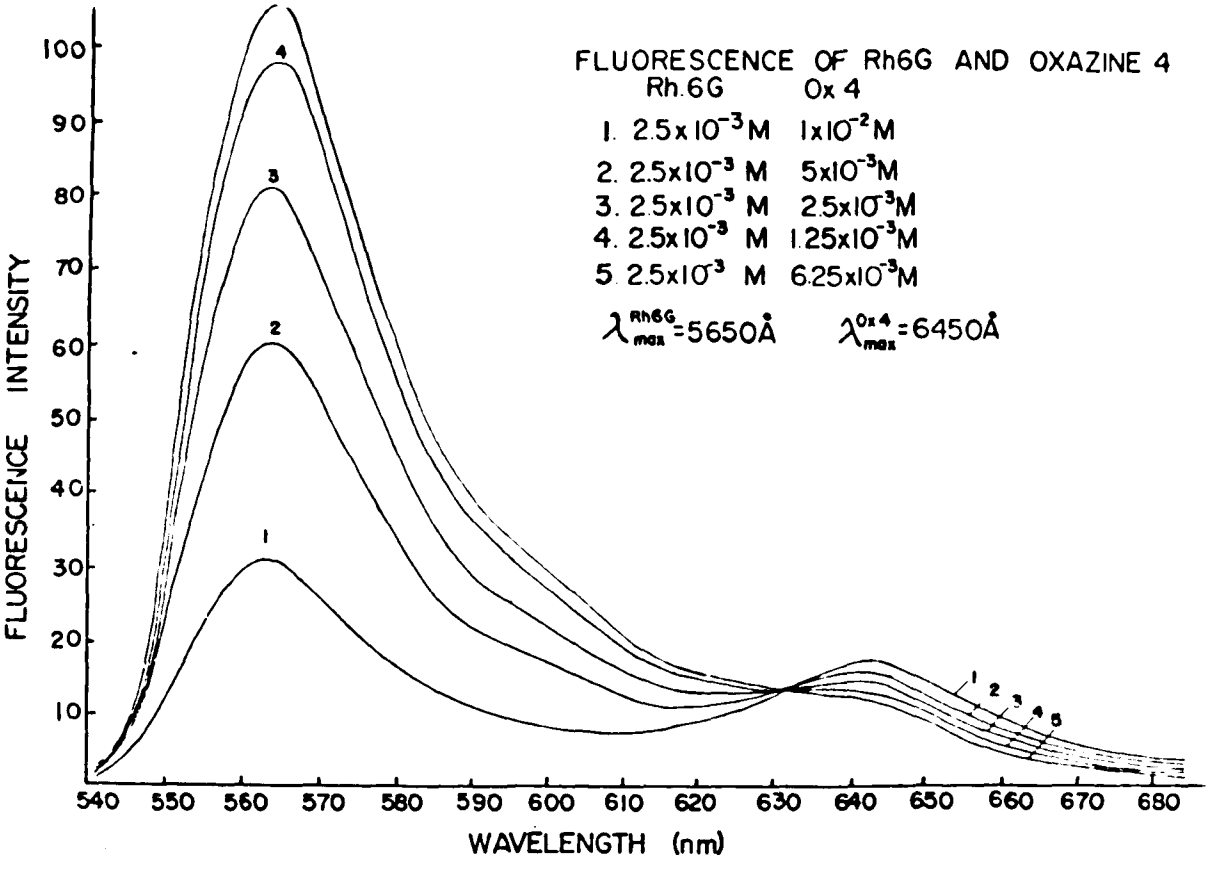

Fig. 5.3 Experimental measurement of the fluorescence spectra from 540 nm to 690 nm for Rhodamine 6G (the donor) at a concentration of 1.25×10^{-3} M and Oxazine 4 Perchlorate (the acceptor) at various concentrations in ethylene glycol. The peak intensity of Rh6G and Ox.4 occurs at 565 nm and 650 nm, respectively

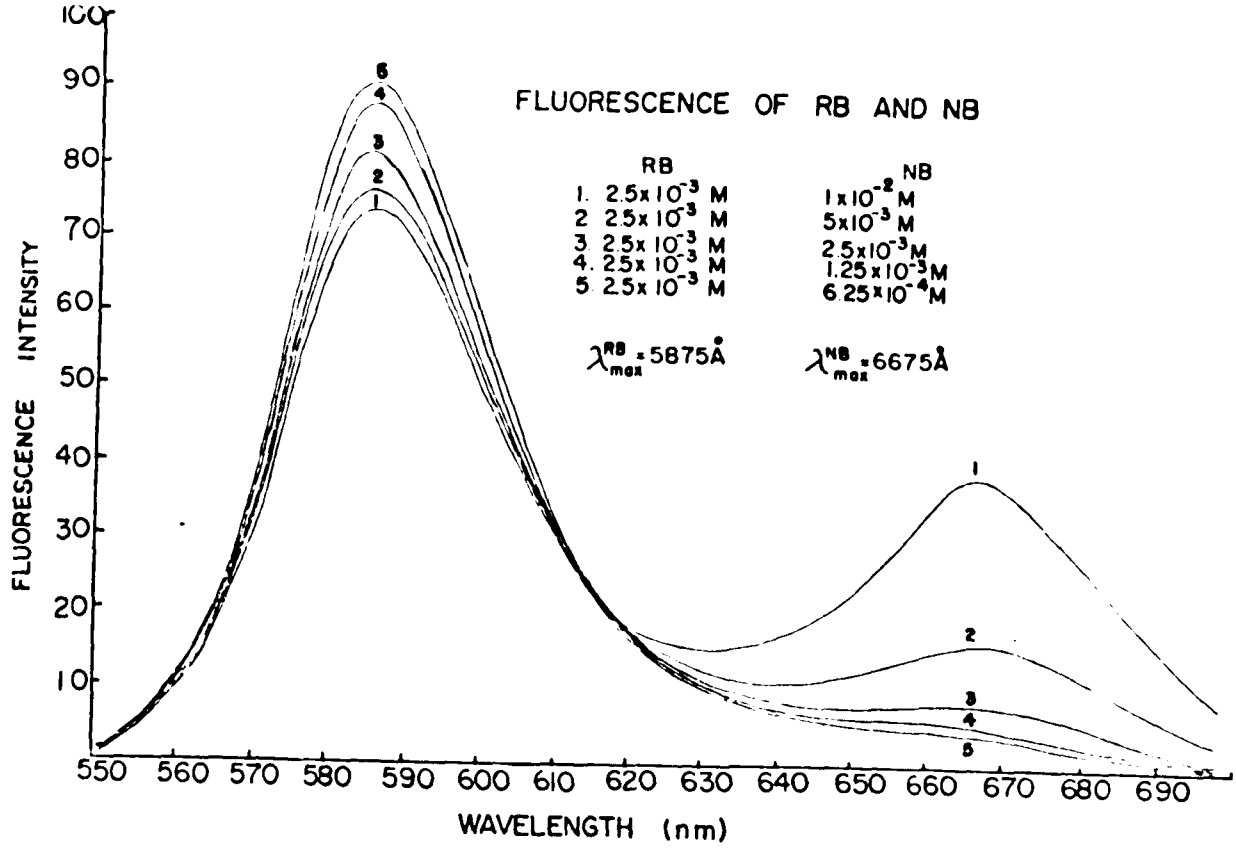

Fig. 5.4 Experimental measurement of the fluorescence spectra from 550 nm to 690 nm for Rhodamine B (the donor) at a concentration of 1.25×10^{-3} M and Nile Blue A Perchlorate (the acceptor) at various concentrations in ethylene glycol. The peak intensity of RhB and NB occurs at 588 nm and 670 nm, respectively

Fig. 5.5 Experimental measurement of time-resolved fluorescence profile of Rhodamine 6G (530 nm $< \lambda <$ 600 nm) at a concentration of 1.25×10^{-3} M mixed with Oxazine 4 Perchlorate at different concentrations: (a) 5×10^{-3} M, (b) 2.5×10^{-3} M, (c) 1.25×10^{-3} M, (d) 6.25×10^{-4} M and (e) 3.13×10^{-4} M in ethylene glycol. The filters used are Corning 3-67 and Cyan Dichroic filters. The measurement is fitted by a solid line generated by equation (5.1). The parameters used to fit the data are: the system risetime of 80 ps, the critical distance $R_o = 55$Å, the absorption ratio $\beta = 22$; the fluorescence decay time 1.82 ns for Rh6G, and fluorescence decay times for neat Ox.4 (a) 1.42 ns, (b) 1.45 ns, (c) 1.47 ns, (d) 1.50 ns, (e) 1.51 ns at the respective concentrations

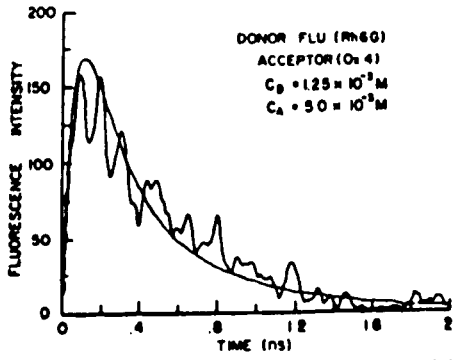

Fig. (a)

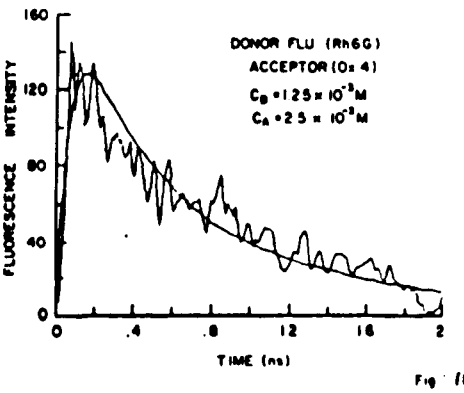

Fig. (b)

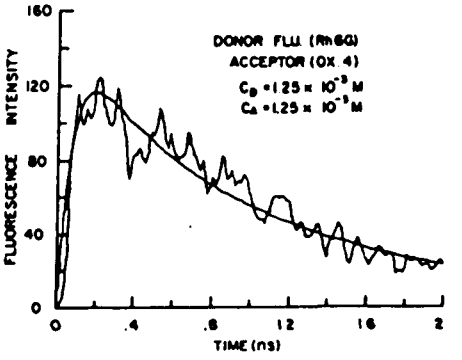

Fig. (c)

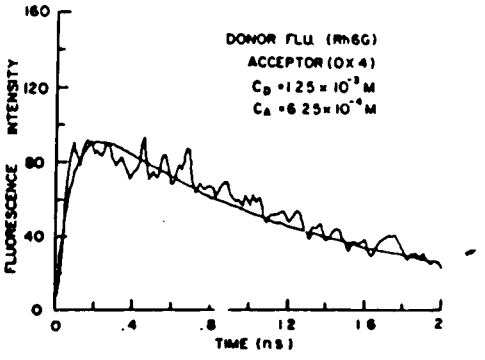

Fig. (d)

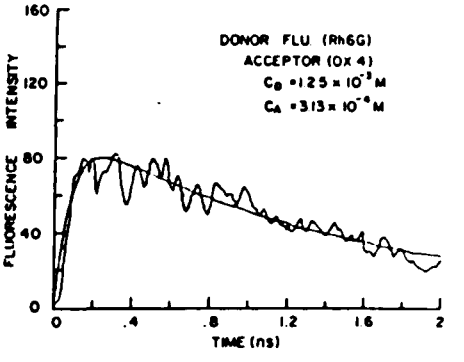

Fig. (e)

Fig. 5.6 Experimental measurement of fluorescence profiles of Oxazine 4 Perchlorate ($\lambda > 660$ nm) at different concentrations (a) 5×10^{-3} M, (b) 2.5×10^{-3} M, (c) 1.25×10^{-4} M, (d) 6.25×10^{-4} M, (e) 3.13×10^{-4} M mixed with Rhodamine 6G at a concentration of 1.25×10^{-3} M in ethylene glycol. The filters used are Corning 3-67 and Hoya R66 filters. The measurement is fitted by a solid line generated by equation (5.2). The parameters used to fit the data are: the system response of 80 ps, the critical distance $R_o = 55$ Å; the absorption ratio $\beta = 22$, the fluorescence decay time for neat Oxazine 4 (a) 1.42 ns, (b) 1.45 ns, (c) 1.47 ns, (d) 1.5 ns, (e) 1.51 ns at the respective concentrations

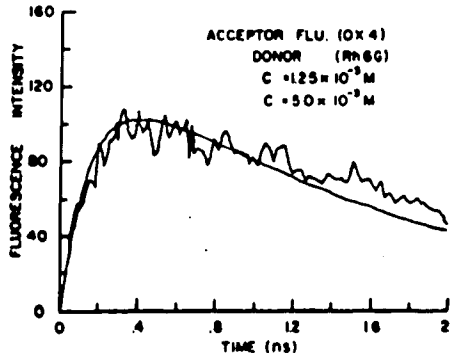

Fig. (a)

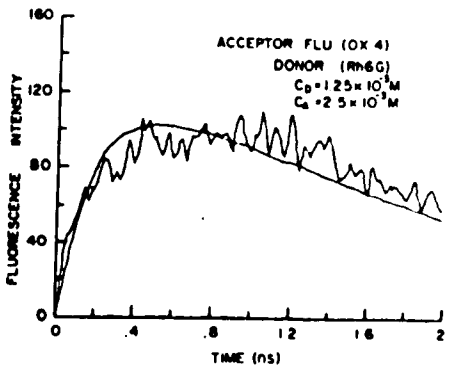

Fig .(b)

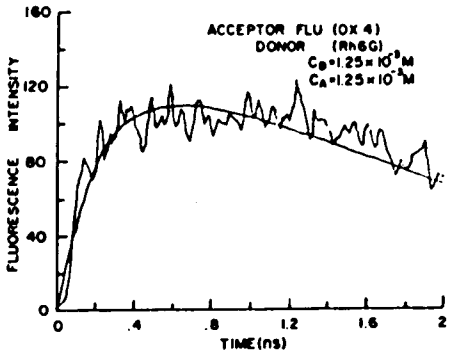

Fig (c)

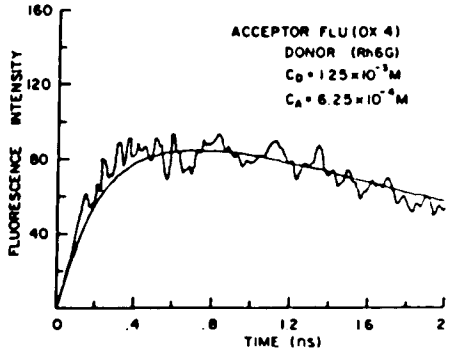

Fig (d)

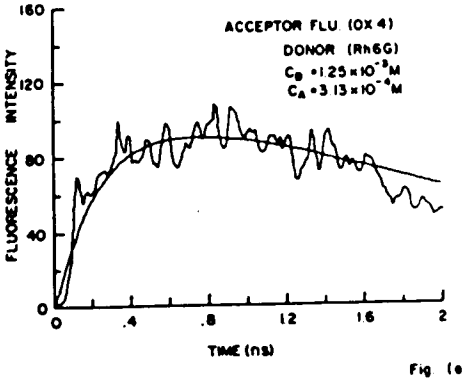

Fig (e)

Fig. 5.7 Experimental measurement of fluorescence profiles of Rhodamine B (530 nm $< \lambda <$ 620 nm) at a concentration of 1.25×10^{-3} M mixed with Nile Blue A Perchlorate at different concentrations (a) 5×10^{-3} M, (b) 2.5×10^{-3} M, (c) 1.25×10^{-3} M, (d) 6.25×10^{-4} M, and (e) 3.13×10^{-4} M in ethylene glycol. The filters used are Corning 3-67 and Ditric short pass filter at 620 nm. The measurements are fitted by a solid line generated by equation (5.1). The parameters used to fit the data are: the system risetime of 80 ps, the critical distance $R_o = 48$Å, the absorption ratio 17.5, the fluorescence decay time 1.62 ns for RhB, and fluorescence decay times for neat Nile Blue A Perchlorate (a) 0.73ns, (b) 0.75 ns, (c) 0.76 ns, (d) 0.77 ns, and (e) 0.77 ns.

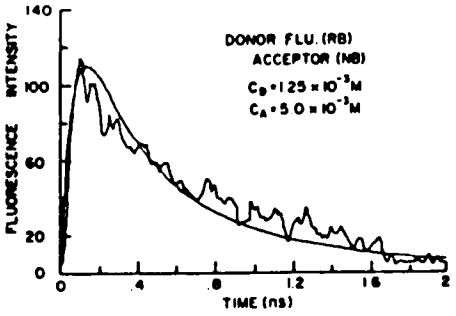

Fig (a)

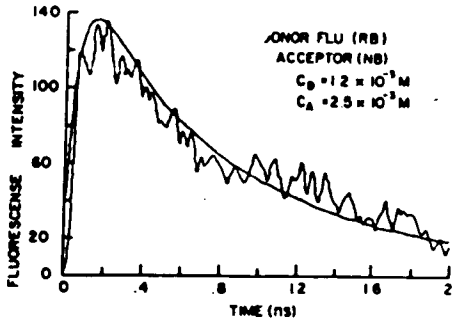

Fig (b)

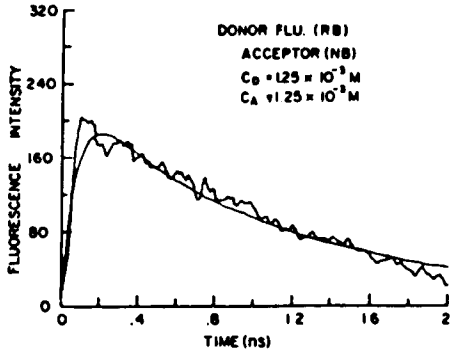

Fig (c)

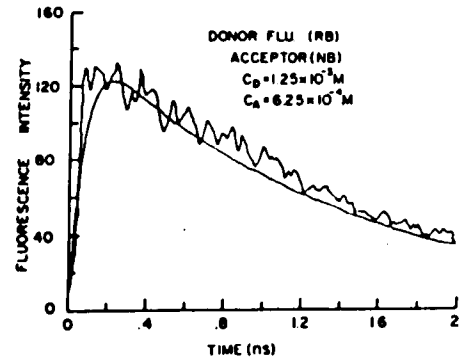

Fig (d)

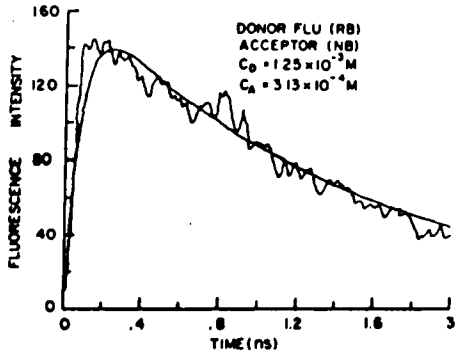

Fig (e)

Fig. 5.8 Experimental measurement of fluorescence profile of Nile Blue A Perchlorate ($\lambda > 680$ nm) at different concentrations (a) 5×10^{-3} M, (b) 2.5×10^{-3} M, (c) 1.25×10^{-3} M, (d) 6.25×10^{-4} M, and (e) 3.13×10^{-4} M mixed with Rhodamine B at a concentration of 1.25×10^{-3} M in ethylene glycol. The filters used are Corning 3-67 and Hoya R68 filters. The measurement is fitted by a solid line generated by equation (5.2). The parameters used to fit the data are the same as fig. 5.7

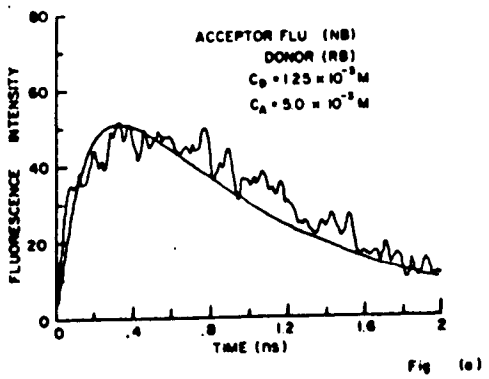

Fig (a)

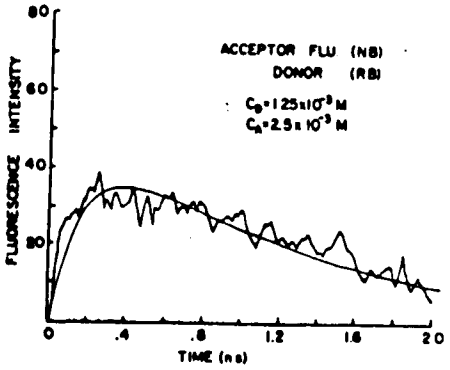

Fig (b)

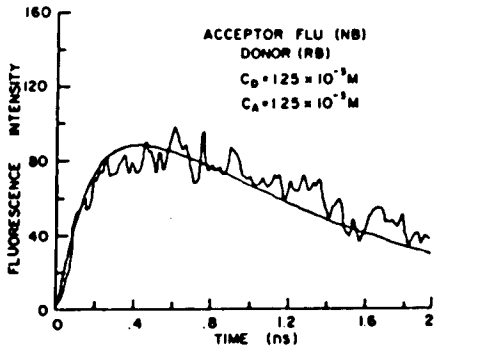

Fig (c)

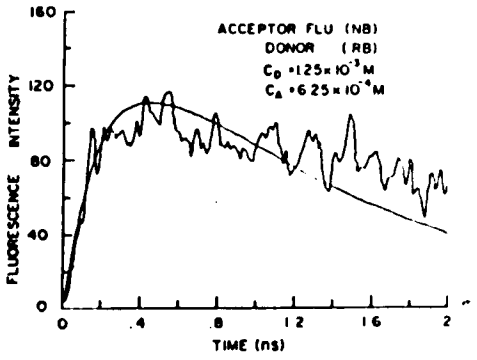

Fig (d)

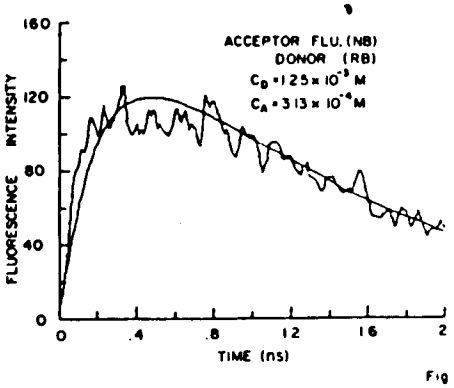

Fig (e)

Rhodamine B and Nile Blue A Perchlorate are shown in figures 5.7 and 5.8. The parameter R_o used in the fittings are 55Å ± 1Å and 48Å ± 2Å for the pair Rh6G and Ox.4, and Rh.B and N.B., respectively.

The risetime of fluorescence of Rhodamine 6G is too fast to be resolved[1] (see figure 5.9(a)) on order of 1 psec. Basically, the observed "risetime" of the time-resolved fluorescence profile of the donor reflects the system response function of the detection system which is 80 ps. The slope of the beginning portion of the time-resolved fluorescence profile of donors mixed with various concentrations of acceptors appears steep. This means the donor in the different acceptor concentrations has a similar tendency to be pumped by the laser. The reason that the peak of fluorescence profile of the donors shifts a little in the mixtures with diluted concentrations of acceptors is because of the longer decay time of donor occurring in these cases.

The decay time is defined as the time period between the peak intensity and its 1/e value. In figure 5.9(b), the decay times for the fluorescence profile of Rh6G (donor) in the solution with different concentrations of acceptors are found to decrease as the concentration of Ox.4 (acceptor) increases. This decrease occurs because there is more energy transferred to the acceptor molecules surrounding the donor molecule. At the higher concentration, the average distance between molecules becomes shorter and below

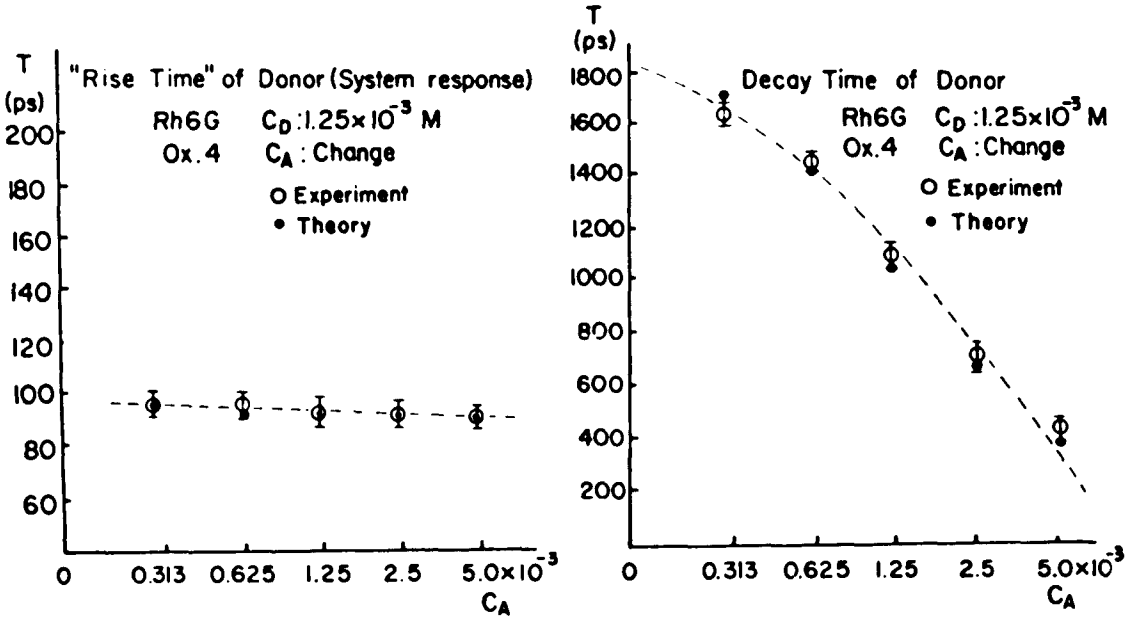

Fig. 5.9 (a) The observed "risetime" of the donor (R6G) at 1.25×10^{-3} M mixed with various concentrations of acceptor (Ox4). This risetime only reflects the system response time (80 ps on the 3.1 ns time scale.

(b) 0: Experimental measurement of decay time (1/e time) of fluorescence profile of Rhodamine 6G at a concentration of 1.25×10^{-3} M mixed with Oxazine 4 Perchlorate at different concentrations from 3.13×10^{-4} M to 5×10^{-3} M in ethylene glycol.
.: the decay time deduced from the theoretical fitting curves

R_o^{DA}. Therefore, there is more efficient long range energy transfer. This causes a faster decay of the excited electronic state of donor molecules. The time separation between the peak intensity and the starting point of the fluorescence profile of the acceptors becomes much longer than that in the neat solution of acceptors. In figure 5.10(a), the risetime of the peak intensity of the fluorescence profile of Ox.4 (acceptor) is more than 400 ps in the mixed solution, which is much longer than the risetime of Ox.4 in neat solution of 80 ps (the response time). The time separation of peak intensity of the fluorescence profile of the acceptor has a tendency to become even longer in the diluted concentration of acceptors. This arises from reduction in the energy transfer from the donor to the acceptor in the diluted case of acceptor in comparison to a faster long range energy transfer in the concentrated case of acceptor. Overall, the decay time (1/e time) of the fluorescence profile of Ox.4 (acceptor) in the binary mixture is longer than that of Ox.4 (1.5 ns) in the neat solution. This is shown in figure 5.10(b). The increased decay time occurs because the donor acts as an energy source which pumps the acceptor molecules causing them to emit longer. According to concentration quenching, the decay time decreases as the concentration increases. Similar results are shown in figures 5.11 and 5.12 for the binary mixture of Rhodamine B and Nile Blue A Perchlorate.

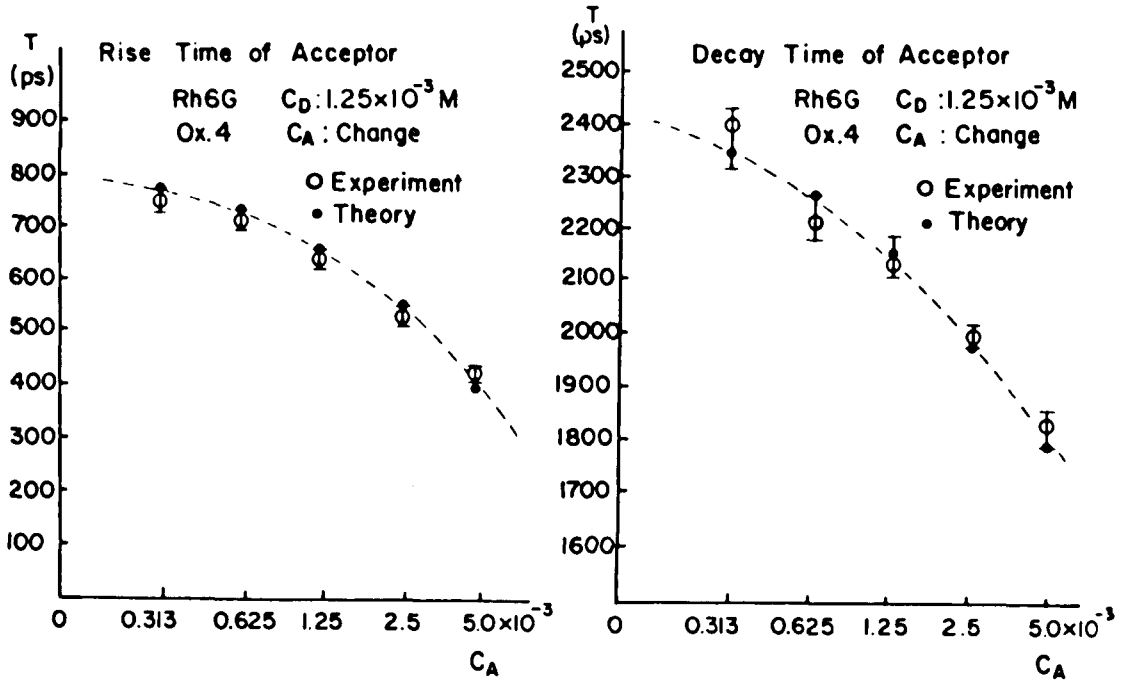

Fig. 5.10 (a) 0: Experimental measurement of time separation between peak intensity and starting point of fluorescence profile of Oxazine 4 Perchlorate at different concentrations from 3.13×10^{-4} M to 5×10^{-3} M mixed with Rhodamine 6G at a concentration of 1.25×10^{-3} M.
.: the time separation between the peak intensity and starting point of the theoretical fitting curve.
(b) 0: Experimental measurement of decay time of fluorescence profiles of Oxazine 4 Perchlorate at different concentrations from 3.13×10^{-4} M to 5×10^{-3} M mixed with Rhodamine 6G at a concentration of 1.25×10^{-3} M in ethylene glycol.
.: the decay time deduced from the theoretical curves

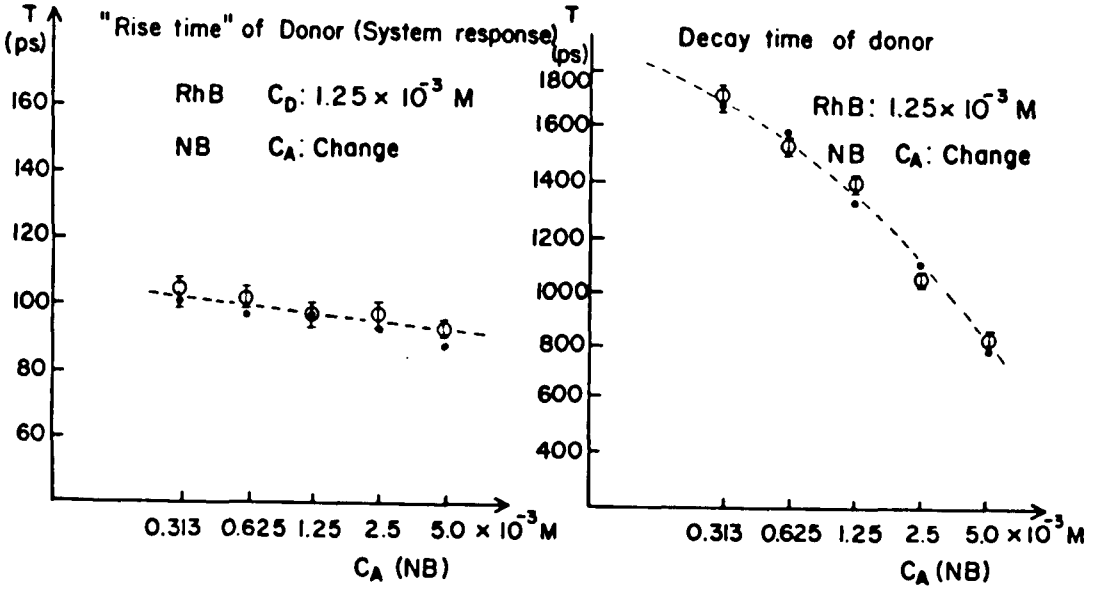

Fig. 5.11 (a) The observed "risetime" of the donor (RB) at 1.25×10^{-3} M mixed with various concentrations of the acceptor (NB). This risetime reflects the system response time (~80 ps).

(b) 0: Experimental measurement of decay time (1/e time) of fluorescence profile of RB at a concentration of 1.25×10^{-3} M mixed with NB at different concentrations from 3.13×10^{-4} M to 5×10^{-3} M in ethylene glycol.

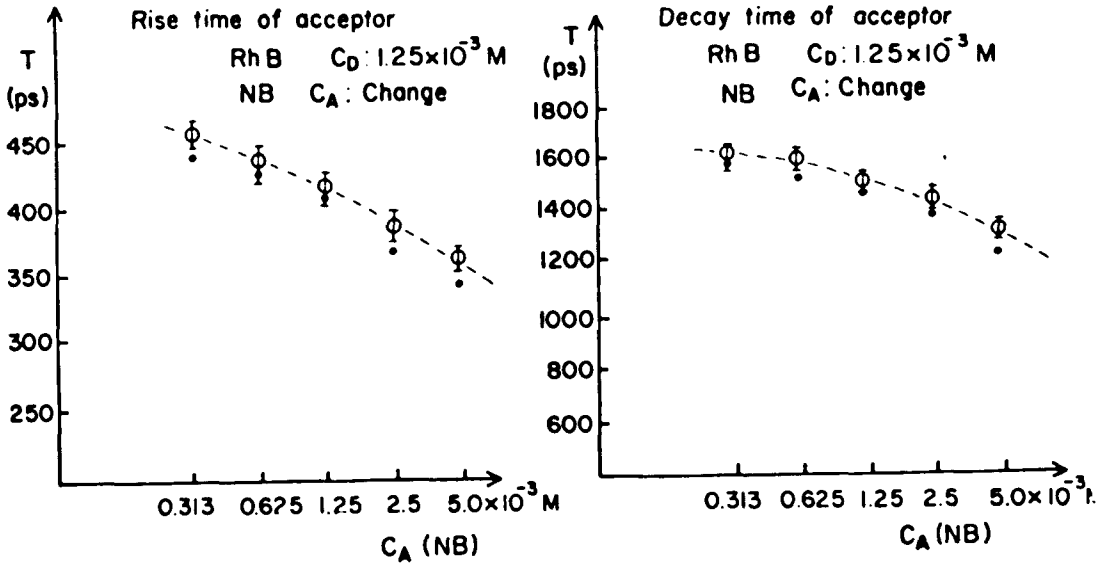

Fig. 5.12 (a) 0: Experimental measurement of time separation of peak intensity of fluorescence profile of NB at different concentrations from 3.13×10^{-4} M to 5×10^{-3} M mixed with RB at a concentration of 1.25×10^{-3} M.
.: the time separation of peak intensity of the theoretical fitting curves.
(b) 0: Experimental measurement of the decay time of the fluorescence profiles of NB at different concentrations from 3.13×10^{-4} M to 5×10^{-3} M mixed with RB at a concentration of 1.25×10^{-3} M in ethylene glycol.
.: the decay time deduced from the theoretical curves

The efficiency of long range energy transfer determined by equations (5.3) and (5.4) are displayed in tables II and III for Rhodamine 6G-Oxazine 4 Perchlorate and Rhodamine B-Nile Blue A Perchlorate, respectively. The experimental results of the energy transfer efficiency are also included in tables II and III for Rh6G-Ox4 and RhB-NB, respectively. These values are plotted in figures 5.13 and 5.14. We find the theoretical model we developed (eq. 5.3) is in better agreement with the experimental data than those obtained from the Forster version given by equation (5.4) for an average energy transfer distance due to the Forster mechanism.

The value of R_o^{DA} in the pair of Rh6G-Ox4 (55A) is larger than that of the pair of RB-NB (48A). Accordingly, the estimation of η_E by equation (5.4), is a little larger in the diluted concentration case of acceptor for the pair of Rh6G-Ox4 and is a little smaller in the concentrated concentration case of acceptor for the pair RB-NB. If we define R_o to be the critical distance at which there is 50% efficiency of energy transfer by equation (5.4), then the values of R_o^{DA} evaluated from figure 5.13 and 5.14 are 54.1 and 49.5 Å for Rh6G-Ox4 and RB-NB, respectively. These values are close to the values of R_o obtained from curve fitting, which are 55 and 48 Å, respectively.

5.4 Discussion and Summary

The steady state fluorescence spectra of the binary mixture solution of donor at a fixed concentration and

Table II

Concentration C_D=1.25×10^{-3} / C_A	Energy Transfer Efficiency (η_E)		
	Experiment Result O	Calculated by Eq.(3) •	Calculatet by Eq.(4) Δ
3.13×10^{-4}M	16.4±3%	16.5 %	30%
6.25×10^{-4}M	27.2±3%	31.0 %	39%
1.25×10^{-3}M	47.7±6%	52.0 %	53%
2.5×10^{-3}M	72.0±7%	68.0 %	71 %
5.0×10^{-3}M	81.5±9%	88.0 %	87%

Table II Energy transfer efficiency between the donor (Rh6G) and the acceptor (Ox.4) in different concentration solution

Table III

Concentration $\frac{C_D=1.2\times10^{-3}}{C_A}$	Energy Transfer Efficiency (η_E)		
	Experiment Result O	Calculated by Eq.(3) •	Calculated by Eq.(4) Δ
3.13×10^{-4} M	15 ± 4 %	14.7 %	15.7 %
6.25×10^{-4} M	20 ± 1 %	24.6 %	21.6 %
1.25×10^{-3} M	41 ± 5 %	40.4 %	33.1 %
2.5×10^{-3} M	64 ± 4 %	61.2 %	52.2 %
5.0×10^{-3} M	81 ± 6 %	80.98 %	75.4 %

Table III Energy transfer efficiency between the donor (RB) and the acceptor (NB) in different concentration solution

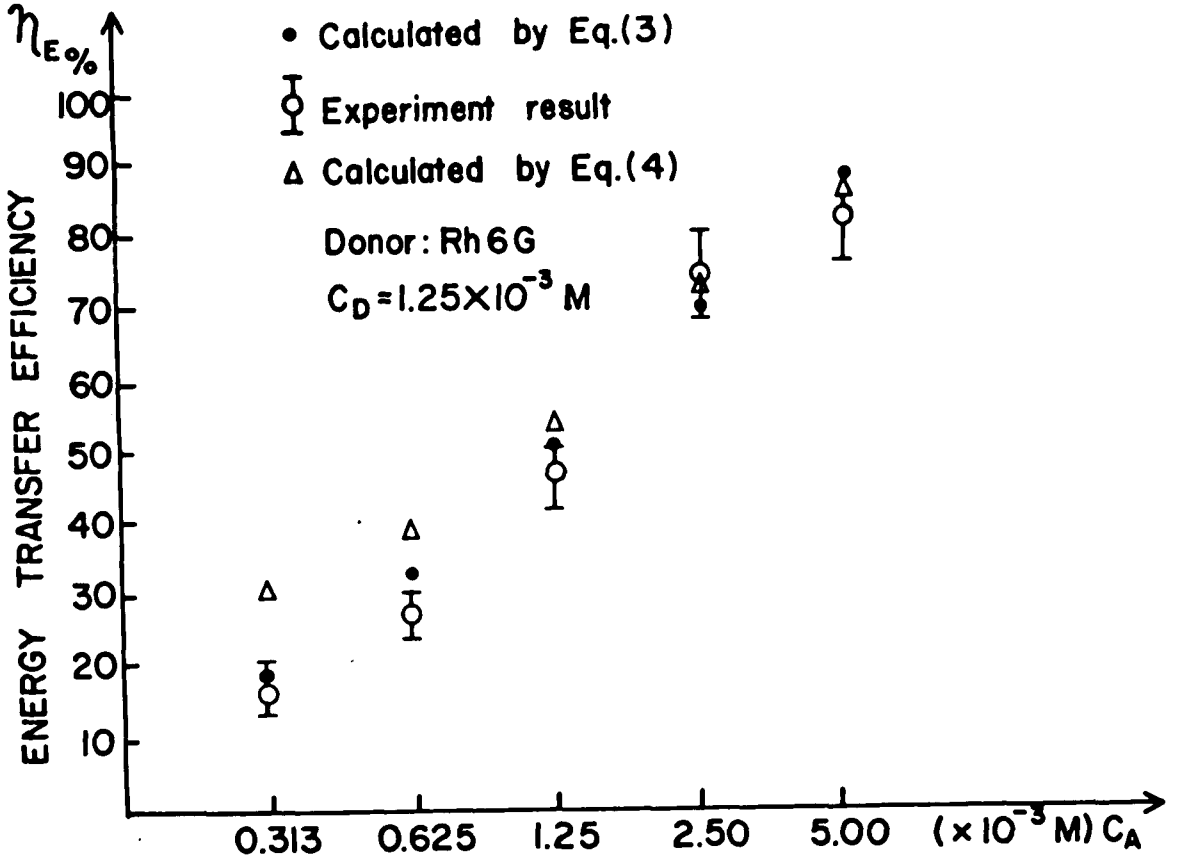

Fig. 5.13 0: Experimental measurements of the efficiency of long range energy transfer for Rh6G and Ox4 in different concentrations
.: theoretical calculations of the efficiency of energy transfer by equation (5.3).
▲: theoretical estimations of the efficiency of energy transfer by equation (5.4)

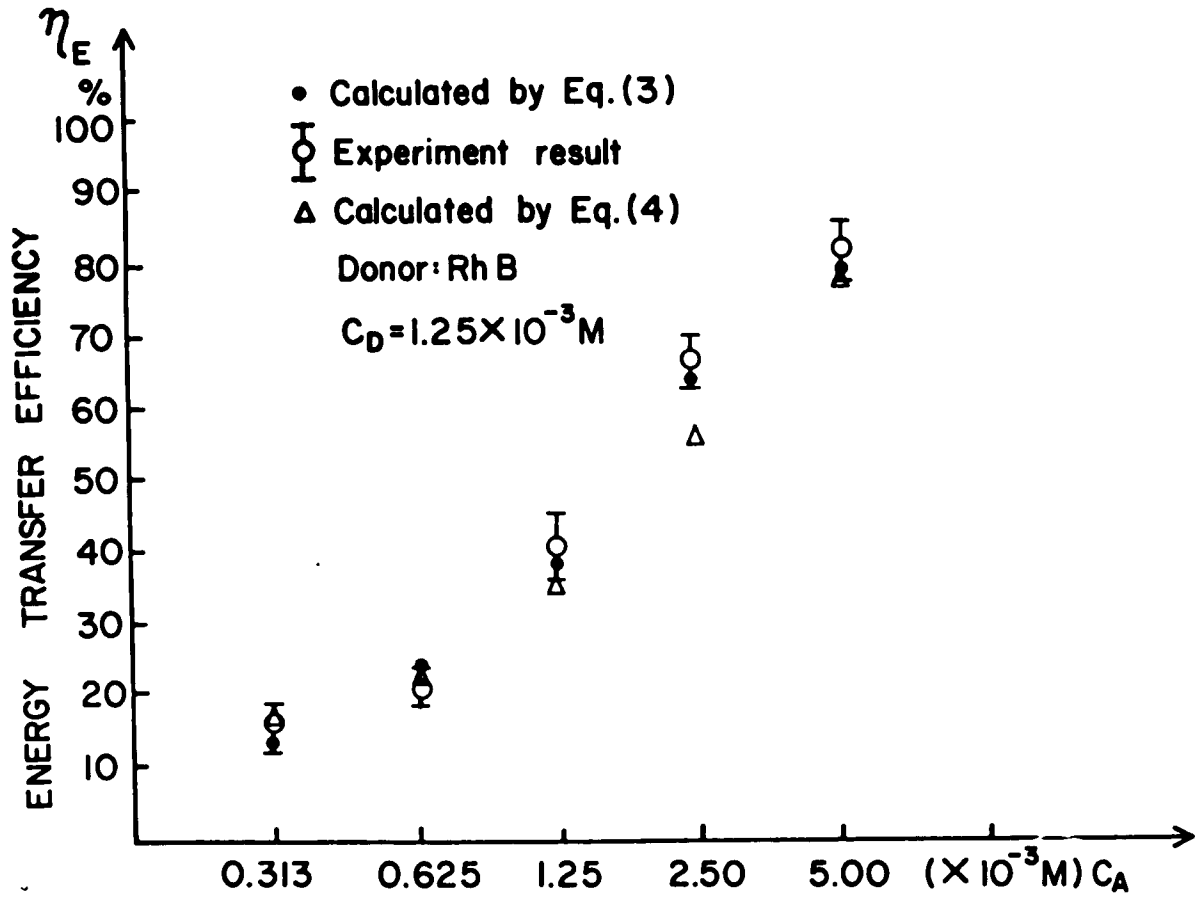

Fig. 5.14 0: Experimental measurement of the efficiency of long range energy transfer for RB and NB in different concentrations.
.: theoretical calculation of efficiency of energy transfer by equation (5.3).
Δ: theoretical estimation of efficiency of energy transfer by equation (5.4)

acceptors at various concentrations were measured. The picosecond time-resolved fluorescence profiles for donor and acceptor molecules were measured by a picosecond laser pulse excitation and streak camera detection system. The risetimes and decay time of the donor and acceptor molecules were determined for the different mixtures. A comparison of these times from calculated values fits well for different concentrations of acceptors. The energy transfer efficiency was measured and calculated. The data are in excellent agreement with our theory for the spatial average over the distance between acceptor and donor molecules in the theoretical expressions given for D(t), A(t) and η_E. We found that the higher efficiency of energy transfer occurs when the donor and acceptor molecules become close enough so that $\overline{R^{DA}} < R_o^{DA}$. Physically, this is due to the stronger long range interaction between the donor and acceptor molecules in the higher concentration cases. In addition, efficient energy transfer occurs when there is more overlapping of the emission spectrum of the donor and the absorption spectrum of the acceptor. The theoretical fitting parameters R_o for each case are the same values used in previous chapter. The theoretical model presented in previous chapter (equations (5.1) and (5.2)) fits the data well for the various concentrations. The concentration dependence in the spatial average calculation is involved in the argument of the exponential term in equation (5.3).

Thus, the efficiency of transfer calculated by equation (5.3) is more accurate and closer to real value than equation (5.4). However, in equation (5.4), the concentration dependence is given by the mean distance R between the molecules.

To check the possibility of a long range energy transfer between donors, a solution, in the condition for which the donor-donor transfer dominates over donor-acceptor transfer, was prepared with a high concentration of the Rh6G (donor) at 5×10^{-3}M mixed with a low concentration of the Ox4 (acceptor) at 1.25×10^{-5}M. The Ox4 acceptor was supposed to probe the D-D transfer.[2] Unfortunately, the fluorescence of the acceptor was so weak that no signal was detected at all. The fluorescence of donor in the binary mixture solution in this case is similar to that in the neat solution at the same concentration 5×10^{-3}M. As we pointed out in last chapter, we chose the pair of donor and acceptor to enhance the long range energy transfer and to reduce the possibility of D-D transfer to a negligible value. Since the absorption of laser beam by the donor molecule is large and the critical transfer distance R_o^{DA} for a donor-acceptor pair is larger than critical distance R_o^{DD} for a donor-donor pair and $R_o^{DD} < \overline{R^{DD}}$, we conclude that donor-donor energy transfer is negligible in samples in our study. Furthermore, these samples are excellent for the study of long range energy transfer between donor-acceptor

binary systems. Our theoretical model is in excellent agreement with the experimental measurements both qualitatively and quantitatively.

SUMMARY

We have completed a detailed study of the energy transfer between donor and acceptor systems via the Forster dipole-dipole interaction. Extension of our previous research to a concentration dependence has confirmed our previous theory and experiments. This has given us a more detailed description of energy loss of the donor with a strong or weak interaction with acceptors at different concentrations. We not only found a decrease of the relaxation decay time of the donors, but also observed a decrease in risetime of the acceptors in the presence of an increase of concentration of acceptors. Both indicate energy transfer. An important point to note is the risetime of the acceptor does not match the decay time of the donor. Our theory fits the rise and decay time data well. This is the first study to measure the efficiency of energy transfer and present theoretical calculations for both donor and acceptors. Diffusion effects on the energy transfer mechanism will be presented in the next chapter.

Reference

1. A. Penzkofer, W. Falkenstein, and W. Kaiser, Chem. Phys. Lett. 44, 82 (1976).

2. D. P. Millar, R. J. Robbins, and A. H. Zewail, J. Chem. Phys. 75, 3649 (1981).

CHAPTER 6 DIFFUSION EFFECTS ON THE LONG RANGE ENERGY TRANSFER BETWEEN DONOR AND ACCEPTOR DYES IN SOLUTION INVESTIGATED WITH PICO-SECOND FLUORESCENCE SPECTROSCOPY

6.1 In the previous chapters, we have investigated long range energy transfer dynamics between molecules in binary solution mixtures using steady state and time-resolved fluorescence spectroscopy. We found an excellent consistency between our theoretical model and our experimental results. The critical distance, Ro, and the efficiency of energy transfer were determined for two binary systems: (1) rhodamine 6G (the donor) and oxazine 4 perchlorate (the acceptor), and (2) rhodamine B (the donor) and nile blue A perchlorate (the acceptor) dissolved in ethylene glycol at room temperature.[1,2] The experimental results show the long range energy transfer efficiency depends on the critical distance R_o and the concentration of the solution[1,2]. The relative absorption cross section of the donor and acceptor and the decay time of the donor and acceptor also affect the energy transfer[1,2]. In these studies the translational diffusion constant for the xanthane and oxazine dyes in ethylene glycol is less than $10^{-6}cm^2/sec$. Since the fluorescence lifetimes are of the order of 1 ns, the diffusion length in this case is less than 3Å. Therefore, the diffusion effects were neglected in our previous research in chapters 4 and 5. The extention to a diffusion

study on the energy transfer process is interesting if the viscosity of the solvent is small so that the translational diffusion of the donor molecule should be taken into account to the energy transfer. In this chapter, we have performed measurments and theoretical calculations on the kinetics of energy transfer between donor (rhodamine 6G) and acceptor (oxazine 4 perchlorate) molecules including the effect of diffusion at different temperatures.

6.2 Theoretical Review

Galanin[3] developed a theoretical model based on the Forster Mechanism[4-6] to study the long range resonance energy transfer assuming immobile molecules in viscous solutions. Waite[7] genelized the random walk diffusion of particles to a continuum of positions in the differential equation describing the energy transfer between the donor and the acceptors. Kurskii et al.[8] considered the Brownian motion of molecules and formulated the kinetic equation for the energy transfer. Later, Samson[9] et al and other investigators[10-12] included the effect of diffusion transfer to describe the rate change for the concentration of donors in the study of resonance energy transfer. Yokota and Tanimoto[13] used the Pade approximation in solving the transformed differential equations for the distribution functions of excited molecules of donor and

acceptor molecules in the study of energy transfer with the effect of diffusion. They obtained a complicated time-dependent decay function of the excited donors. Furthermore, Gosele[14-16] obtained a simpler functional form of for the decay of the donors. Recently, Millar[17] et al. have used the result of Gosele[14-16] to satisfactorily fit their measurements for the energy transfer including translation between donors and acceptors.

The translational diffusion term can be added to our theoretical model [1,2] of the study of energy transfer between molecules in a solvent with low viscosity. The equations describing the energy dynamics for photoexcited donors in chapter 3 are modified to take into account diffusion as follows:

$$\dot{D}_{2n} + \rho_D D_{2n} = \sigma_D I_0 \delta(t) \tag{6.1}$$

$$\dot{D}_{1n} + (\gamma_D + \Gamma_D) D_{1n} = \rho_D D_{2n} - \sum_m^{NA} \delta_{nm} D_{1n} + \partial \nabla^2 D_{1n} \tag{6.2}$$

where

$I_0\delta(t)$=ultrashort laser pulse (I_0=number of photons/area)

D_{jn} =probability for the nth donor molecules to be in the jth vibronic excited state of S_1.

ρ_D =excited state vibrational relaxation rate of the donor molecule.

σ_D =absorption cross sections in the acceptor molelcule.

γ_D =nonradiative decay rate of the donor molecule.

Γ_D =radiative decay rate of the donor molecule.

Equation (6.2) is similar to the equation (2) in Yokota et al's paper[13]. The solution to equation (6.2) is given by a complicated form. However, Gosele[14-16] found a much simpler form for the solution to this kind of equation without loss of accuracy. Therefore, we adopt the Gosele's treatment and the fluorescence per unit volume for the donor is:

$$\frac{\phi(t)}{\Gamma_D \sigma_D I_0} = n_D \rho_D \int_0^t d\tau \exp\left[-\rho_D(t-\tau) - g_D\tau - \frac{4\pi}{3} n_A \sqrt{\pi \mathcal{D}\tau} - 4\pi \mathcal{D} r_F n_A \tau\right] \tag{6.3}$$

where $n_D = \frac{N_D}{V}$ = number of donors per unit volume,

$$r_F = 0.676 \left(\frac{R_0^6}{\tau_D \mathcal{D}}\right)^{\frac{1}{4}}$$

δ_{nm} = transfer rate from the nth donor to the mth acceptor,

$$= \frac{1}{\tau_D}\left(\frac{R_0}{R}\right)^6$$

τ_D =fluorescence decay time of the donor,

R_0 =the critical distance at which the rate of energy transfer is equal to the sum of all other donor deactivation rates,

$\mathcal{D}$ =diffusion constant for the donors and acceptors,

$$= \frac{kT}{6\pi\eta r_D} + \frac{kT}{6\pi\eta r_A}$$

and

K =Boltzmann constant,

T =absolute temperature,

η =viscosity of the solvent,

r_D =effective radius of the donor molecule,

r_A =effective radius of the acceptor molecule.

The diffusion constant is given by Stoke's law and Einstein's relation in the sticky model[18] of viscosity of a fluid. This expression is similar to the equation in our previous paper[1,2] except for an additional term $4\pi \mathcal{D} r_F n_A \tau$ in the argument of exponential. This is the effect of the translational diffusion of molecules. Substituting the diffusion factor and equation (6.3) into the equations in chapter 3, we obtain the solution for the fluorescence per unit volume of the acceptors:

$$
\begin{aligned}
A(t) = r_A \sigma_A I_0 \Big\{ & n_D \rho_D \beta \frac{(e^{-\rho_D t} - e^{-g_A t})}{g_A - \rho_D} + n_A \rho_A \frac{(e^{-\rho_A t} - e^{-g_A t})}{g_A - \rho_A} \\
& - \left(\frac{g_D - \rho_D}{g_A - \rho_D}\right) n_D \rho_D \beta e^{-\rho_D t} \int_0^t d\tau \exp\left[(\rho_D - g_D)\tau - \frac{4\pi}{3} n_A \sqrt{\pi \Delta \tau} - 4\pi \mathcal{D} r_F n_A \tau\right] \\
& + \left(\frac{g_D - \rho_D}{g_A - \rho_D}\right) n_D \rho_D \beta e^{-g_A t} \int_0^t d\tau \exp\left[(g_A - g_D)\tau - \frac{4\pi}{3} n_A \sqrt{\pi \Delta \tau} - 4\pi \mathcal{D} r_F n_A \tau\right] \\
& - n_D \rho_D \beta e^{-g_A t} \int_0^t d\tau \exp\left[(g_A - g_D)\tau - \frac{4\pi}{3} n_A \sqrt{\pi \Delta \tau} - 4\pi \mathcal{D} r_F n_A \tau\right] \Big\}
\end{aligned}
\tag{6.4}
$$

Using equations (6.3) and (6.4), the fluorescence intensity versus time were calculated for different values of the diffusion constant from room temperature to -90°C. The results are shown in figure 6.1.

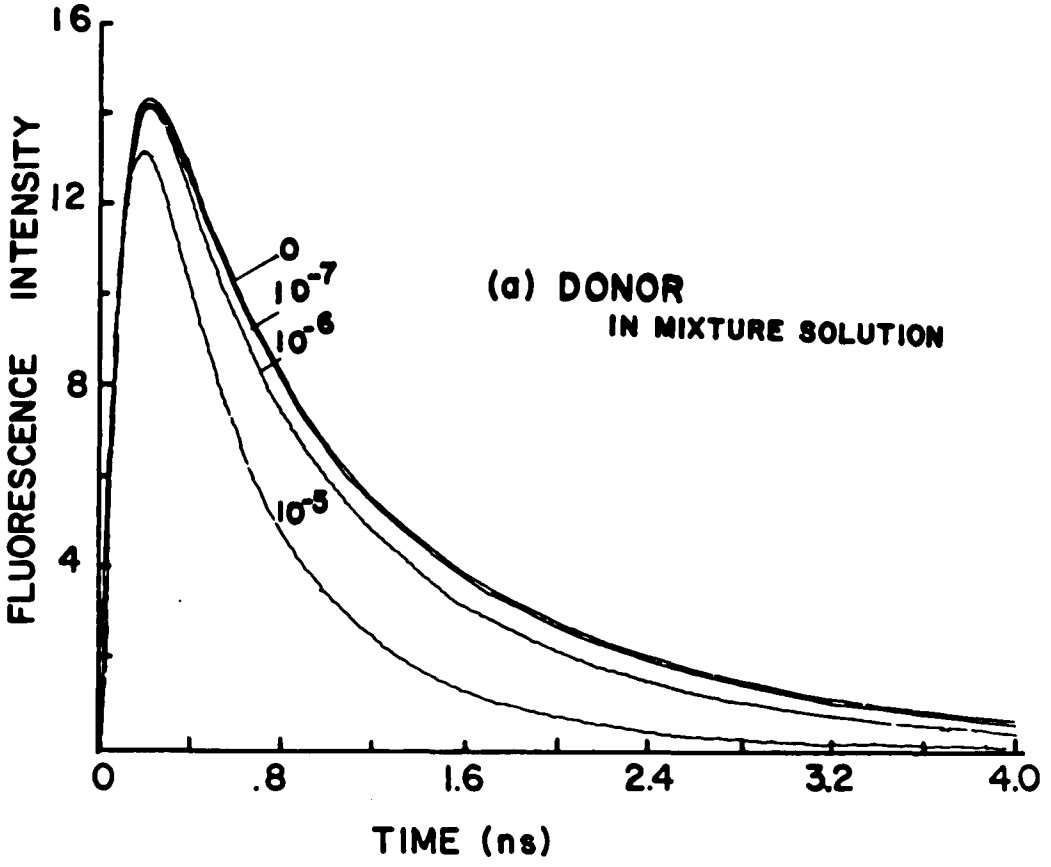

Fig. 6.1 The theoretical calculation of the fluorescence profiles versus time obtained by equations (6.3) and (6.4) for (a) donor (b) acceptor at a concentration of 1.25×10^{-3} M at different diffusion constants from 10^{-5} cm^2/sec to 0 cm^2/sec. The detection system risetime is assumed to be 80 ps considering the convolution of signal and streak camera. The critical transfer distance R_o is assumed to be 55 Å. The ratio of absorption of donor to acceptor is 22. The decay time of donor is 1.8 ns. The decay time of acceptor is 1.5 ns.

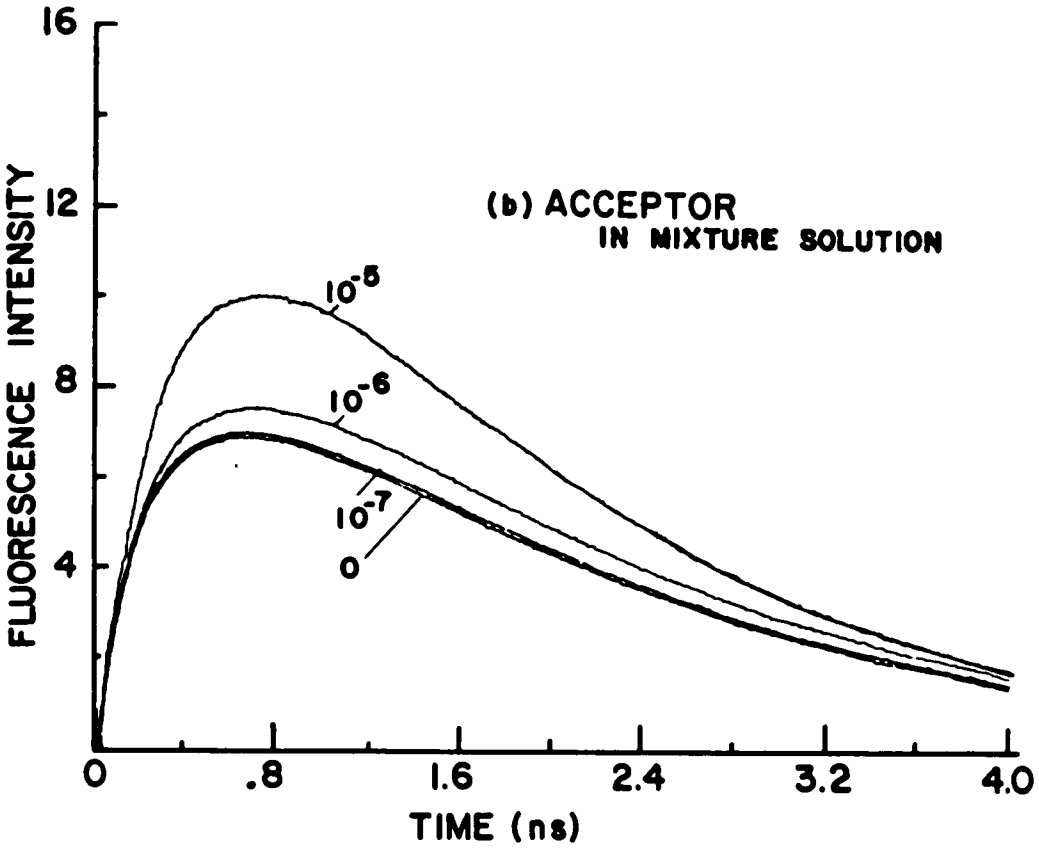
16
12
8
4
FLUORESCENCE INTENSITY
(b) ACCEPTOR
IN MIXTURE SOLUTION
10-5
10-6
10-7
0
0
.8
1.6
2.4
3.2
4.0
TIME (ns)

Fig. 6.1 (b)

From the fluorescence profiles displayed figure 6.1(a), the decay time of fluorescence of the donor molecule becomes faster and the quantum yield decreases as the diffusion constant increases. From the fluorescence profiles displayed in figure 6.1(b) the risetime and quantum yield of the acceptor molecule increases as the diffusion increases. Basically, the energy deactivation of the donors is due to the long range energy transfer to the acceptor. Diffusion helps in moving the donors and acceptors effectively closer, so that energy can be transferred to the acceptor more readily.

For a neat solution of rhodamine 6G (or oxazine 4 perchlorate), the intensity versus time is described by the equation (6.5)(R_0=0)

$$F(t) = \frac{\rho_F}{\rho_F - g_F}\left[e^{-g_F t} - e^{-\rho_F t}\right] \qquad (6.5)$$

The efficiency of energy deactivation of the donor molecule taking into account the diffusion effect is defined to be

$$\epsilon_1 = 1 - \frac{\int_0^\infty\int_0^t d\tau dt \exp\left[-\rho_D(t-\tau) - g_0\tau - \frac{4\pi}{3}n_A\sqrt{\pi\Delta\tau} - 4\pi\Delta r_F n_A \tau\right]}{\int_0^\infty\int_0^t d\tau dt \exp\left[-\rho_D(t-\tau) - g_0\tau\right]} \qquad (6.6)$$

We also define the efficiency of energy deactivation without the diffusion effect to be

$$\epsilon_2 = 1 - \frac{\int_0^\infty\int_0^t d\tau dt \exp\left[-\rho_D(t-\tau) - g_D\tau - \frac{4\pi}{3}n_A\sqrt{\pi\Delta\tau}\right]}{\int_0^\infty\int_0^t d\tau dt \exp\left[-\rho_D(t-\tau) - g_D\tau\right]} \qquad (6.7)$$

The contribution of the diffusion effect on the long range energy transfer can be evaluated by the following equation:

$$f_d = 1 - \frac{\int_0^\infty \int_0^t d\tau dt \, exp[-\rho_D(t-\tau) - g_D\tau - \frac{4\pi}{3} n_A \sqrt{\pi D \tau} - 4\pi D r_F n_A \tau]}{\int_0^\infty \int_0^t d\tau dt \, exp[-\rho_D(t-\tau) - g_D\tau - \frac{4\pi}{3} n_A \sqrt{\pi D \tau}]} \quad (6.8)$$

The value of f_d will be zero when there is no diffusion (D =0). The total efficiency of energy deactivation can also be obtained from the sum of the efficiency of energy deactivation without diffusion (long range energy transfer) and the partial contribution due to diffusion according to the relation

$$\epsilon_3 = \epsilon_2 (1 + f_d) \quad (6.9)$$

The value obtained from ϵ_3 can be compared to the value obtained from ϵ_1 .

6.3 Samples

Laser-grade dyes of rhodamine 6G and oxazine 4 perchlorale from the Eastman Kodak Company were dissolved in 1-propanol without further purification. The solution of single component dyes and binary mixtures of two kinds of dyes were made at a concentration of 1.25×10^{-3} M. The average distance R between the donor-acceptor molecules in the mixed solution is 54.1Å. The mean distance between the like molecules (donor and donor, or acceptor and acceptor) is 68.2Å. The value of the critical transfer distance R_o

from the spectroscopic data of the fluorescence spectrum of the donor and the absorption spectrum of the acceptor is 56 Å. The solution was contained in a 1 mm or 2 mm optical path cuvette. The cuvette was put in an optical dewar with a nitrogen gas flow around it. The temperature of the sample was controlled by the flow rate of cooled nitrogen gas and read from a Keithley 177 digital microvoltmeter connected with a copper constantan thermocouple. The temperature was lowered from room temperature to - 90°C. The temperature versus viscosity[19] and diffusion constant of 1-propanol from table IV is displayed in figure 6.3. The ratio of the absorption cross section β at λ = 527 nm for rhodamine to that of oxazine 4 perchlorate was measured to be 22. At this high absorption ratio there will be little direct excitation of acceptor by the laser pulse.

6.4 Experimental and Theoretical Results

Typical time-resolved fluorescence profiles emtted from neat rhodamine 6G and oxazine 4 perchlorate in 1-propanol at 25°C and at -90°C are displayed in figures 6.3 and 6.4. The decay time of R6G and oxazine 4 perchlorate are about 1.8ns and 1.50 ns at room temperature. Similarly, at - 90°C by fitting single exponential profiles for neat rhodamine 6G and oxazine 4 perchlorate we obtain fluorescence decay times for neat R6G and ox 4 of 2.2 and 2.1 ns at -90°C, respectively. Using the value of temperature and

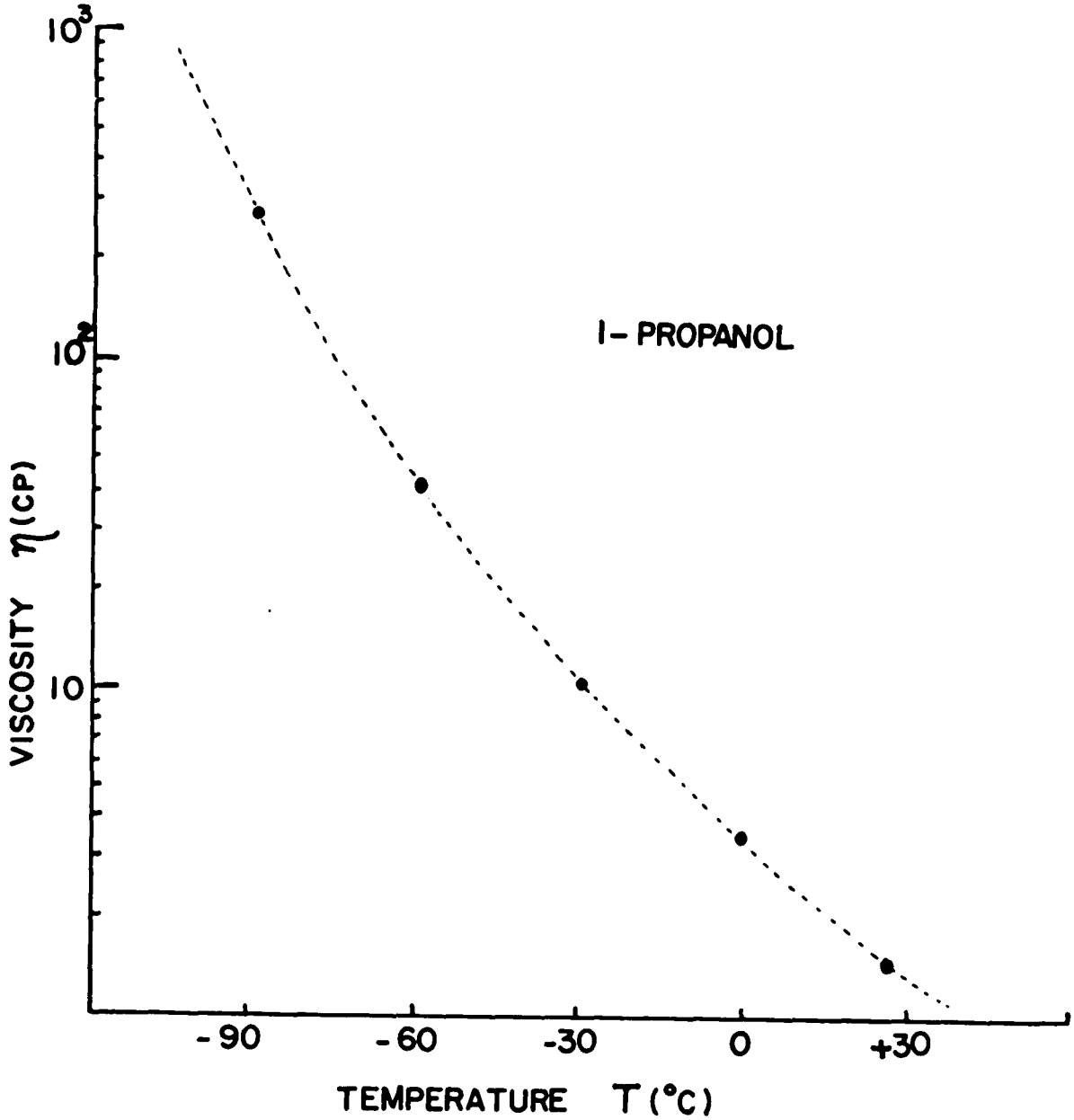

Fig. 6.2 The relation between the viscosity and temperature, and the diffusion constant and temperature are shown in (a) and (b) respectively

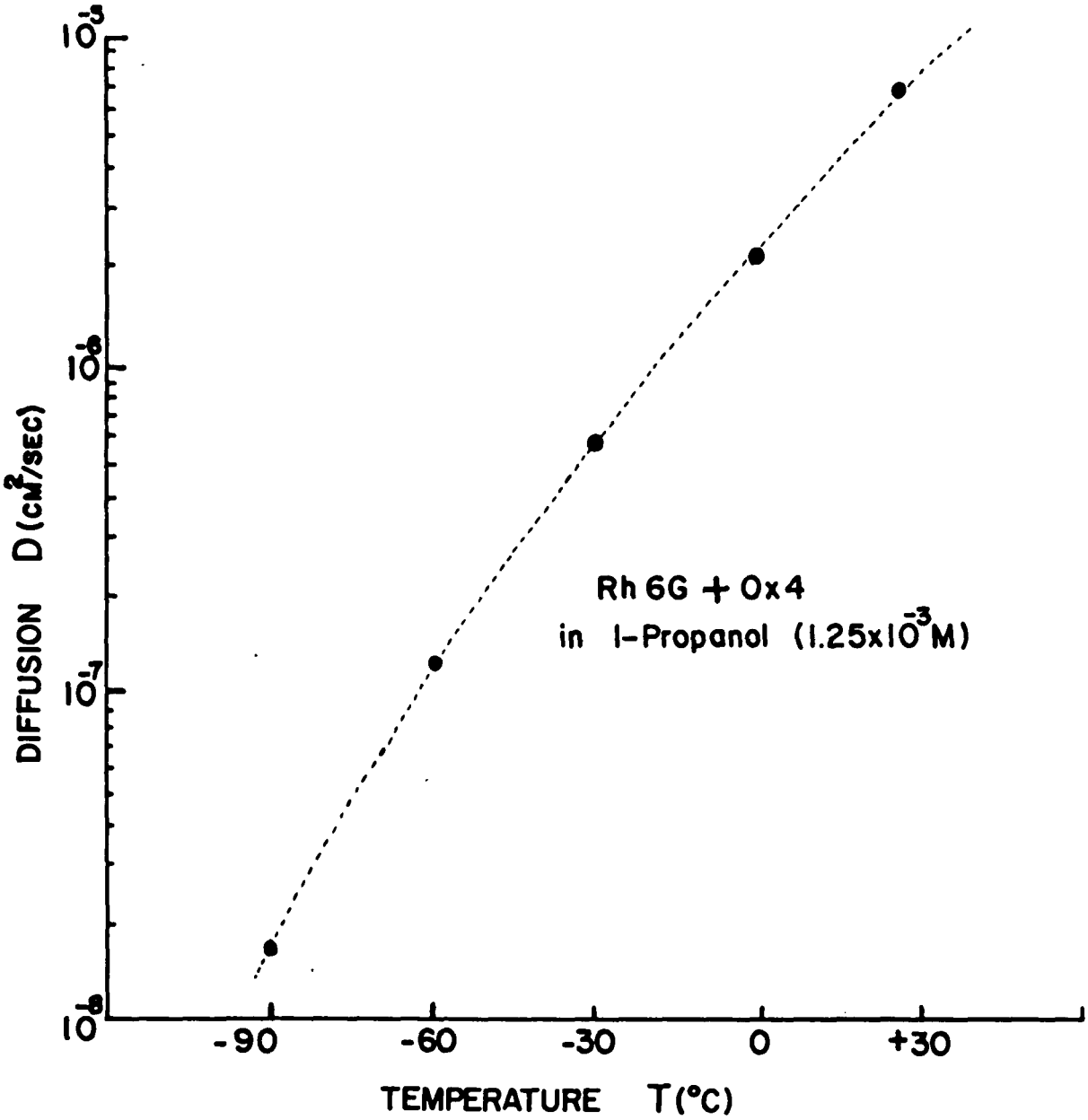
DIFFUSION D (cm²/sec)
10⁻⁵
10⁻⁶
10⁻⁷
10⁻⁸
Rh 6G + Ox4
in I-Propanol (1.25x10⁻³M)
-90
-60
-30
0
+30
TEMPERATURE T(°C)

Fig. 6.2 (b)

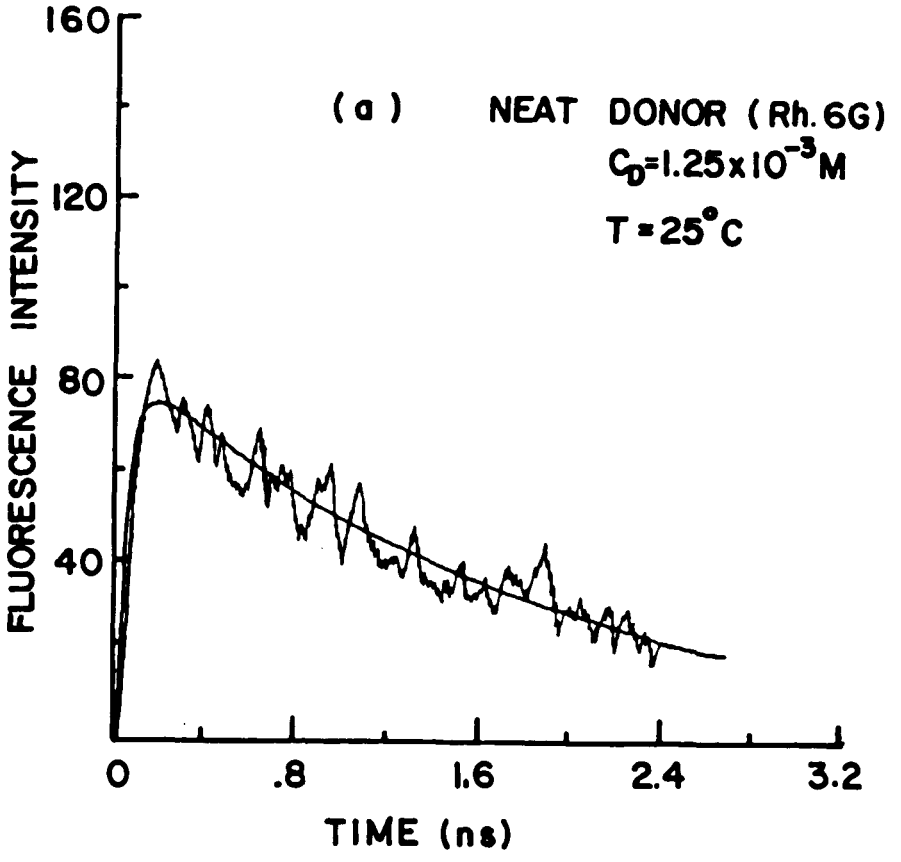

Fig. 6.3 Experimental measurement of the time-resolved fluorescence profiles of neat rhodamine 6G (530 nm $<\lambda<$ 600 nm) at a concentration of 1.25×10^{-3} M in 1-propanol at (a) room temperature (b) -90°C. The measurements are fitted by a solid line generated by equation (6.5). The decay time on the fitting is found to be 1.8 and 2.2 ns for figure (a) and (b) respectively.[1,2] The system risetime response is 80 ps.

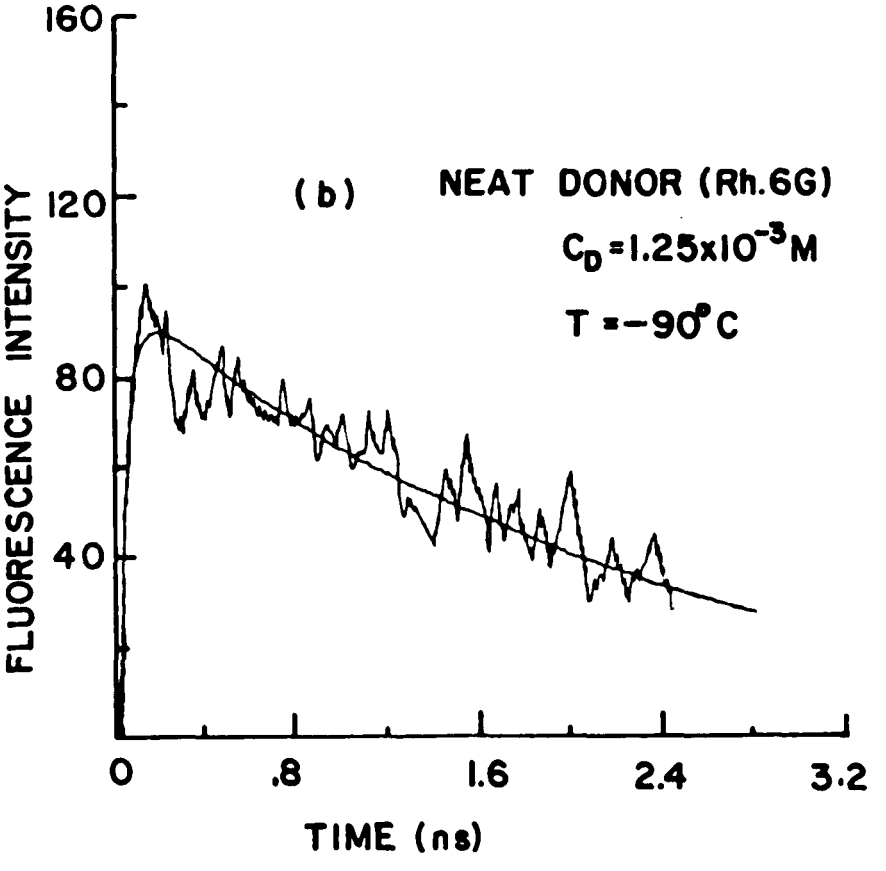
160
120
80
40
FLUORESCENCE INTENSITY
(b)
NEAT DONOR (Rh.6G)
$C_D = 1.25 \times 10^{-3} M$
T = −90°C
0
.8
1.6
2.4
3.2
TIME (ns)

Fig. 6.3 (b)

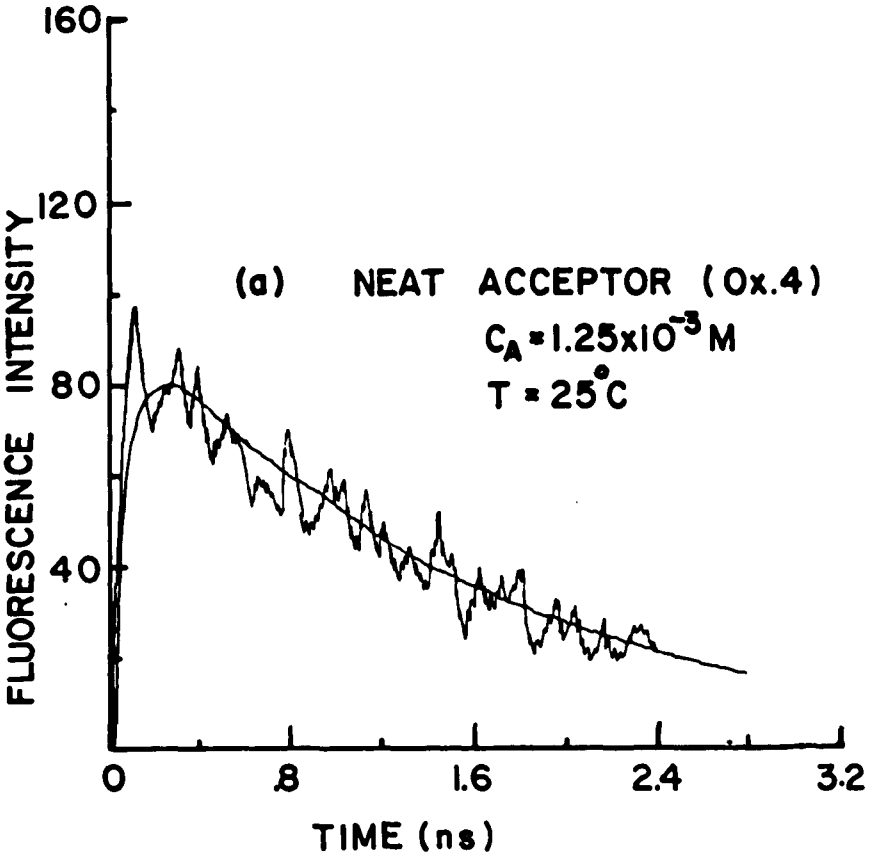

Fig. 6.4 Experimental measurement of the time-resolved fluorescence profiles of neat oxazine 4 perchlorate ($\lambda > \sim 660$ nm) at a concentration of 1.25×10^{-3} M in 1-propanol at (a) room temperature and (b) -90°C. The measurement is fitted by a solid line generated by equation (6.5). The decay time in this fitting is found to be 1.5 and 2.1 ns for figure (a) and (b) respectively. The system risetime is 80 ps.

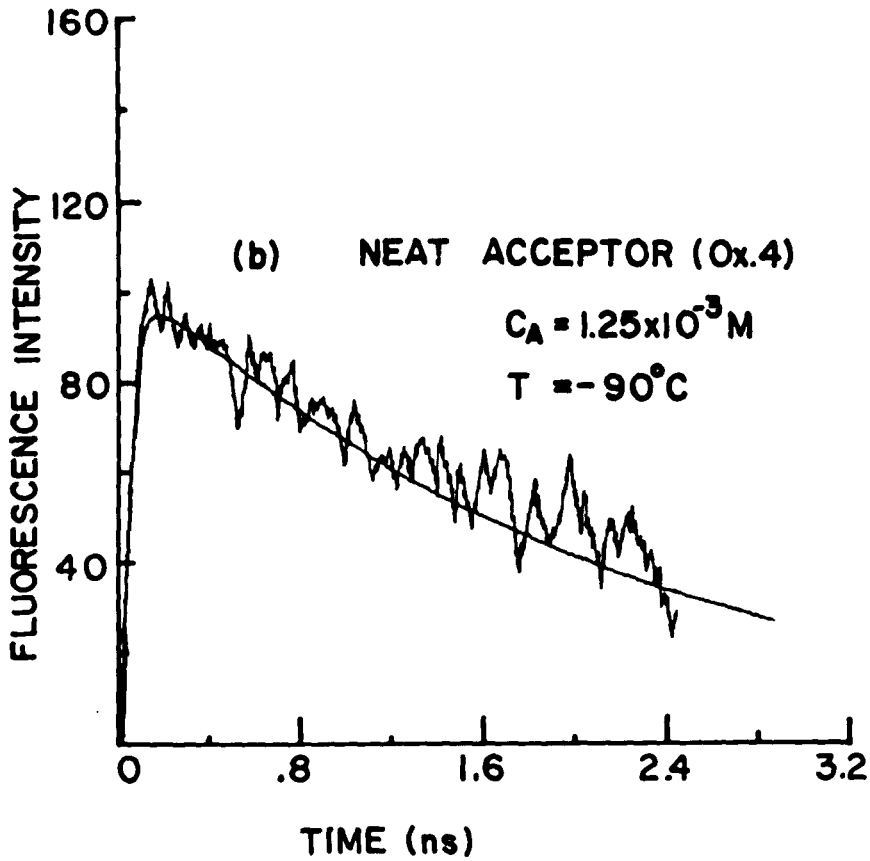
160
120
80
40
FLUORESCENCE INTENSITY
(b) NEAT ACCEPTOR (Ox.4)
$C_A = 1.25 \times 10^{-3} M$
T = -90°C
0
.8
1.6
2.4
3.2
TIME (ns)

Fig. 6.4 (b)

viscosity at a given temperature (see fig. 6.2), and other parameters, the fluorescence intensity profiles versus time were fitted to the donor and acceptor profiles generated by equations (6.3) and (6.4). An effective molecular radius r_D and r_A on the order of 6Å was used for curve fitting. The theoretical fittings and the data are in excellent agreement as shown in figures(6.5) and (6.6). The fluorescence decay time ($\frac{1}{e}$ time) of the donor at different diffusion constants (different temperature and viscosity regions) are shown in figure 6.7. The decay time decreases when the diffusion constant increases. This is attributed to the fact that translational motion of molecules combined with the long range energy transfer causes the energy deactivation of the donor molecule to occur more efficiently. In other words, when the diffusion constant increases, the decay time of the donor becomes shorter due to the process of energy transfer to the acceptor. The efficiency of energy deactivation with (ϵ_1) and without (ϵ_2) diffusion effects for different temperatures were calculated by equations (6.6) and (6.7) in order to obtain more information on the influence of the diffusion effect on the long range energy transfer between donors and acceptors. The diffusion contribution to the long range energy transfer was calculated for f_d by equation (6.8). The total energy deactivation efficiency with the diffusion effect was compared with experimental data and with theoretical expression ϵ_3 . These results are shown

Fig. 6.5 Experimental measurements of fluorescence profiles 530 nm$<\lambda<$600 nm of rhodamine 6G (the donor) mixed with oxazine 4 (the acceptor) at a concentration of 1.25×10^{-3} M in 1-propanol at temperatures of (a) 25°C, (b) 0°C, (c) -30°C, (d) -60°C, and (e) -90°C. The filters used are Corning 3-67 and Ditric short pass filter at 620 nm. The measurements are fitted by a solid line generated by equation (6.3). The parameters used to fit the data are: the system risetime of 80 ps. The critical distance R_o = 55Å, the absorption ratio β = 22 and the effective radius of molecule is 6Å. The fluorescence decay times for neat R6G and Ox are (a) 1.8 ns and 1.5 ns, (b) 1.82 ns and 1.51 ns, (c) 1.87 ns and 1.56 ns, (d) 1.95 ns and 1.88 ns, and (e) 2.2 ns and 2.1 ns. The diffusion constants are for different labs (a) 5.47×10^{-6}, (b) 1.74×10^{-6}, (c) 5.9×10^{-7}, (d) 1.27×10^{-7} and (e) 1.7×10^{-8} cm^2/sec

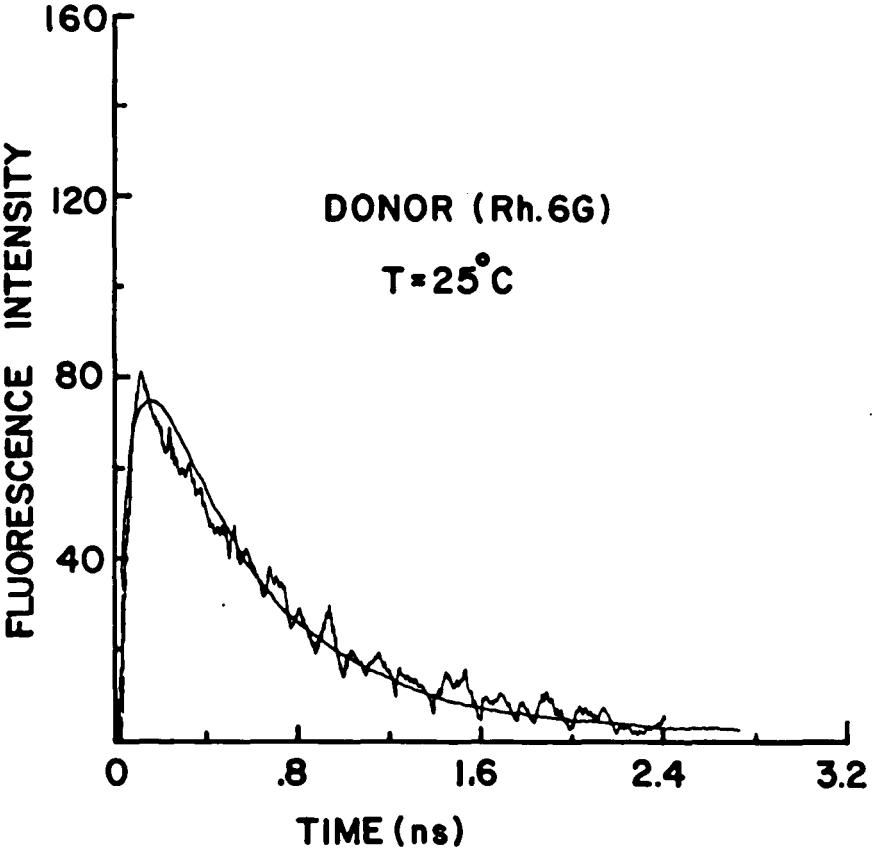
160
120
80
40
FLUORESCENCE INTENSITY
DONOR (Rh.6G)
T=25°C
0
.8
1.6
2.4
3.2
TIME (ns)

Fig. 6.5 (a)

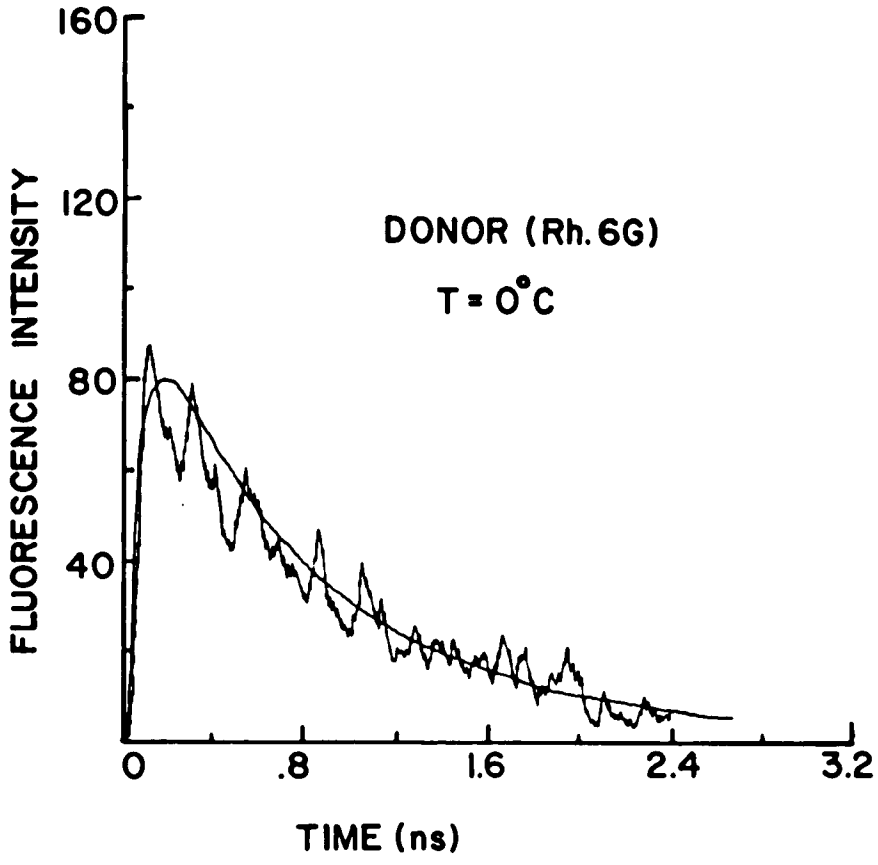
160
120
80
40
FLUORESCENCE INTENSITY
DONOR (Rh. 6G)
T = 0°C
0
.8
1.6
2.4
3.2
TIME (ns)

Fig. 6.5 (b)

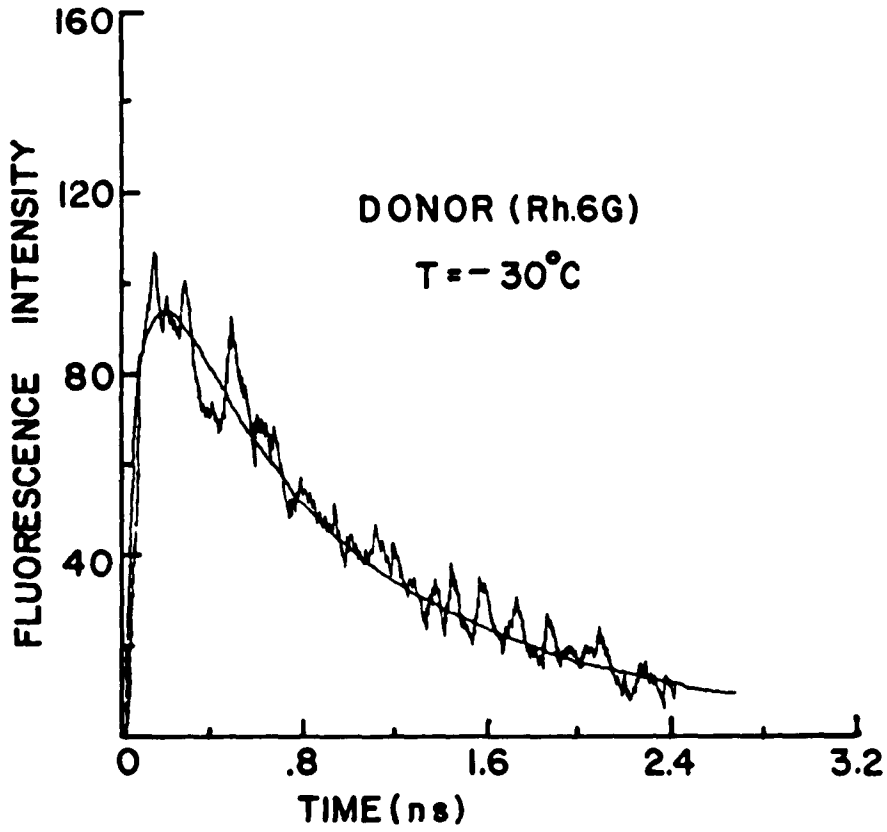
160
120
80
40
FLUORESCENCE INTENSITY
DONOR (Rh.6G)
T = - 30°C
0
.8
1.6
2.4
3.2
TIME (ns)

Fig. 6.5 (c)

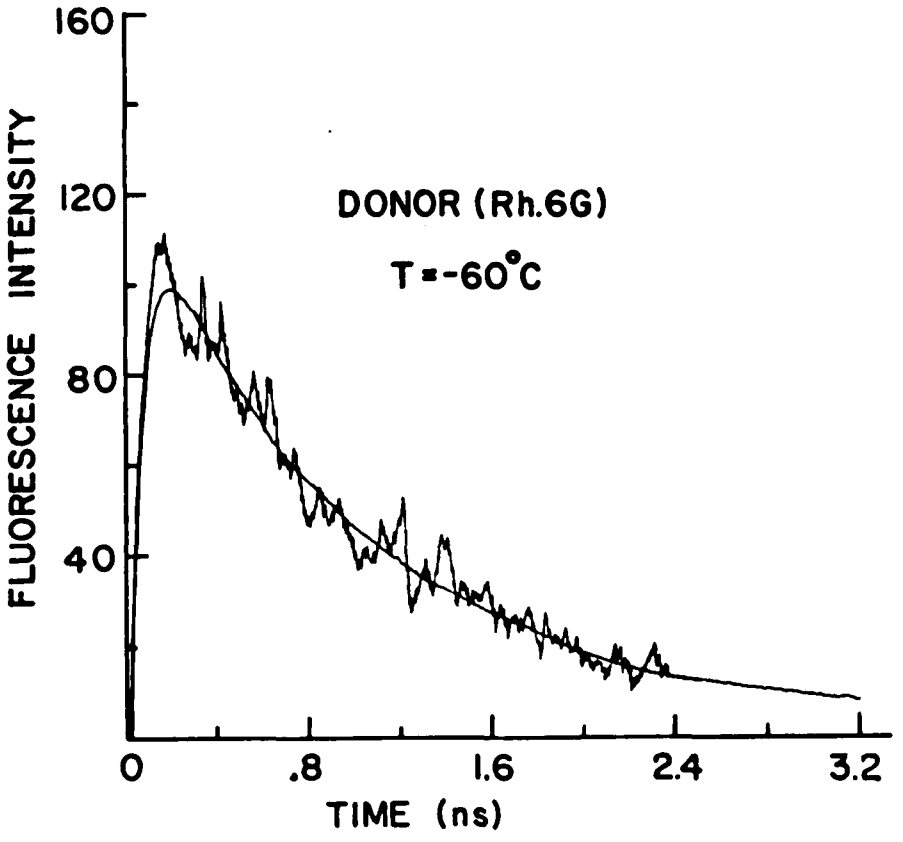
160
120
80
40
FLUORESCENCE INTENSITY
DONOR (Rh.6G)
T=-60°C
0
.8
1.6
2.4
3.2
TIME (ns)

Fig. 6.5 (d)

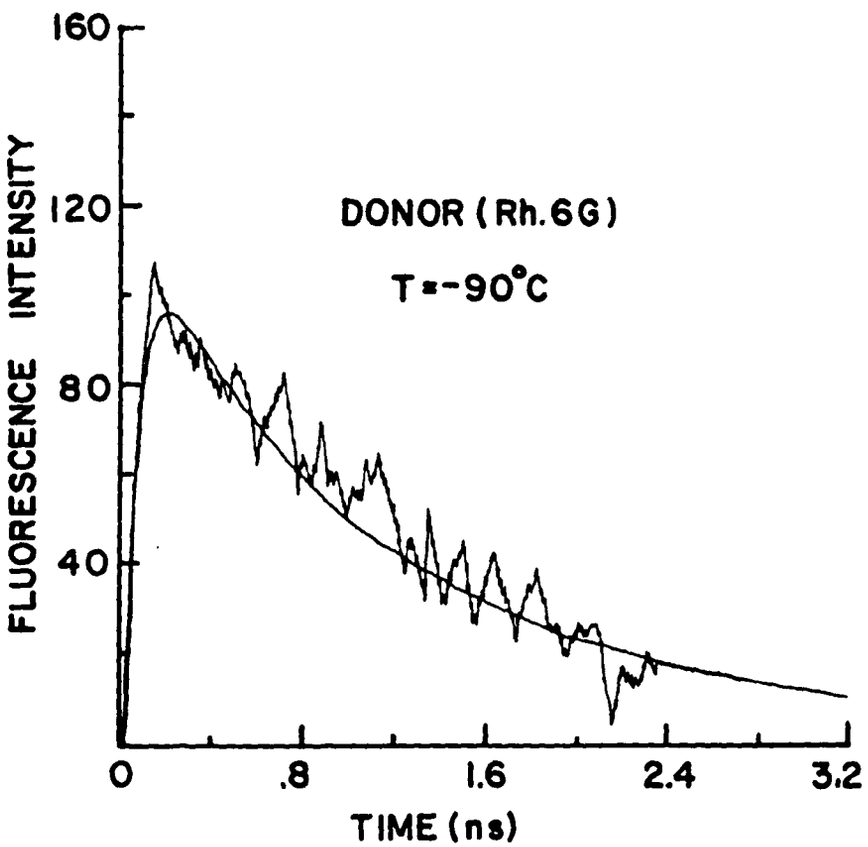
160
120
80
40
FLUORESCENCE INTENSITY
DONOR (Rh.6G)
T=-90°C
0
.8
1.6
2.4
3.2
TIME (ns)

Fig. 6.5 (e)

Fig. 6.6 Experimental measurements of fluorescence profiles ($\lambda > 660$ nm) of oxazine 4 Perchlorate (the acceptor) mixed with rhodamine 6G (the donor) at a concentration of 1.25×10^{-3} M in 1-propanol at the temperatures of (a) 25°C, (b) 0°C, (c) -30°C, (d) -60°C, and (e) -90°C. The filters used are Corning 3-67 and Hoya R-66 filters. The measurements are fitted by a solid line generated by equation (6.4). The parameters used to fit the data are: the system risetime of 80 ps, the critical distance $R_o = 55$Å, the absorption ratio $\beta = 2.2$, the effective radius of molecule is 6Å. The fluorescence decay times for neat R6G and Ox 4, and the diffusion constants are the same as in Fig. 6.5

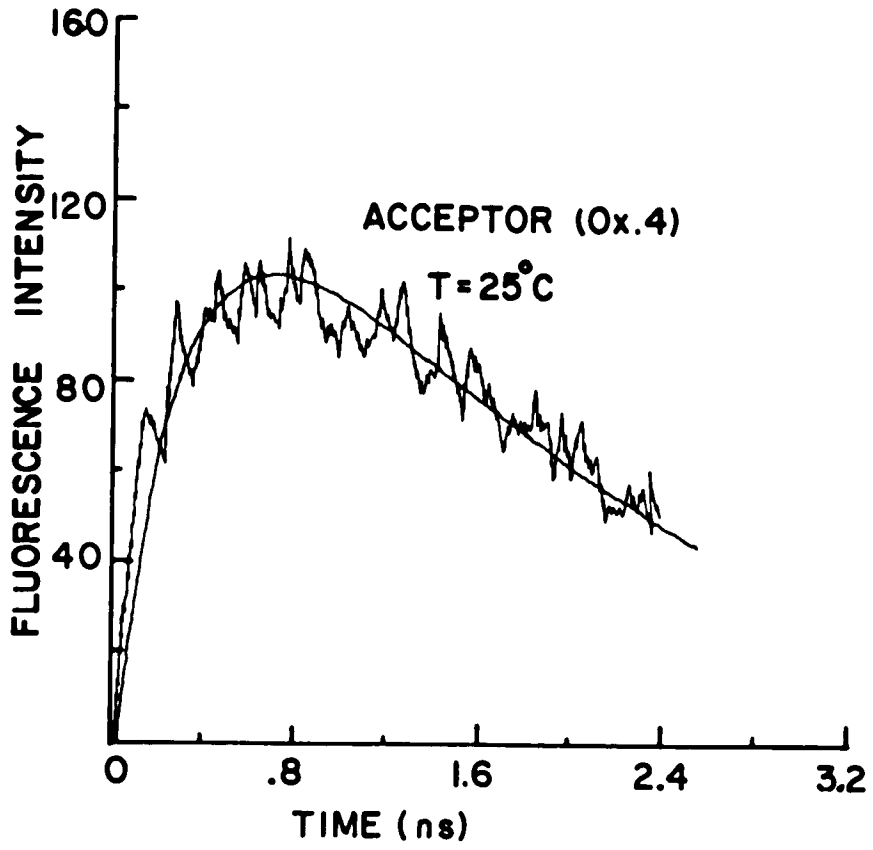
160
120
80
40
FLUORESCENCE INTENSITY
ACCEPTOR (0x.4)
T=25°C
0
.8
1.6
2.4
3.2
TIME (ns)

Fig. 6.6 (a)

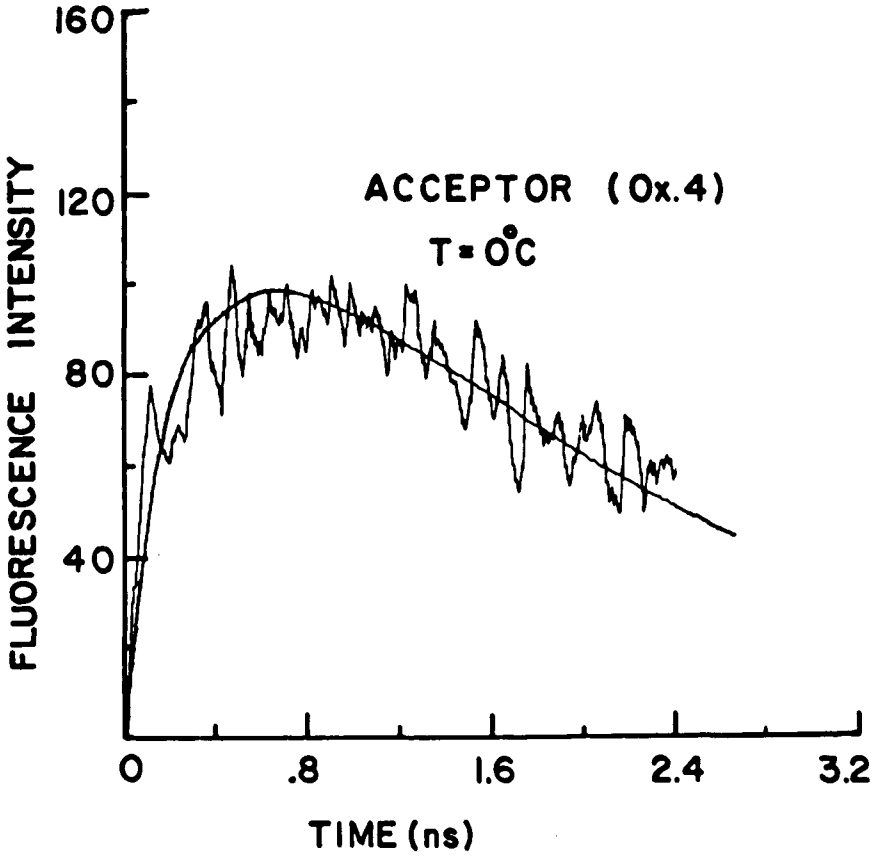
160
120
80
40
FLUORESCENCE INTENSITY
ACCEPTOR (0x.4)
T = 0°C
0
.8
1.6
2.4
3.2
TIME (ns)

Fig. 6.6 (b)

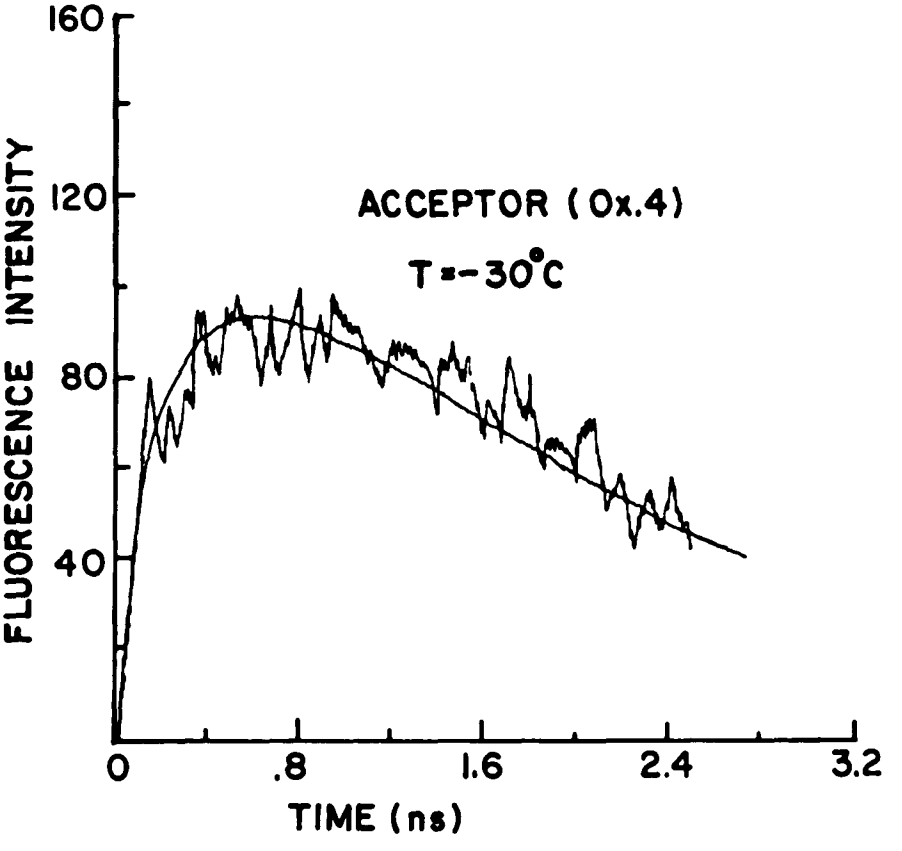
160
120
80
40
FLUORESCENCE INTENSITY
ACCEPTOR (0x.4)
T=-30°C
0
.8
1.6
2.4
3.2
TIME (ns)

Fig. 6.6 (c)

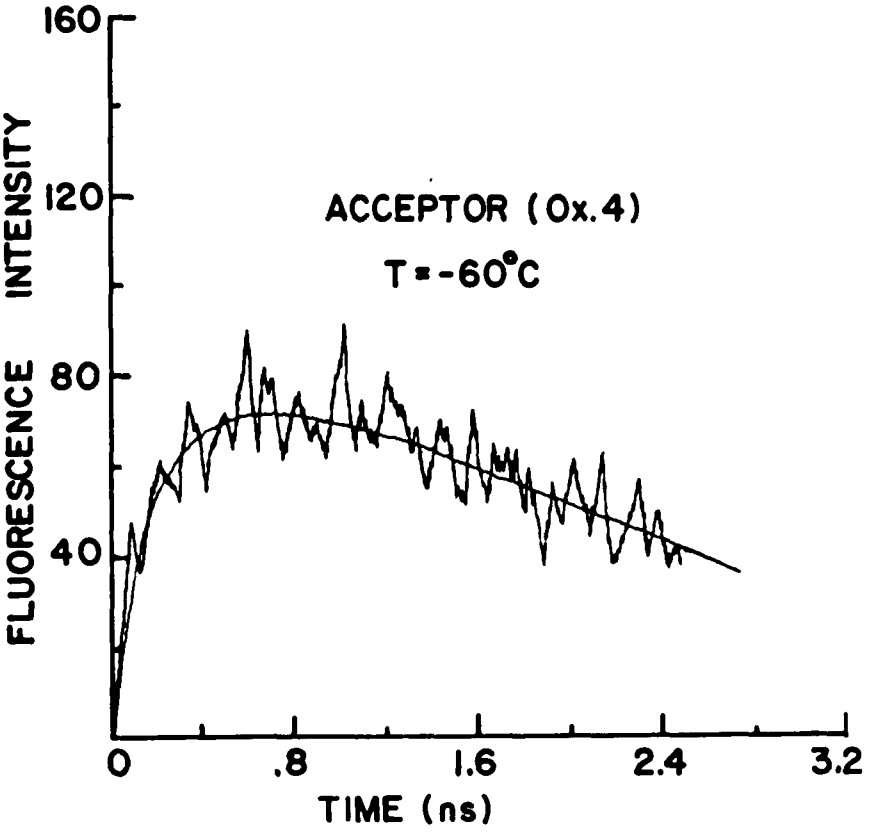
160
120
80
40
FLUORESCENCE INTENSITY
ACCEPTOR (Ox.4)
T=-60°C
0
.8
1.6
2.4
3.2
TIME (ns)

Fig. 6.6 (d)

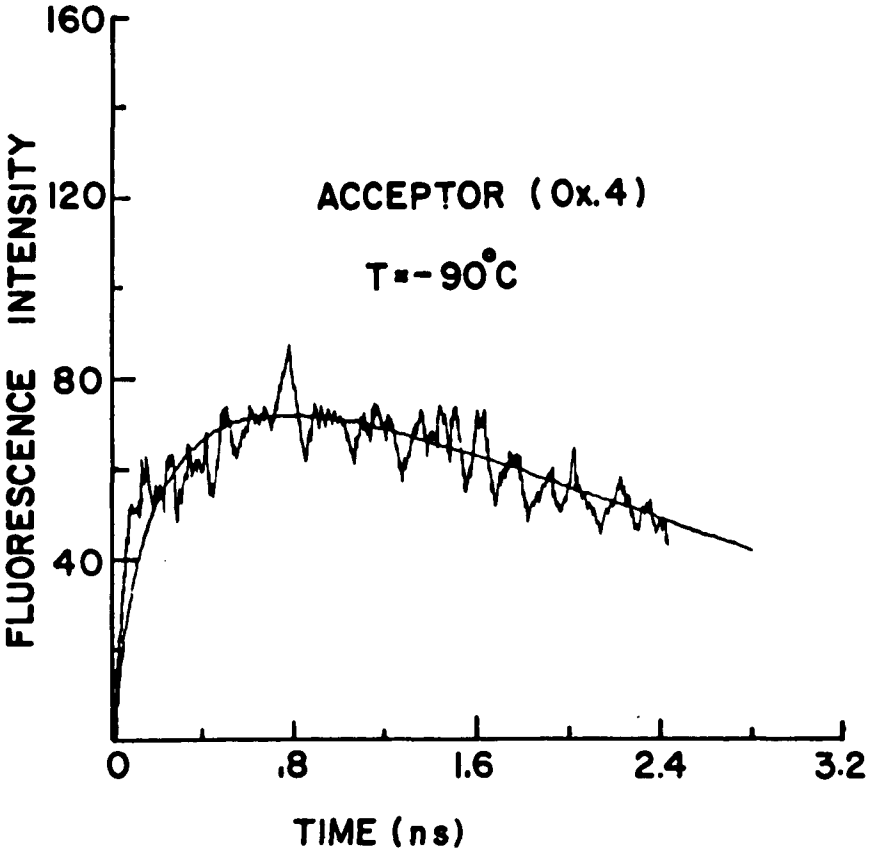
160
120
80
40
FLUORESCENCE INTENSITY
ACCEPTOR (0x.4)
T=-90°C
0
.8
1.6
2.4
3.2
TIME (ns)

Fig. 6.6 (e)

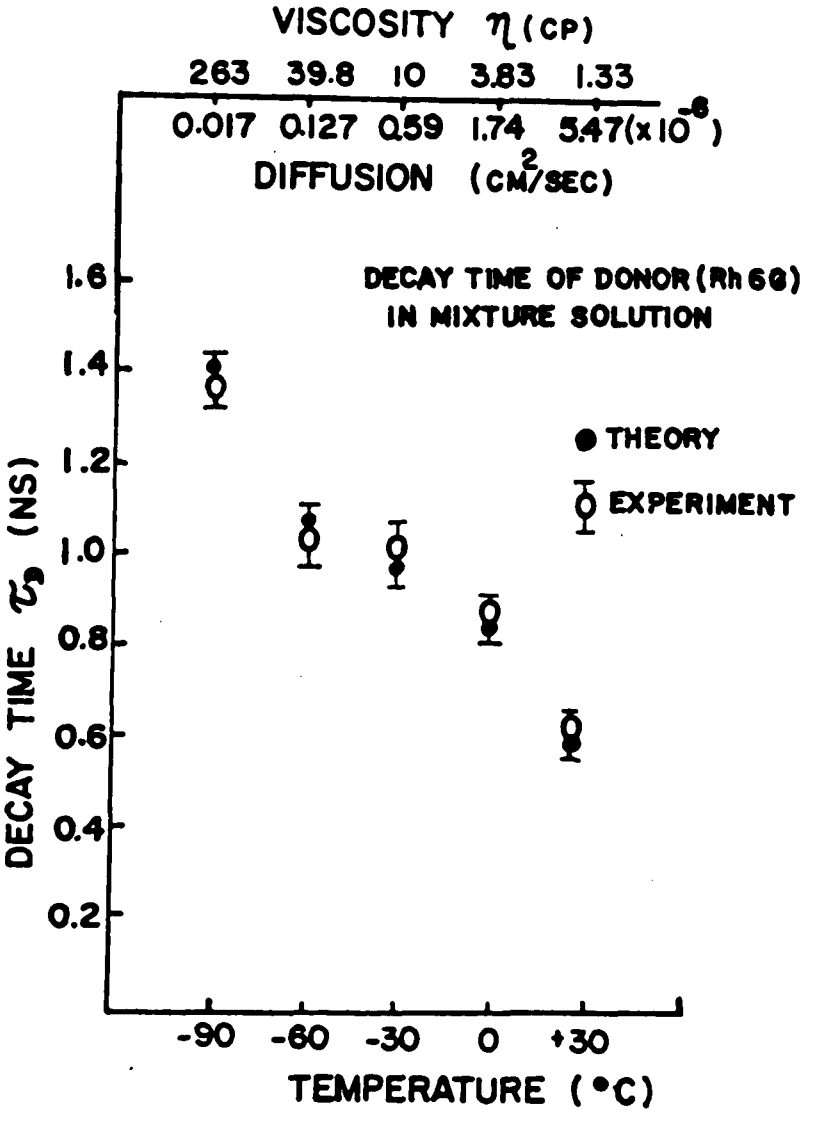

Fig. 6.7 Experimental measurement of decay time ($\frac{1}{e}$ time) of fluorescence profile of R6G at a concentration of 1.25×10^{-3}M mixed with Ox4 in 1-propanol for temperatures ranging from room temperature to -90°C. Decay time deduced from theoretical fitting

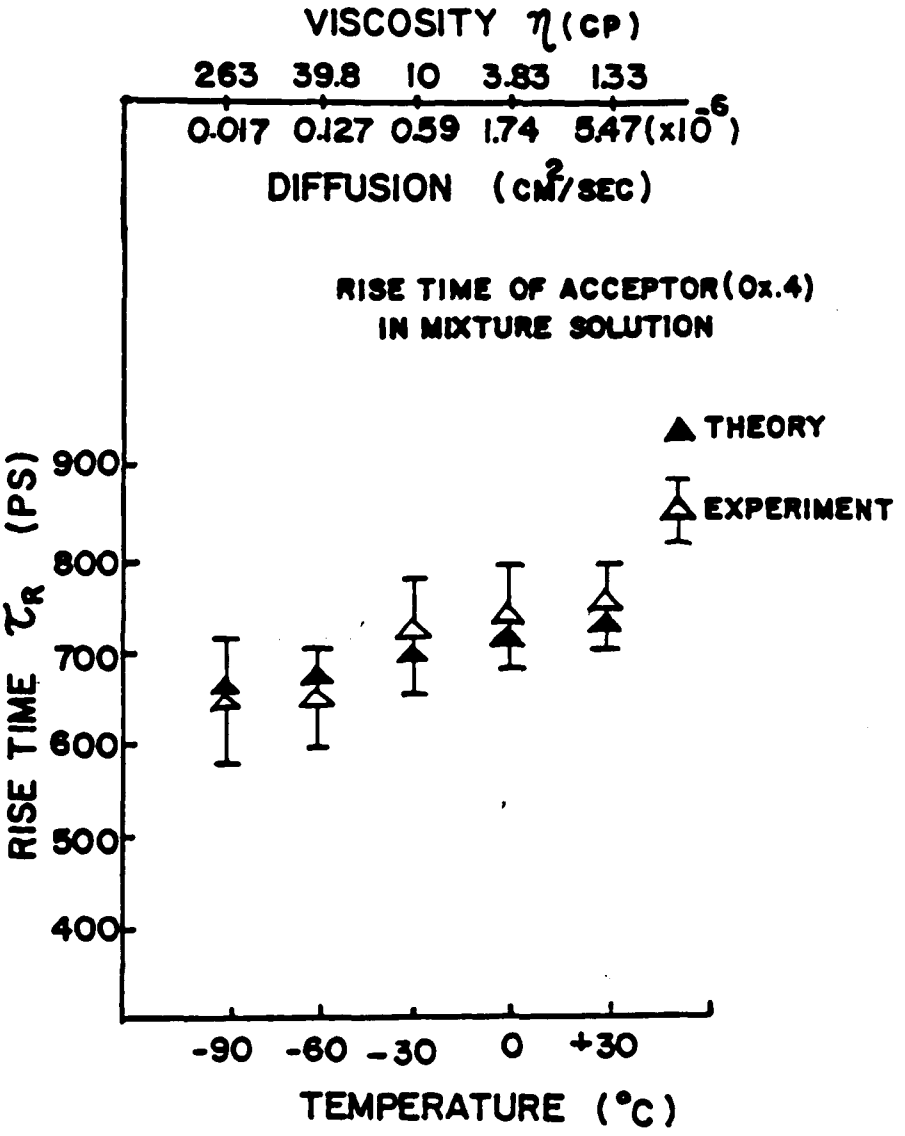

Fig. 6.8 Experimental measurement of time separation between the peak and starting point of fluorescence profile of 0x4 mixed with R6G at a concentration of 1.25×10^{-3} in 1-propanol for temperatures ranging from room temperature to -90°C, and the time separation between the peak and starting point of fluorescence profile deduced from the theoretical fitting

in Table IV. We found that as the diffusion effect increases, the long range energy transfer increases from 0.66% to 38% as the temperature increases from -90°C to room temperature as shown in Fig. 6.9. The total efficiency, calculated by equation (6.6) is equal to that calculated by $\epsilon_2(1+f_d)$ .This means the total efficiency of energy loss of the donors is due to the long range energy transfer to the acceptor with the diffusion of molecules. This agreement shows that the measurements and calculations are consistent.

6.5 Discussion

The diffusion of molecules in solution is most important for energy transfer. The larger the diffusion, the more the energy is transferred. Diffusion increases the close collisional encounter with other molecules in order for the interaction between donor and acceptor molecules to occur more effectively. The diffusion constant can be altered by the temperature and viscosity of the solvent. For a high temperature and less viscous fluid, the Brownian motion makes the molecule move more easily. As we have learned from this chapter, the contribution of diffusion decreases when the temperature is lowered. If the diffusion constant reaches the order of 10^{-7} cm^2/sec, the contribution of the diffusion effect on the long range energy transfer is less than 3%. In our previous papers[1,2] the diffusion

Table IV: Efficiency of energy deactivation with and without the effect of diffusion (Rh6G & Ox4 in 1-Propanol)

T (°C)	η (CP)	D (CM²/SEC)	ε_1 Theory with diffusion	ε_1 Experiment with diffusion	ε_2 Theory without diffusion	f_d Contribution of diffusion	$\varepsilon_3 = \varepsilon_2(1+f_d)$
25	1.33	5.47×10^{-6}	68.9%	77±3%	50.2%	38.4%	69.4%
0	3.83	1.74×10^{-6}	58.6%	60.2±3%	50.1%	17.1%	58.6%
-30	10	5.9×10^{-7}	54.0%	56.7±2%	49.8%	8.4%	53.9%
-60	39.8	1.27×10^{-7}	51.3%	49±2%	49.6%	2.9%	51.0%
-90	263	1.7×10^{-8}	49.2%	51±5%	49.2%	0.66%	49.5%

Table IV Efficiency of the long range energy transfer between R6G (donor) and Ox 4 (acceptor) with and without diffusion effects at different temperatures

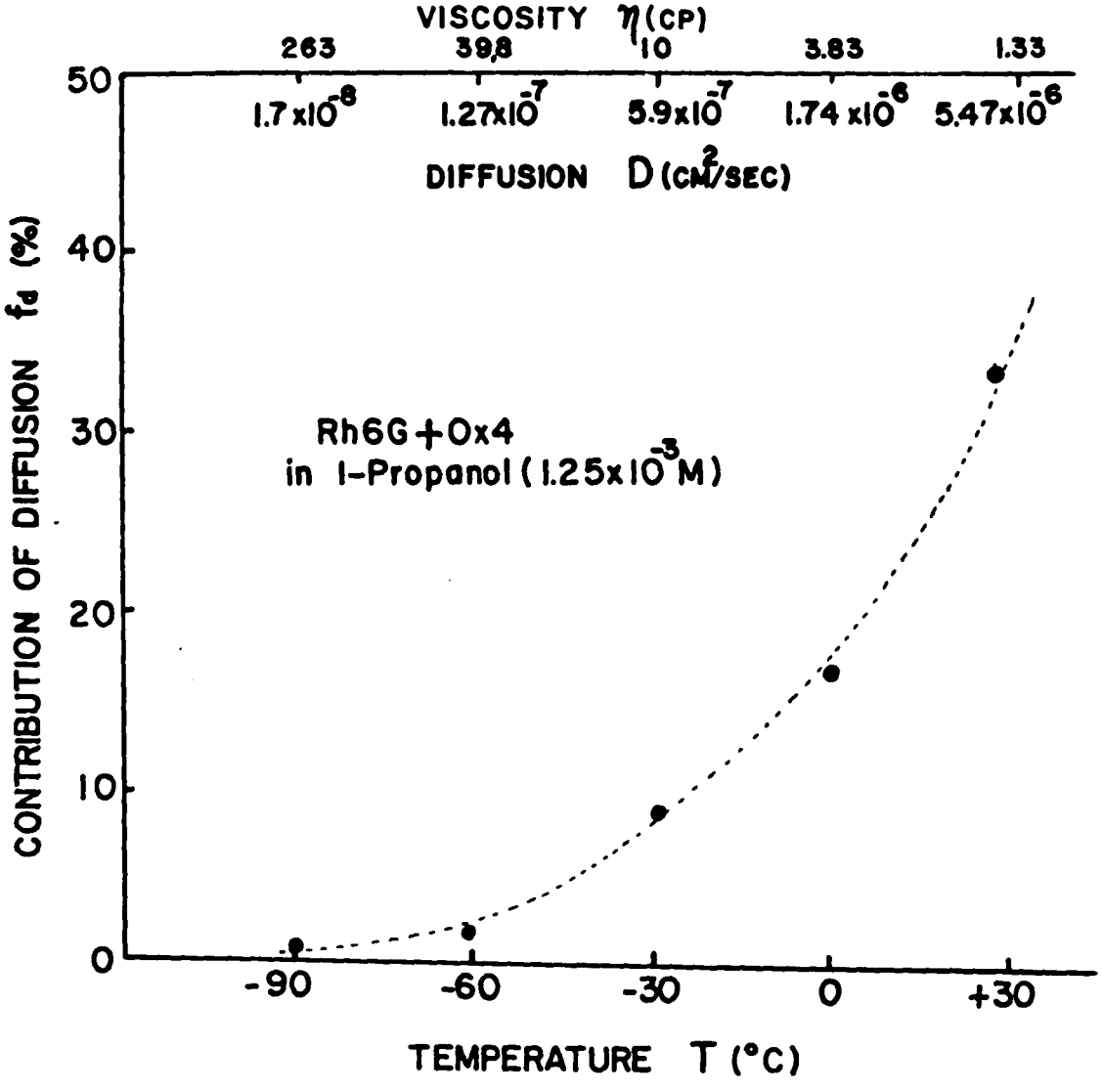

Fig. 6.9 The percentage of contribution of diffusion effect on the energy transfer versus temperature

constant was about 3.7×10^{-7} cm^2/sec for the binary mixture in ethylene glycol at room temperature. In this case the contribution of the diffusion effect on the long range energy transfer is estimated to be less than 6%. Therefore, in that case we have neglected the diffusion effect. For the R6G and OX4 binary mixture in 1-propanol, we have completed the first measurements of the kinetics study of the long range energy transfer including the diffusion effect from a non-negligible value of 10^{-5} cm^2/sec (room temperature) to a neglibible value of 10^{-8} cm^2/sec (low temperature). Theoretical fittings to the experimental measurements of the time resolved fluorescence profiles are in excellent agreement. The total efficiency of energy deactivation of the donor molecule was calculated and compared experimentally. Since the temperature varied in a limited region ($25^{o}C$ to $-90^{o}C$), the vibrational and rotational effects of the molecule are neglected. The percentage contribution of the diffusion effect required to increase the long range energy transfer was determined. In conclusion, the energy transfer via dipole-dipole long range interaction plays a dominant role in the mechanisms of energy transfer between donors and acceptors. This work will be extended to study energy transfer of mixed dyes in glass and crystal states.

References

1. P. Y. Lu, Z. X. Yu, R. R. Alfano, and J. I. Gersten, Phys. Rev. A (June 1982)
2. P. Y. Lu, Z. X. Yu, R. R. Alfano, and J. I. Gersten, submitted for publication
3. M. D. Galanin, Soviet Phys. -JETP, 1, 317 (1955)
4. Th Forster, Ann. Physik 2, 55 (1948). Dis Far Soc. 27, 7 (1959)
5. J. B. Birks, Photophysics of Aromatic Molecules, John Wiley (1970)
6. R. G. Powell and Z. G. Soons, J. Lum 11, 1 (1975)
7. T. R. Waite, J. of Chem. Phys. 28, 103 (1958)
8. Yu. K. Kurskii and A. S. Selivanenko, Opt. and Spectro. 8, 340 (1960)
9. A. M. Samson, Opt. and Spectro. 13, 285 (1962)
10. N. N. Tunitskii and Kh. S. Bagdasar' yan, Opt. and Spectro. 15, 50 (1963)
11. Kh. S. Bagdasaryan and A. L. Muler, Opt. and Spectr. 18, 558 (1965)
12. Y. Elkana, J. Feitelson, and E. Katchalski, J. of Chem. Phys. 48, 2399 (1968)
13. M. Yokota and O. Tanimoto, J. of Phys. Soc. of Japan, 22, 779 (1967)
14. U. Gosele and M. Hauser, U.K.A. Klein and R. Frey, Chem. Phys. Lett. 34, 519 (1975)

15. U. K. A. Klein, R. Frey, M. Hauser, and U. Gosele, Chem. Phys. Lett. 41, 139 (1976)

16. U. Gosele, Chem. Phys. Lett. 43, 61 (1976)

17. D. P. Millar, R. J. Robbins, and A. H. Zewail, J. Chem. Phys. 75, 3649 (1981)

18. P. P. Ho, Ph.D. Dissertation "Reorientational Relaxation Kinetics of Polyatomic Molecules in Different States of Condensed Media", City University of New York, 1978 (Chap. 2)

19. D. J. Denney, J. of Chem. Phys. 30, 159 (1959)

CHAPTER 7 SUMMARY, CONCLUSION AND FUTURE RESEARCH

7.1 Summary

In this research, the experimental measurements of the absorption and fluorescence spectra of rhodamine 6G, rhodamine B, oxazine 4 perchlorate, nile blue A perchlorate in neat and binary mixed solutions were performed. The good overlapping of the fluorescence spectrum of rhodamine 6G and absorption spectrum of oxazine 4 perchlorate implied a resonant long range energy transfer may occur between the donor (R6G) and acceptor (OX4) by Forster mechanism. Similar behavior was observed for the rhodamine B and nile blue A perchlorate. The R_o is 56Å and 54Å for R6G-Ox4 and RB-NB respectively. Measurements of time-resolved fluorescence spectroscopy of rhodamine 6G and oxazine 4 perchlorate were then undertaken in order to find out the physical quantities such as decay time and rise time of the donor and acceptor in neat and binary mixed solution on energy transfer. From these measurements, the decay time of donor becomes shorter (1.8 ns to 1.1 ns for R6G) and rise time of acceptor becomes slower (1 ps to 400 ps for Ox4) in the binary mixed solutions compared to that in neat solutions. A theoretical model of the rate equations for the excited probability of donor and acceptor was established to fit the experimental results by varying R_o only. For a better understanding of how strong the interaction between the donor and acceptor may affect the long range energy transfer,

the measurements of time resolved fluorescence spectroscopy of the donor and acceptor component were undertaken for a fixed concentration of donor (1.25×10^{-3} M) mixed with various concentrations of the acceptor (3.13×10^{-4} to 5.0×10^{-3} M). The efficiency of energy transfer was also determined theoretically and experimentally. From the theoretical and experimental results, the larger change of decay time (100 ps to 1300 ps) of donor and rise time (400 ps to 800 ps) of acceptor, and the larger efficiency (15% to 80%) of energy transfer in the more concentrated solution reflects a stronger interaction between the donor and acceptor because the average distance between donor and acceptor is closer. However, for the fluid solution with low viscosity, the diffusion of molecules can increase the encounter probability and may affect the long range energy transfer. The temperature controlled solution can give rise to different diffusion constants at different temperatures. From the experimental measurement and modified theoretical model including the diffusion effect, a contribution of diffusion of molecule to the long range energy transfer was determined from a negligible value (low temperature and high viscosity) to a non-negligible value (room temperature and low viscosity). Theory and experiments are in excellent agreement. The diffusion can increase the efficiency (0.66% at $-90^{\circ}C$ to 38% at RT) of long range energy transfer. In short, the energy deactivation of donor molecule is

dominantly due to the dipole-dipole interaction in the Forster mechanism and the strength of interaction is affected by the concentration of acceptor. The efficiency of transfer can be increased when the solution is more concentrated with lower viscosity and larger diffusion constant.

In this research, the factors effecting the long range energy transfer rate are (1) the critical transfer distance R_o^{DA}, (2) the concentration of the solution, (3) the diffusion of molecule in different temperature and viscosity region, (4) the decay time of donor, (5) the relative ratio of absorption cross section of donor and acceptor, and (6) the overlap integral of the absorption and fluorescence spectra of donor.

The critical distance R_o^{DA} of the pair of rhodamine 6G and oxazine 4 perchlorate (55Å) is greater than that of the pair of rhodamine B and nile blue A perchlorate (48Å) and induced a more efficient energy transfer for the former pair in the same solvent at the same concentration and temperature as the latter one. The various concentrations of acceptor mixed with the donor at fixed concentration gives a different separation distance between donor and acceptor and hence a different efficiency of energy transfer appears. An efficiency up to 80% corresponds to a concentrated solution of 5×10^{-3}M. The diffusion of molecules in the mixed solution at room temperature help the

energy transfer efficiency increase to 38% and decrease to 0.66% at -90°C in the solvent of 1-propanol. A longer decay time of donor can induce a larger quantum yield and then fluorescence intensity of donor molecule also increases. This gives rise to a decrease of energy transfer rate ($\sim \frac{1}{\tau_D}$) because energy is spread out over a larger time interval. The relative absorption ratio of donor and acceptor, β , defines the relative amount of laser energy absorbed by the donor molecule. The fluorescence of acceptor via energy transfer from donor will be increased in the case of larger because more photon energy is absorbed by donor.

The overlap integral of the absorption and fluorescence spectra of donor defines a possible energy transfer between the donor and donor molecules. In the particular pairs of xanthane and oxazine dye we used, the energy transfer between donor and donor molecules is neglected because of the large overlap integral of the absorption spectrum of acceptor and the fluorescence spectrum of donor, and the large relative ratio of absorption cross section of donor and acceptor. The R_o^{DA} is 55Å and 48Å for R6G-Ox and RB-NB, while R_o^{DD} is 41Å and 40Å for R6G and RB respectively.

7.2 Conclusion

The detailed measurements of the time-resolved fluorescence spectroscopy for the long range resonant energy

transfer from an energy donor molecule to an energy acceptor molecule were completed. The theoretical calculations and fittings were in excellent agreement with the experimental results. In conclusion, the long range dipole-dipole interaction in the Forster mechanism is the dominant mechanism during the process of energy transfer from the donor to the acceptor. The critical transfer distance R_o^{DA}, the relative absorption cross section of donor and acceptor β, and the concentration of the solution define the condition for the long range energy transfer from donor to acceptor with negligible transfer from donor to donor. The important factors which affect the rate and efficiency of energy transfer are critical transfer distance R_o^{DA}, the concentration, viscosity and temperature of the solution, and the fluorescence decay time of donor. We completed a self consistent theory and experimental measurements on the study of long range energy transfer between dyes, the results of this research can be applied to understand the energy conversion in some energy storage device and operation of dye lasers because not only the fundamental physical phenomena but also the important controlling factors which affects the energy transfer were found in detail in this research.

7.3 Future Research

The following are the areas for future research:

1. In order to have more efficient energy transfer and the

information on exchange effect, a crystalline or powder mixture of rhodamine 6G (the donor) and oxazine 4 perchlorate (the acceptor) may be prepared for the kinetics study of energy transfer. If the Forster mechanism in our theoretical model is applicable to this system, a high efficiency of long range energy transfer will be obtained. If the exchange effect exists, an exponential decay dependence of the transfer rate[1] is expected for $R \sim 10\text{Å}$.

2. In order to have the information on the dye sensitized luminescence of silver halides, a cyanine dye contacted with the silver halides may be prepared. The fluorescence kinetics of silver halides and silver halides contacted with cyanine dye will be investigated to compare the intrinsic luminescence of silver halides and sensitized luminescence of silver halides contacted with cyanine dye. It is expected that the cyanine dye, after absorbing the photon energy will transfer the electron from its S_1 state to the conduction band of silver halides. Then a sensitized luminescence of silver halides will emit by the transition of the electron from the conduction to the valence band of silver halides.[2]

References:

1. D. L. Dexter, J. Chem. Phys. 21, 836 (1953)
2. H. Hediger, P. Junod, and R. Steiger, J. of Lum. 24, 881 (1981)

APPENDIX

EVALUATION OF DONOR INTEGRAL

$$\frac{\mathcal{D}(t)}{\Gamma_D \sigma_D I_0} = n_D \rho_D \int_0^t e^{-\rho_D(t-\tau) - \vartheta_D \tau - \frac{4\pi}{3} n_A \sqrt{\pi \Delta \tau}} d\tau$$

```
DIMENSION VAL (4000), X(4000)
DEFINE (RD,0.012)          #VIBRATION DECAY RATE
DEFINE(ADA, 17.5)  #RATIO OF ABSORPTION OF DONOR TO ACCEPTOR
DEFINE(GD, 6.6E-4) #TOTAL DECAY RATE EXCEPT TRANSFER
DEFINE(PAN, 1.412E-4)    #CONSTANT
DEFINE(CA,.0025)          #CONCENTRATION OF ACCEPTOR
DEFINE(RO,40)             #CRITICAL DISTANCE BETWEEN DONOR
                          ACCEPTOR
COMMON T, TAUD
EXTERNAL F
DOUBLE PRECISION FILNAM
TYPE 1 ; 1 FORMAT(2X,'ENTER TAUD(NS)')
ACCEPT 2,TAUD  ; 2 FORMAT(1G)
TYPE 3 ; 3 FORMAT(2X,'ENTER TIME(PS)')
ACCEPT 2,TI
TYPE  4  ;4 FORMAT(2X,'ENTER OUTPUT DATA FILENAME')
ACCEPT 5,FILNAM ; 5 FORMAT(A10)
CALL OFILE(21,FILNAM)
FOR(I=1;I < =TI;I=I+1)
[
T=FLOAT(I)-1
```

```
      IF(T < 0.)BREAK
      CALL QUAD(F,0.,T,1.0E-4,AND,ER) #PORT  ROUTINE FOR
      INTEGRAL
      X(I)=T
      VAL(I)=1*ADA*RD*ANS
      WRITE(21,50)X(I),VAL(I)
50    FORMAT(2F)
      ]
      CALL RELEASE(21)
      STOP
      END
      FUNCTION F(TAU)
      COMMON T,TAUD
      ARG=-RD*(T-TAU)-GD*TAU-PAN*CA*RO*RO*RO*SQRT(TAU/TAUD)
      F=EXP(ARG)
      RETURN
      END
```

#EVALUATION OF ACCEPTOR INTEGRAL

$$\rho_D \beta \frac{(e^{-\rho_D t} - e^{-g_A t})}{g_A - \rho_D} + \frac{n_A}{n_D} \rho_A \frac{(e^{-\rho_A t} - e^{-g_A t})}{g_A - \rho_A}$$

```
DIMENSION VAL(4000),X(4000)
DEFINE(RD,0.012)     #VIBRATION DECAY RATE
DEFINE(RA,0.012)     #VIBRATION DECAY RATE
DEFINE(ADA,17.5)     #RATIO OF ABSORPTION OF DONOR TO
ACCEPTOR
DEFINE(GD,6.6E-4)    #TOTAL DECAY RATE EXCEPT TRANSFER
DEFINE(GA,13.3E-4)
DEFINE(PAN,1.412E-4) #CONSTANT
DEFINE(CD,.0025)
DEFINE(CA,.0025)     #CONCENTRATION OF ACCEPTOR
DEFINE(RO,40)  #CRITICAL DISTANCE BETWEEN DONOR )
ACCEPTOR
DOUBLE PRECISION FILNAM
TYPE 1 ; 1 FORMAT(2X,'ENTER TAUD')
ACCEPT  2,TAUD ;  2 FORMAT(1G)
TYPE  3 ; 3 FORMAT(2X,'ENTER TI')
ACCEPT 2,TI
TYPE 4 ;4 FORMAT(2X,'ENTER OUTPUT DATA FILENAME')
ACCEPT 5,FILNAM ; 5  FORMAT(A10)
CALL OFILE(21,FILENAM)
FOR(I=1;I <=  TI;I=I+1)
[
T=FLOAT(I)-1
IF(T <  0.)BREAK
```

```
      X(I)=T
      VAL(I)=RD*ADA*(EXP(-RD*T)-EXP(-GA*T))/(GA-RD)
      VAL(I)=VAL(I)+CA/CD*RA*(EXP(-RA*T)-EXP(-GA*T))/(GA-RA)
      WRITE(21,50)X(I),VAL(I)
50    FORMAT(2F)
      ]
      CALL RELEASE(21)
      STOP
      END
```

#EVALUATION OF ACCEPTOR INTEGRAL

$$-\left(\frac{g_D - \rho_D}{g_A - \rho_D}\right) n_D \rho_D \beta e^{-\rho_D t} \int_0^t d\tau\, e^{(\rho_D - g_D)\tau - \frac{4\pi}{3} n_A \sqrt{\pi \Delta \tau}}$$

```
DIMENSION VAL(4000),X(4000)
DEFINE(RD,0.012)    #VIBRATION DECAY RATE
DEVINE(RA,0.012)    #VIBRATION DECAY RATE
DEFINE(ADA,17.5)    #RATIO OF ABSORPTION OF DONOR TO ACCEPTOR
DEFINE(GD,6.6E-4)   #TOTAL DECAY RATE EXCEPT TRANSFER
DEFINE(GA,13.3E-4)
DEFINE(PAN,1.412E-4) #CONSTANT
DEFINE(CD,.0025)
DEFINE(CA,.0025)    #CONCENTRATION OF ACCEPTOR
DEFINE(RO,40) #CRITICAL DISTANCE BETWEEN DONOR ) ACCEPTOR
COMMON T,TAUD
EXTERNAL F
DOUBLE PRECISION FILNAM
TYPE1 ; 1 FORMAT(2X,'ENTER TAUD')
ACCEPT 2,TAUD ; 2 FORMAT(1G)
TYPE 3 ; 3 FORMAT(2X,'ENTER  TI')
ACCEPT  2,TI
TYPE4 ;4 FORMAT(2X,'ENTER OUTPUT DATA FILENAME')
ACCEPT 5,FILNAM ; 5 FORMAT(A10)
CALL OFILE(21,FILNAM)
FOR(I=1;I<=TI;I=I+1)
[
```

```
      T=FLOAT(I)-1
      IF(T < 0.)BREAK
      CALL QUAD(F,0.,T,1.0E-4,ANS,ER) #PORT ROUTINE FOR
      INTEGRAL
      X(I)=T
      VAL(I)=-(RD-GD)/(RD-GA)*ADA*RD*ANS
      WRITE(21,50)X(I),VAL(I)
50    FORMAT(2F)
      ]
      CALL RELEASE(21)
      STOP
      END
      FUNCTION F(TAU)
      COMMON T,TAUD
      ARG=-RD*(T-TAU)-GD*TAU-PAN*CA*RO*RO*RO*SQRT(TAU/TAUD)
      F=EXP(ARG)
      RETURN
      END
```

#EVALUATION OF ACCEPTOR INTEGRAL

$$+\left(\frac{g_D - \rho_D}{g_A - \rho_D}\right) n_D \rho_D \beta\, e^{-g_A t} \int_0^t d\tau\, e^{(g_A - g_D)\tau - \frac{4\pi}{3} n_A \sqrt{\pi \Delta \tau}}$$

```
      DIMENSION VAL(4000),X(4000)
      DEFINE(RD,0.012)     #VIBRATION DECAY RATE
      DEFINE(RA,0.012)     #VIBRATION DECAY RATE
      DEFINE(ADA,17.5)     #RATIO OF ABSORPTION OF DONOR TO
      ACCEPTOR
      DEFINE(GD,6.6E-4)    #TOTAL DECAY RATE EXCEPT TRANSFER
      DEFINE(GA,13.3E-4)
      DEFINE(PAN,1.412E-4) #CONSTANT
      DEFINE(CD,.0025)
      DEFINE(CA,.0025)     #CONCENTRATION OF ACCEPTOR
      DEFINE(RO,40)  #CRITICAL DISTANCE BETWEEN DONOR) ACCEPTOR
      COMMON  T,TAUD
      EXTERNAL F
      DOUBLE PRECISION FILNAM
      TYPE1 ; 1 FORMAT(2X,'ENTER TAUD')
      ACCEPT 2,TAUD; 2 FORMAT(1G)
      TYPE 3 ; 3 FORMAT(2X,'ENTER TI')
      ACCEPT 2,TI
      TYPE 4 ;4 FORMAT(2X,'ENTER OUTPUT DATA FILENAME')
      ACCEPT 5,FILNAM; 5 FORMAT(A10)
      CALL OFILE(21,FILNAM)
      FOR(I=1;I <=TI;I=I+1)
      [
```

```
      T=FLOAT(I)-1
      IF(T < 0.)BREAK
      CALL QUAD(F.0.,T,1.'0E-4,ANS,ER) #PORT ROUTINE FOR
      INTEGRAL
      X(I)=T
      VAL(I)=(RD-GD)/(RD-GA)*ADA*RD*ANS
      WRITE(21,50)X(I),VAL(I)
50    FORMAT(2F)
      ]
      CALL RELEASE(21)
      STOP
      END
      FUNCTION F(TAU)
      COMMON T,TAUD
      ARG=-GA*(T-TAU)-GD*TAU-PAN*CA*RO*RO*SQRT(TAU/TAUD)
      F=EXP(ARG)
      RETURN
      END
```

EVALUATION OF ACCEPTOR INTEGRAL

$$-n_D \rho_D \beta e^{-g_A t} \int_0^t d\tau\, e^{(g_A - g_D)\tau - \frac{4\pi}{3} n_A \sqrt{\pi D \tau}}$$

```
DIMENSION VAL(4000),X(4000)
DEFINE(RD,0.012)     #VIBRATION DECAY RATE
DEFINE(RA,0.012)     #VIBRATION DECAY RATE
DEFINE(ADA,17.5)     #RATIO OF ABSORPTION OF DONOR TO
ACCEPTOR
DEFINE(GD,6.6E-4)    #TOTAL DECAY RATE EXCEPT TRANSFER
DEFINE(GA,13.3E-4)
DEFINE(PAN,1.412E-4)      #CONSTANT
DEFINE(CD,.0025)
DEFINE(CA,.0025)     #CONCENTRATION OF ACCEPTOR
DEFINE(RO,40)  #CRITICAL DISTANCE BETWEEN DONOR) ACCEPTOR
COMMON T, TAUD
EXTERNAL F
DOUBLE PRECISION FILNAM
TYPE 1 ; 1 FORMAT(2X,'ENTER TAUD')
ACCEPT 2,TAUD ; 2 FORMAT(1G)
TYPE 3 ; 3 FORMAT (2X,'ENTER TI')
ACCEPT 2,TI
TYPE 4 ;4 FORMAT(2X,'ENTER OUTPUT DATA FILENAME')
ACCEPT 5,FILNAM; 5 FORMAT(A10)
CALL OFILE(21,FILNAM)
FOR(I=1;I < =TI;I=I+1)
[
```

```
      T=FLOAT(I)-1
      IF(T < 0.)BREAK
      CALL QUAD(F,0.,T,1.0E-4,ANS,ER) #PORT ROUTINE FOR
      INTEGRAL
      X(I)=T
      VAL(I)=-ADA*RD*ANS
      WRITE(21,50)X(I),VAL(I)
50    FORMAT(2F)
      ]
      CALL RELEASE(21)
      STOP
      END
      FUNCTION F(TAU)
      COMMON T,TAUD
      ARG=-GA*(T-TAU)-GD*TAU-PAN*CA*RO*RO*RO*SQRT(TAU/TAUD)
      F=EXP(ARG)
      RETURN
      END
```

```
DOUBLE PRECISION FILNAM,TYT


        DIMENSION X(4000),Y(4000),VAL(4000)
        TYPE 6000
6000    FORMAT(2X,'INPUT THE TITLE')
        ACCEPT 100,TYT
100     FORMAT(A10)
        TYPE 6500
6500    FORMAT(2X,'ENTER TI')
        ACCEPT 200,TI
200     FORMAT(F)
        FOR(I=1;I <=TI;I=I+1)
        [
        VAL(I)=0
        ]
        TYPE 10
10      FORMAT(2X,'ENTER NO. OF FILE')
        ACCEPT 15,N
15      FORMAT(I4)
        REPEAT
        [
        TYPE 7000
7000    FORMAT(2X,'ENTER THE INPUT DATA FILE')
        ACCEPT 100,FILNAM
        CALL IFILE(20,FILNAM)
```

```
          I=0
1         I=I+1
          READ(20,150,END=2)X(I),Y(I)
          VAL(I)=VAL(I)+Y(I)
          GO TO 1
2         NP=I-1
          CALL RELEASE(20)
150       FORMAT(2F)
          N=N-1
          IF(N==0.)BREAK
          ]
          TYPE 30
30        FORMAT(2X,'ENTER THE OUTPUT FILENAME")
          ACCEPT 100,FILNAM
          CALL OFILE(21,FILNAM)
          FOR(I=1;I < =TI;I=I=1)
          [
          WRITE(21,80)X(I),VAL(I)
80        FORMAT(2F)
          ]
          CALL RELEASE(21)
          STOP
          END
```